HYDROTHERMAL INFLUENCES ON THE HOLOCENE ENVIRONMENTAL HISTORY OF CENTRAL YELLOWSTONE NATIONAL PARK

by

Christopher Michael Schiller

A dissertation submitted in partial fulfillment
of the requirements for the degree

of

Doctor of Philosophy

in

Earth Sciences

MONTANA STATE UNIVERSITY
Bozeman, Montana

November 2020

ACKNOWLEDGEMENTS

Foremost thanks belong to my advisor, Dr. Cathy Whitlock, without whom I might never have had the opportunity to study ancient ecosystems, stand at the edge of geysers, hear the elk bugle as we anchor our boat for the night, or spend so many nights in the backcountry of Yellowstone. Her mentorship made me into the scientist I am now, and I am honored to join the ranks of scholars to come out of her labs. I am grateful to the guidance provided by my committee, Drs. Dave McWethy, Lisa Morgan, and Devon Orme. To Lisa, I will carry parts of your careful, meticulous research style with me through my career. Thank you to the members of the Paleoecology research group at Montana State University for your patient teaching and friendship, particularly Pico Alt, Dr. Buzz Nanavati, Dr. Virginia Iglesias, James Benes, Dr. Laurie Stahle, and Nick Kichas. My peers on the HD-YLAKE project, Dr. Sabrina Brown, Dr. Rosine Cartier, and Petra Zahajská were and are a constant source of inspiration. Finally, I need to thank my parents and brother who have encouraged my geology since the beginning.

The research contained in this dissertation was funded by a National Science Foundation grant to Cathy Whitlock (EAR-1515353) and a research fellowship from the Montana Institute on Ecosystems to myself. Thanks are owed to the National Lacustrine Core Facility (LacCore) and Large Lakes Observatory at the University of Minnesota, the National Ocean Sciences Accelerator Mass Spectrometry Facility, and the Montana Nanotechnology Facility (ICAL) for analytical support. Field work was conducted as part of this dissertation solely in Yellowstone National Park; thanks are further owed to those who enabled us to do our work in the world's first national park. Samples were collected under permits YELL-(2016, 2017, 2018)-SCI-0009, YELL-2016-SCI-5054, and YELL-2016-SCI-7018.

TABLE OF CONTENTS

TABLE OF CONTENTS CONTINUED

TABLE OF CONTENTS CONTINUED

TABLE OF CONTENTS CONTINUED

LIST OF TABLES

LIST OF FIGURES

Figure Page

LIST OF FIGURES CONTINUED

Figure Page

LIST OF FIGURES CONTINUED

Figure Page

LIST OF FIGURES CONTINUED

LIST OF FIGURES CONTINUED

Figure Page

LIST OF FIGURES CONTINUED

Figure Page

ABSTRACT

The postglacial vegetation history of Yellowstone National Park is well established by past paleoecological studies, but the role of hydrothermal activity—pervasive in areas of the park—in that history is poorly understood. To address this unknown, pollen and charcoal records were examined from lake sediment cores at multiple sites in central Yellowstone National Park to reconstruct Holocene vegetation. First, radiocarbon ages obtained from pollen concentrates were compared with other age controls at Yellowstone Lake, revealing ages that were up to 4300 cal years too old. Erroneous ages were due to either old carbon contamination from magmatic or hydrothermally degassed CO_2 or old pollen reworked from an unknown source. Second, Holocene vegetation and fire history were reconstructed from a Yellowstone Lake sediment core. The record was characterized by gradually increasing closure or extent of *Pinus contorta* forest and increasing fire activity to the present, consistent with reduced summer insolation creating cooler, effectively wetter conditions in central Yellowstone National Park. No impact of hydrothermal activity was detected in the regional Holocene-long vegetation and fire histories. Third, Holocene vegetation and fire history were studied at Goose Lake in Lower Geyser Basin, an area with abundant modern hydrothermal activity. The vegetation and fire history diverged from the regional trend at 3800 cal yr BP, synchronous with geochemical indicators indicating reorganization of hydrothermal activity in the basin, suggesting an abrupt ecological response to shifting hydrothermal activity. Finally, a variety of volcanic and hydrothermal processes were investigated as disturbances in the Northern Rocky Mountains and Yellowstone National Park through high-resolution pollen analysis. Hydrothermal explosion deposits were found to be synchronous with conifer morality, in some records, indicating that the effects of hydrothermal explosions are local and short-lived. At a regional scale, it is evident that vegetation changes were chiefly responding to millennial-scale, insolation-driven climate change. However, the impacts of hydrothermal activity were locally important where pervasive, as in Lower Geyser Basin, and in areas recently affected by hydrothermal explosions.

CHAPTER ONE

INTRODUCTION TO THE DISSERTATION

Introduction

The environmental history of Yellowstone National Park is established by a rich collection of archives. In addition to Eocene fossil forests (Dorf, 1964; Fritz, 1980) and pollen records recovered from limited outcrop exposures of interglacial (MIS 5?) lake sediments (Baker and Richmond, 1978; Baker, 1986; Love et al., 2007), Yellowstone National Park hosts many lakes from which postglacial vegetation history has been studied (Figure 1.1). Postglacial vegetation development was first investigated through pollen records from lake sediments nearly 50 years ago to provide environmental context for Paleoindian use of the region (Waddington and Wright, 1974) and vegetation history (Baker, 1976). Subsequent studies have refined our understanding of late-glacial and Holocene ecosystem dynamics by focusing on: (1) the influence of past climate variations (Gennett and Baker, 1986; Whitlock, 1993; Whitlock and Bartlein, 1993; Whitlock et al., 1995, 2012; Huerta et al., 2009; Krause and Whitlock, 2013; Iglesias et al., 2018; Stegner et al., 2019); (2) the nature of postglacial conifer establishment (Whitlock, 1993; Whitlock and Millspaugh, 2001; Krause and Whitlock, 2013); (3) the use of charcoal as a fire proxy (Millspaugh and Whitlock, 1995; Whitlock and Millspaugh, 1996); (4) the long-term linkages between changes in fire, climate, and vegetation (Millspaugh et al., 2000, 2004; Huerta et al., 2009; Higuera et al., 2010); (5) the long-term influence of geological substrate on vegetational development (Whitlock, 1993); (6) the environmental changes since

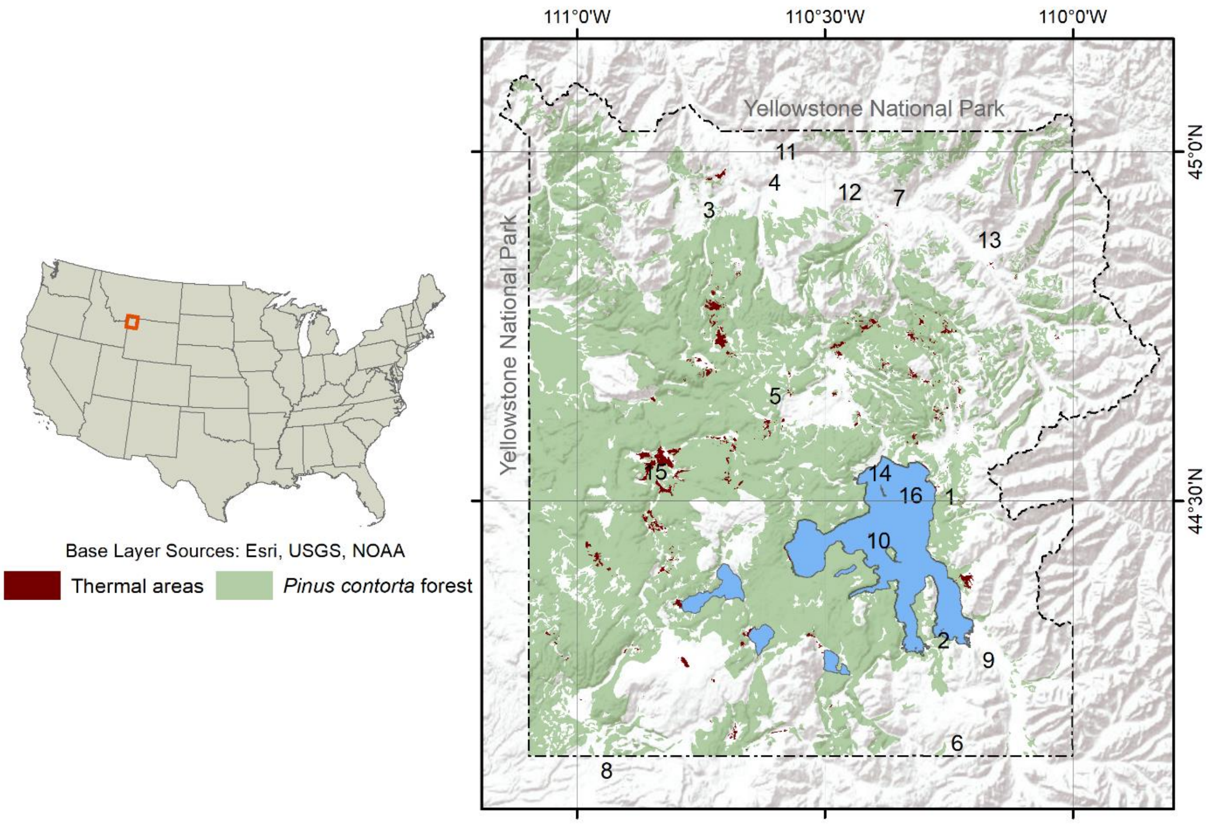

Figure 1.1: Map of Yellowstone National Park, documenting sites of postglacial vegetation history study, including sites contributed by this dissertation (14–16). Site data are juxtaposed with the distribution of pre-1988 fires *Pinus contorta* forest (Despain, 1990) and active thermal areas based on satellite measurements of heat flux (Vaughan et al., 2014). Sites are listed in Table 1.1.

Yellowstone National Park was established (Engstrom et al., 1991); and (7) the projections of ecological change with future global warming (Bartlein et al., 1997).

The Yellowstone Plateau Ecoregion (17j in Figure 1.2A; Chapman et al., 2004), a component of the Middle Rockies Ecoregion, is a set of broad volcanic plateaus that comprise much of central and southwestern Yellowstone National Park and adjacent, forested regions of southwestern Montana, eastern Idaho, and northwestern Wyoming. Latest Pliocene and Pleistocene volcanism, through violent, caldera-forming eruptions and post-caldera rhyolite flows (Christiansen, 2001), produced high, subdued topography with elevations from roughly 1900 to 2600 m.

Table 1.1. Postglacial vegetation history sites in Yellowstone National Park

Site No.	Site Name	References
1	Cub Creek Pond	Waddington and Wright, 1974; Chapter 5
2	Buckbean Fen	Baker, 1976
3	Gardiner's Hole	Baker, 1983
4	Blacktail Pond	Gennett and Baker, 1986; Huerta et al., 2009; Krause and Whitlock, 2013
5	Cygnet Lake	Whitlock, 1993; Millspaugh et al., 2000
6	Mariposa Lake	Whitlock, 1993
7	Slough Creek Pond	Whitlock and Bartlein, 1993; Millspaugh et al., 2004
8	Loon Lake	Whitlock et al., 1995
9	Trail Lake	Whitlock et al., 2003
10	Yellowstone Lake (YL92-1A)	Theriot et al., 2006
11	Crevice Lake	Whitlock et al., 2008, 2012
12	Floating Island Lake	Firmage, 2019
13	Foster Lake	Firmage, 2019
14	Yellowstone Lake (YL16-2C)	Chapter 3 (This dissertation)
15	Goose Lake	Chapter 4 (This dissertation)
16	Yellowstone Lake (YL16-5A)	Chapter 5 (This dissertation)

The climate of the Yellowstone Plateau is strongly influenced by location and topography. The high elevation leads to cold winters and mild summers (mean annual temperatures ~0-4.5 °C; PRISM Climate Group, 2004). Annual precipitation (~600-1400 mm; PRISM Climate Group, 2004) also varies strongly with elevation, with the greatest precipitation received at the highest elevations of the Madison and Pitchstone Plateaus. The season of highest precipitation varies greatly at different locations on the Plateau. Island Park, ID receives the most precipitation in winter (231 mm DJF, 132 mm JJA; 30-year normals, Arguez et al., 2010). At Lake Yellowstone, WY, in contrast, precipitation is more evenly distributed through the year, with slightly more received in early summer (124 mm DJF, 139 mm JJA; 30-year normals, Arguez et al., 2010). The source of winter precipitation is dominantly from frontal storms funneled eastward through the low-elevation channel of the Snake River Plain (Bryson and Hare, 1974). Summer precipitation is generally sourced from convective storms with Gulf of Mexico and subtropical Pacific moisture sources. The northern edge of the Plateau receives a majority of annual precipitation in spring and summer from convective storms and has been termed "summer-wet" (Figure 1.2B; Whitlock and Bartlein, 1993; Mock, 1996). In contrast, the climate of most of the Yellowstone Plateau is dominated by winter precipitation and referred to as "summer-dry" (Whitlock and Bartlein, 1993; Mock, 1996). During the early Holocene, summers were warmer and drier than present in summer-dry regions, because the direct effects of insolation increased temperatures, and the indirect effect of changes in atmospheric circulation expanded and strengthened the northeastern Pacific subtropical high pressure system in summer (Bartlein et al., 1998).

Latest Pliocene and Pleistocene volcanism on the present Yellowstone Plateau produced large volume rhyolite lava flows and ignimbrites (Christiansen, 2001); Figure 2C), resulting in rhyolitic soils throughout most of the region, which are well-drained and nutrient-poor. The Yellowstone Plateau was repeatedly glaciated during the Pleistocene, including the most recent Pindedale Glaciation (locally 22-13 ka; Licciardi and Pierce, 2018). At the last glacial maximum,

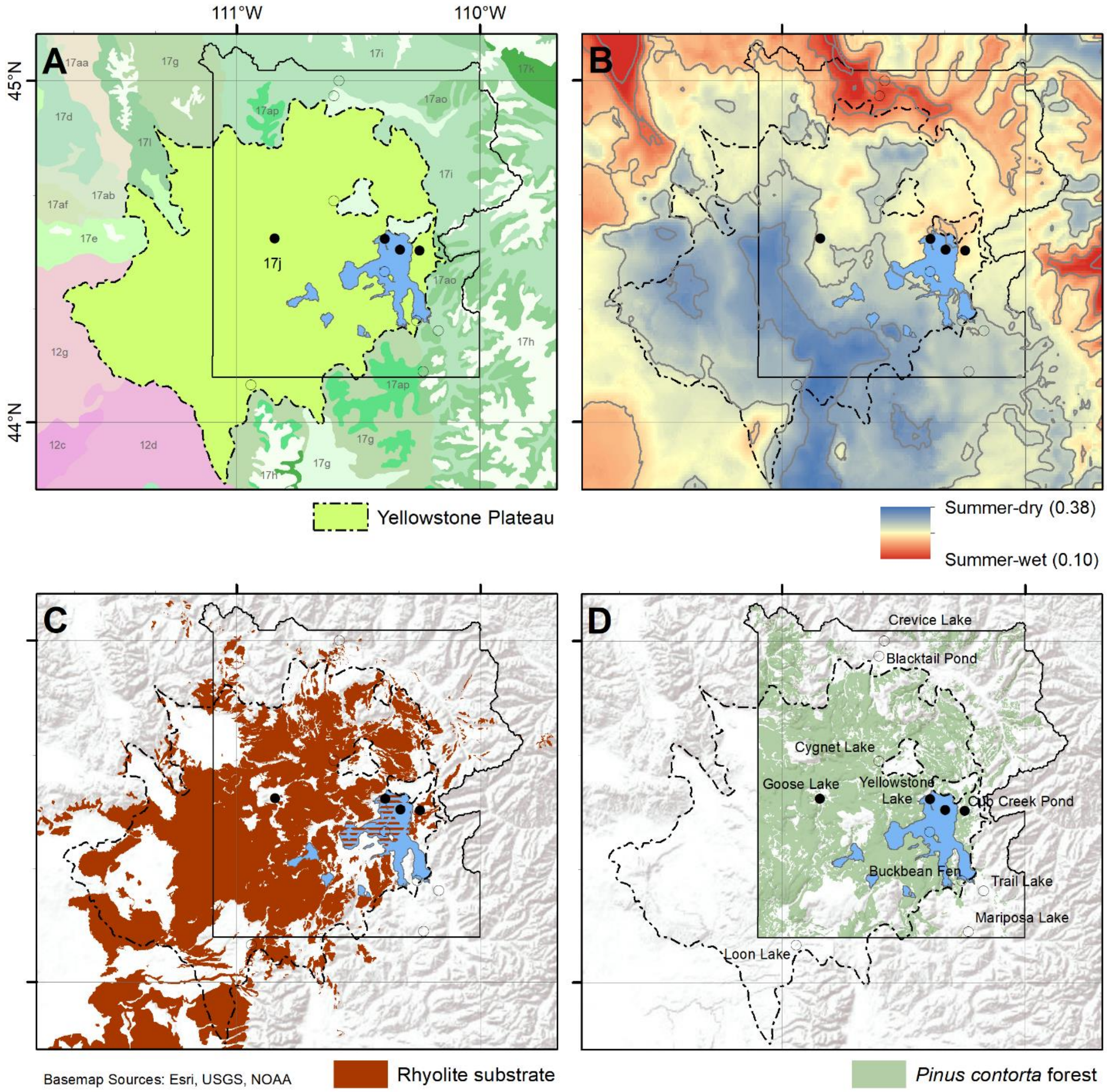

Figure 1.2: The Yellowstone Plateau ecoregion characterized by (A) EPA level IV ecoregions (Chapman et al., 2004), (B) summer-dry versus summer-wet regions based on the average ratio of winter to annual precipitation (30-year normals, PRISM Climate Group, 2004), (C) the distribution of rhyolitic substrate (Bond et al., 1978; Green et al., 1994; Green et al., 1999; Christiansen, 2001; Morgan et al., 2007), and (D) the extent of *Pinus contorta* forest within Yellowstone National Park (Despain, 1990). Dots indicate sites from this dissertation (solid dots) and other sites referenced in the text (open dots).

more than 1000 vertical m of ice was located over Yellowstone Lake, comprising the center of a vast ice complex (Licciardi and Pierce, 2018). Most of the Plateau was probably ice-free by ~14 ka based on correlation to recessional moraines in northern Yellowstone National Park (Licciardi and Pierce, 2008) and basal ages from existing sediment cores (Whitlock, 1993; Theriot et al., 2006). Deglaciation produced many kettle and glacial scour lakes, although the largest lakes, such as Yellowstone Lake, are of volcanic origin (Otis et al., 1977).

Most of the Yellowstone Plateau is covered by *Pinus contorta* forests (Figure 1.2D). *P. contorta* is well-suited to well-drained, nutrient-poor rhyolitic substrates and stand-replacing fires of intermediate (~150–300 years) frequency (Pfister and Daubenmire, 1975; Despain, 1983, 1990). In particular, some *P. contorta* stands are serotinous, wherein closed cones retain mature seeds until released by fire, which allows for rapid regeneration following stand-replacement fires (Tinker et al., 1994; Schoennagel et al., 2003). Although *Abies lasiocarpa* is considered the climax species in most of these middle Rocky Mountain forests at these elevations (Despain, 1990), the combination of edaphic constraints and stand-replacing fires makes *P. contorta* the dominant tree in these forests (Figure 1.2D). Other forest types with components of *A. lasiocarpa*, *Pseudotsuga menziesii*, and/or *Pinus albicaulis* are found on non-rhyolitic substrates surrounding the Yellowstone Plateau where nutrient levels and soil moisture are higher (Despain, 1990). Islands of steppe and grassland vegetation are found within the Yellowstone Plateau, most clearly in Hayden and Pelican Valleys (Figure 1.2D), which are underlain by Pleistocene proglacial lake sediments (Richmond, 1977). The dominant steppe taxa are *Artemisia tridentata* or *Artemisia cana*, with *Bromus carinatus*, *Festuca idahoensis*, *Phleum pratense, Poa pratensis* and abundant herbs (Despain, 1990). Pollen records from the Yellowstone Plateau suggest that

Artemisia steppe or grassland was established soon after ice recession and mostly replaced by *P. contorta* forest after 11,000 ka, with little compositional change since that time (Whitlock, 1993; Iglesias et al., 2018).

The largest concentration of hydrothermal features associated with Yellowstone volcanism, including numerous thermal pools, fumaroles, mud pots, and geysers, occurs on the Yellowstone Plateau at the edges of rhyolite lava flows (Figure 1.1; Morgan and Shanks, 2005; Vaughan et al., 2014; Hurwitz and Lowenstern, 2014). Craters that result from past hydrothermal explosions are found in several regions of Yellowstone (Muffler et al., 1971; Morgan et al., 2009). At least 20 hydrothermal explosion craters are large (diameter >100 m) and their formation blanketed areas of 0.1-5 km^2 with explosion debris in the past (Morgan et al., 2009). The impact of hydrothermal activity on modern vegetation is evidenced by recent tree mortality and stunted growth as a result of heated soils (White et al., 1988; Lowenstern et al., 2003; Vaughan et al., 2020) and contact with hot, mineral-saturated fluids (Pitt and Hutchinson, 1982; Channing and Edwards, 2003). Many hydrothermal landscapes, such as Upper and Lower Geyser Basins, are covered by diminutive grasses adapted to heated, salt-rich soils (Despain, 1990), and barren flats of sinter and diatomaceous mud. The prevalence of hydrothermal activity on the Yellowstone Plateau suggests that it may have played a significant role in the region's environmental history.

Objectives

The objective of this dissertation is to examine the influence of hydrothermal activity on the Holocene vegetation and environmental history of the Yellowstone Plateau ecoregion. To address this objective, the impacts of past hydrothermal activity were examined in different settings to answer the following questions:

- How does hydrothermal activity influence the radiocarbon content of lake sediments and the development of a chronology for documenting environmental change (Chapter 2)?
- How did vegetation and fire respond to hydrothermal explosions and long-term climate change in the Yellowstone Lake area (Chapter 3)?
- What was the influence of hydrothermal activity on local vegetation history, in comparison to the influences of broad-scale climate change (Chapter 4)?
- What was the relative influence of volcanism, ashfall, and hydrothermal activity in shaping the Quaternary vegetation history of the Yellowstone Plateau and the Northern Rocky Mountains (Chapter 5)?

Research history

This project was initially conceived and primarily funded as part of the HD-YLAKE project led by Dr. Robert Sohn (Woods Hole Oceanographic Institute), under NSF Grant No. 1515353 to C. Whitlock. The aim of the HD-YLAKE project was to understand how hydrothermal systems respond to tectonic, magmatic, and climatic forcings on short (seconds to years) to long (centennial to millennial) timescales by focusing on the subaqueous hydrothermal fields of Yellowstone Lake. A geophysical team has conducted short-term measurements of heat flux, microseisms, high-resolution bathymetry, and magnetism of Yellowstone Lake. Another team was responsible for the collection and analysis of sediment cores to determine the influence of Holocene hydrothermal activity and climate change on the terrestrial and limnobiotic history. For the latter goal, analyses were undertaken of fossil pollen and charcoal (myself, C. Whitlock), diatom analysis (S.R. Brown, S.C. Fritz), biogenic silica (P. Zahajská, D. Conley), oxygen isotopes of diatoms (R. Cartier, D. Conley), lithology (L.A. Morgan), and geochemistry (W.C. Shanks III).

Work detailed in this dissertation included and expanded on the goals of HD-YLAKE. Initial radiocarbon age determinations made from Yellowstone Lake sediment cores, the subject of multi-proxy analysis, were erroneously old, demanding examination of the source of old carbon (Chapter 2). Results from the multi-proxy analysis showed little terrestrial impact from past hydrothermal explosions in comparison to the long-term influence of insolation-driven climate change (Chapter 3). Goose Lake, in Lower Geyser Basin near multiple, large (> 100 m diameter) hydrothermal explosion craters, did not produce any sediments attributed to a hydrothermal explosion, but produced a clear history of the environmental impact of shifting hydrothermal activity (Chapter 4). Pollen data from the Yellowstone Plateau and elsewhere in the western U.S. were examined to understand the ecological importance of different volcanic processes (e.g., lava flows, ashfall from distal, and hydrothermal activity) on vegetation dynamics (Chapter 5).

Structure and attribution of contents

This dissertation is written as four stand-alone articles, with contributions from several co-authors, in addition to this Introduction and a Conclusion:

- Chapter 2, "Erroneously old radiocarbon ages from terrestrial pollen concentrates in Yellowstone Lake, Wyoming, USA", is currently in press in the journal *Radiocarbon*. I was responsible for palynological lab work, statistical analyses, and led manuscript preparation. C. Whitlock funded the analyses through NSF Grant No. 1515353 and helped conceptualize and develop the manuscript. K.L. Elder supervised accelerator mass spectrometry lab work and contributed to the manuscript. N.A. Iverson conducted electron microprobe analyses and interpreted tephra data. M.B. Abbott contributed unpublished radiocarbon ages and edited the manuscript.

- Chapter 3 is a component of a manuscript, "Multi-proxy record of Holocene paleoenvironmental conditions from Yellowstone Lake, Wyoming, USA", in preparation for *Quaternary Science Reviews*, led by Dr. Sabrina R. Brown (Defiance College). I participated in field work and conducted radiocarbon, pollen, and charcoal analyses. R. Cartier (Lund University) conducted oxygen isotope analyses of diatoms and contributed to the manuscript. C. Whitlock provided funding and helped conceptualize and develop the manuscript. L.A. Morgan (U.S. Geological Survey) conducted lithological descriptions, advised on lithological interpretations, and contributed to the manuscript.
- Chapter 4, "Holocene geo-ecological evolution in Lower Geyser Basin, Yellowstone National Park", is in preparation for submission to the *Geological Society of America Bulletin.* I was responsible for project conception, led field work, conducted lab work (except diatom and biogenic silica analyses), and led manuscript preparation. C. Whitlock providing funding and guided the development of the manuscript. S.R. Brown conducted analysis of diatoms. P. Zahajská (Lund University) analyzed biogenic silica content of sediments.
- Chapter 5, "Vegetation responses to Quaternary volcanic and hydrothermal disturbances in the Northern Rocky Mountains and Greater Yellowstone Ecosystem", was published in *Paleogeography, Palaeoclimatology, Palaeoecology* (Schiller et al., 2020). I led field

work at Cub Creek Pond and Goose Lake, conducted new pollen analyses at Cub Creek Pond, Goose Lake, and Yellowstone Lake, completed statistics, and led manuscript development. C. Whitlock provided funding and help conceive of and edited the manuscript. M. Alt (Montana State University) contributed new pollen data from Twin Lakes, MT and contributed to the manuscript. L.A. Morgan provided lithological descriptions and edited the manuscript.

- Chapter 6 presents the key findings of this project and offers some thoughts for future research.

CHAPTER TWO

ERRONEOUSLY OLD RADIOCARBON AGES FROM TERRESTRIAL POLLEN CONCENTRATES IN YELLOWSTONE LAKE, WYOMING, USA

Contribution of Authors and Co-Authors

Manuscript in Chapter 2

Author: Christopher M. Schiller

Contribution: Conducted palynological lab work, statistical analyses, and led manuscript preparation.

Co-Author: Cathy Whitlock

Contribution: Provided funding and helped conceptualize and develop the manuscript.

Co-Author: Kathryn L. Elder

Contribution: Supervised accelerator mass spectrometry lab work and contributed to the manuscript.

Co-Author: Nels A. Iverson

Contribution: Conducted electron microprobe analyses and interpreted tephra data.

Co-Author: Mark B. Abbott

Contribution: Added unpublished radiocarbon ages and contributed to the manuscript.

Manuscript Information

Christopher M. Schiller, Cathy Whitlock, Kathryn L. Elder, Nels A. Iverson, Mark B. Abbott

Radiocarbon

Status of Manuscript:
_____ Prepared for submission to a peer-reviewed journal
_____ Officially submitted to a peer-reviewed journal
__×__ Accepted by a peer-reviewed journal
_____ Published in a peer-reviewed journal

Cambridge University Press
October 22, 2020

CHAPTER TWO

ERRONEOUSLY OLD RADIOCARBON AGES FROM TERRESTRIAL POLLEN CONCENTRATES IN YELLOWSTONE LAKE, WYOMING, USA

Abstract

Accelerator mass spectrometry (AMS) dating of pollen concentrates is used often in lake sediment records where large, terrestrial plant remains are unavailable. Ages produced from chemically concentrated pollen as well as manually picked Pinaceae grains in Yellowstone Lake (Wyoming) sediments were consistently 1700 to 4300 cal years older than ages established by terrestrial plant remains, tephrochronology, and the age of the sediment-water interface. Previous studies have utilized successfully the same laboratory space and methods, suggesting the source of old-carbon contamination is specific to these samples. Manually picking pollen grains precludes admixture of non-pollen materials. Furthermore, no clear source of old pollen grains occurs on the deglaciated landscape, making reworking of old pollen grains unlikely. High volumes of CO_2 are degassed in the Yellowstone Caldera, potentially introducing old carbon to pollen. While uptake of old CO_2 through photosynthesis is minor ($F^{14}C$ approximately 0.99), old-carbon contamination may still take place in the water column or in surficial lake sediments. It remains unclear, however, what mechanism allows for the erroneous ages of highly refractory pollen grains while terrestrial plant remains were unaffected. In the absence of a satisfactory explanation for erroneously old radiocarbon ages from pollen concentrates, we propose steps for further study.

Introduction

Lake sediments are the primary archive for reconstructing late-Quaternary terrestrial climate, vegetation, fire, and limnobiotic processes. Correlation between sites and comparison of independent proxies and paleoclimate model simulations requires sedimentary records with high-resolution age-depth control, most commonly accomplished through radiocarbon dating. The utility of radiocarbon dating pollen concentrates with accelerator mass spectrometry (AMS) has been well established in lacustrine settings where terrestrial plant remains are unavailable and where total organic carbon of (bulk) sediments are potentially contaminated by refractory carbon and reservoir effects. Pollen concentration through mechanical separation (Brown et al., 1989; Long et al., 1992; Mensing and Southon, 1999), chemical maceration (Doher, 1980), heavy liquid separation (Vandergoes and Prior, 2003), and flow cytometry (Tennant et al., 2013) selectively removes anachronous sources of carbon (e.g. carbonates, algal remains, humic acids) from the sample. Although some studies suggest dating errors as a result of incomplete separation of non-pollen material (Regnéll, 1992; Richardson and Hall, 1994) or incorporation of reworked pollen grains (Mensing and Southon, 1999; Zimmerman et al., 2019), pollen-concentrate ages typically produce more reliable chronologies than bulk-sediment ages where reservoir effects are a concern (e.g. Brown et al., 1989; Vandergoes and Prior, 2003; Newnham et al., 2007; Fletcher et al., 2017).

Yellowstone Lake, Wyoming (44.5° N, 110.3° W, elev. 2360 m.a.s.l.), a large (341 km^2), temperate, subalpine lake (Figure 2.1), is a good candidate for AMS dating of pollen concentrates, as few sufficiently large, terrestrial plant remains were recovered from recent

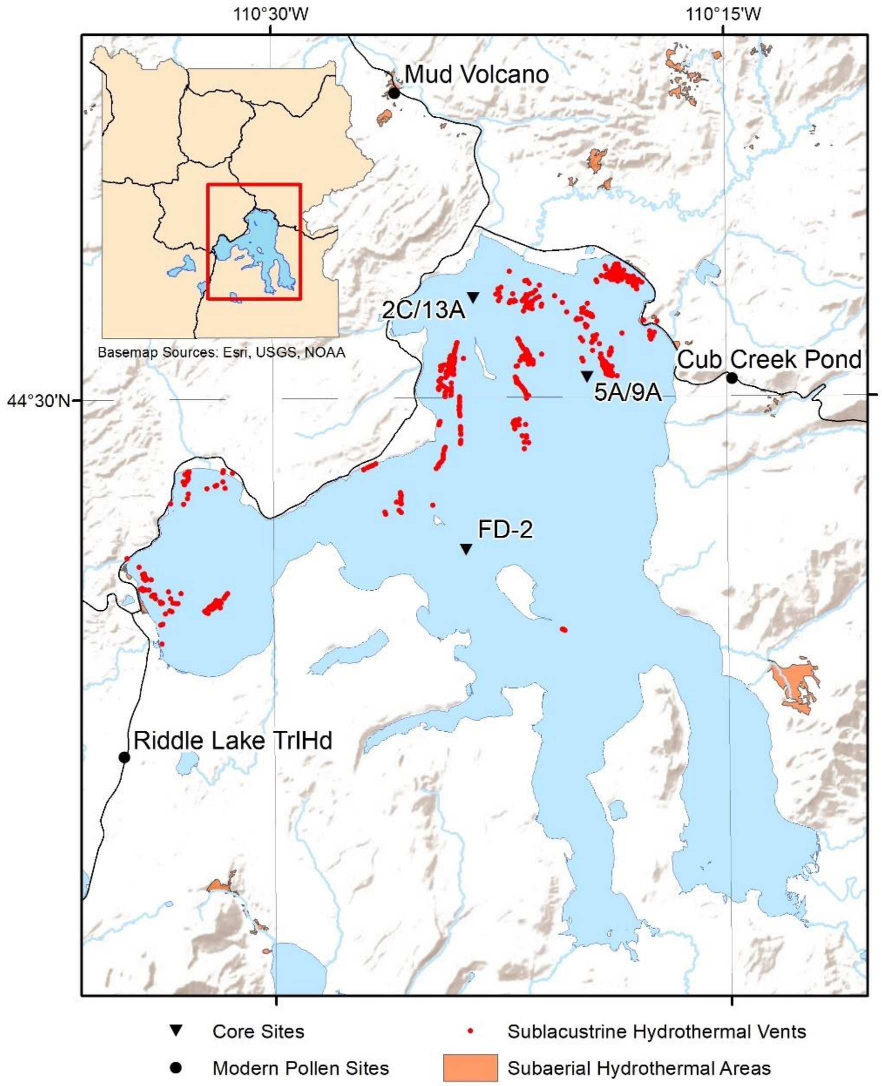

Figure 2.1: Map of the Yellowstone Lake basin, showing location of the collection of sediment cores and modern pollen samples. Subaerial hydrothermal areas based on Vaughan et al. (2014) and sublacustrine hydrothermal vents based on Morgan et al. (2007). All sites are located within or near the eastern half of the Yellowstone Caldera, where the majority of CO_2 degassing occurs from acid-sulfate hydrothermal vents (Werner and Brantley 2003).

coring efforts (2016, Table 2.1). The geology of the watershed is complex, resulting from an interplay of volcanic, glacial, hydrothermal, and tectonic processes. The northern two-thirds of the lake basin lies within the Yellowstone Caldera that was formed ~631 ka (Christiansen, 2001; Matthews et al., 2015; Wotzlaw et al., 2015), and the entire lake basin was covered by the

Yellowstone glacial complex, 22,000-13,000 BP (Licciardi and Pierce, 2018). The lake floor today has more than 660 active or recently active hydrothermal vents (Figure 2.1; Morgan et al., 2007a, b).

Previous studies of sediment cores from Yellowstone Lake provide a postglacial limnogeologic (Tiller, 1995) and paleoenvironmental (Theriot et al., 2006) record, making high-resolution age control desirable. In addition, Yellowstone Lake sediments preserve deposits from past hydrothermal explosions (Tiller, 1995; Morgan et al., 2009) and volcanic ashes from eruptions in the Cascade Range to the west (Tiller, 1995; Theriot et al., 2006). Sediment cores collected in 1992 (FD-2; Figure 2.1) were dated with radiocarbon ages from terrestrial plant remains (Tiller, 1995; Table 2.1). However, previously unpublished radiocarbon ages collected from humic acid and humin during that study were up to thousands of years older than associated terrestrial plant remains (Table 2.1) and demonstrate the presence of an old-carbon pool (Figure 2.2). Radiocarbon ages of bulk sediments and pollen concentrates from Cub Creek Pond (44.505° N, 110.246° W, elev. 2510 m.a.s.l.) ~4 km east of Yellowstone Lake also yielded calibrated ages thousands of years older than established by terrestrial plant remains or tephrochronology (Whitlock, 1993; Lu et al., 2017).

Our objective in this study was to answer the following questions: (1) How do radiocarbon ages from different terrestrial materials in Yellowstone Lake sediments compare? (2) What is the carbon source for pollen concentrates from Yellowstone Lake sediments that might lead to erroneously old ages? To answer these questions, we explore a suite of AMS radiocarbon ages from several sediment cores from the northern basin of Yellowstone Lake and compare them with independent age controls and the radiocarbon ages of living plant material.

Methods

Sediment cores from the northwest area (core 2C, 44.53927° N, 110.38922° W, water depth 61 m) and southeast area (core 5A, 44.50782 °N, 110.32685 °W, water depth 102 m) of the northern basin of Yellowstone Lake were collected in September 2016 with a Kullenberg sampler (Figure 2.1; Kelts et al., 1986). Additional cores were retrieved near the 2C (13A) and 5A (9A) sites with a gravity sampler in July 2017 to recover the most recent sediments. Cores were transported to the National Lacustrine Core Facility (LacCore, University of Minnesota) where they were longitudinally split, photographed, and stored under refrigeration except when sampled or during core-scanning analyses. Kullenberg and gravity cores were correlated on the basis of core imagery and charcoal stratigraphy, producing two complete records for analysis, core 2C/13A and core 5A/9A.

Initial stratigraphic AMS age determinations for core 2C/13A were derived from terrestrial plant remains (needles, charcoal, or unidentified wood fragments) and pollen concentrates. Bulk-sediment ages were avoided based on erroneously old ages previously obtained from humin in the FD-2 core (Figure 2.2; Table 2.1). Plant remains were collected wherever present, identifiably terrestrial, and large enough for analysis. Five terrestrial plant remains were identified, extracted from core sediments, washed in distilled water, and placed under a dissection microscope where extraneous sediment was removed with a teasing needle. Initial pollen samples were collected from 1-cm intervals immediately above and below a thick hydrothermal explosion deposit and wherever substantial stratigraphic gaps occurred in the spacing of terrestrial plant remains. Pollen was concentrated by traditional pollen maceration

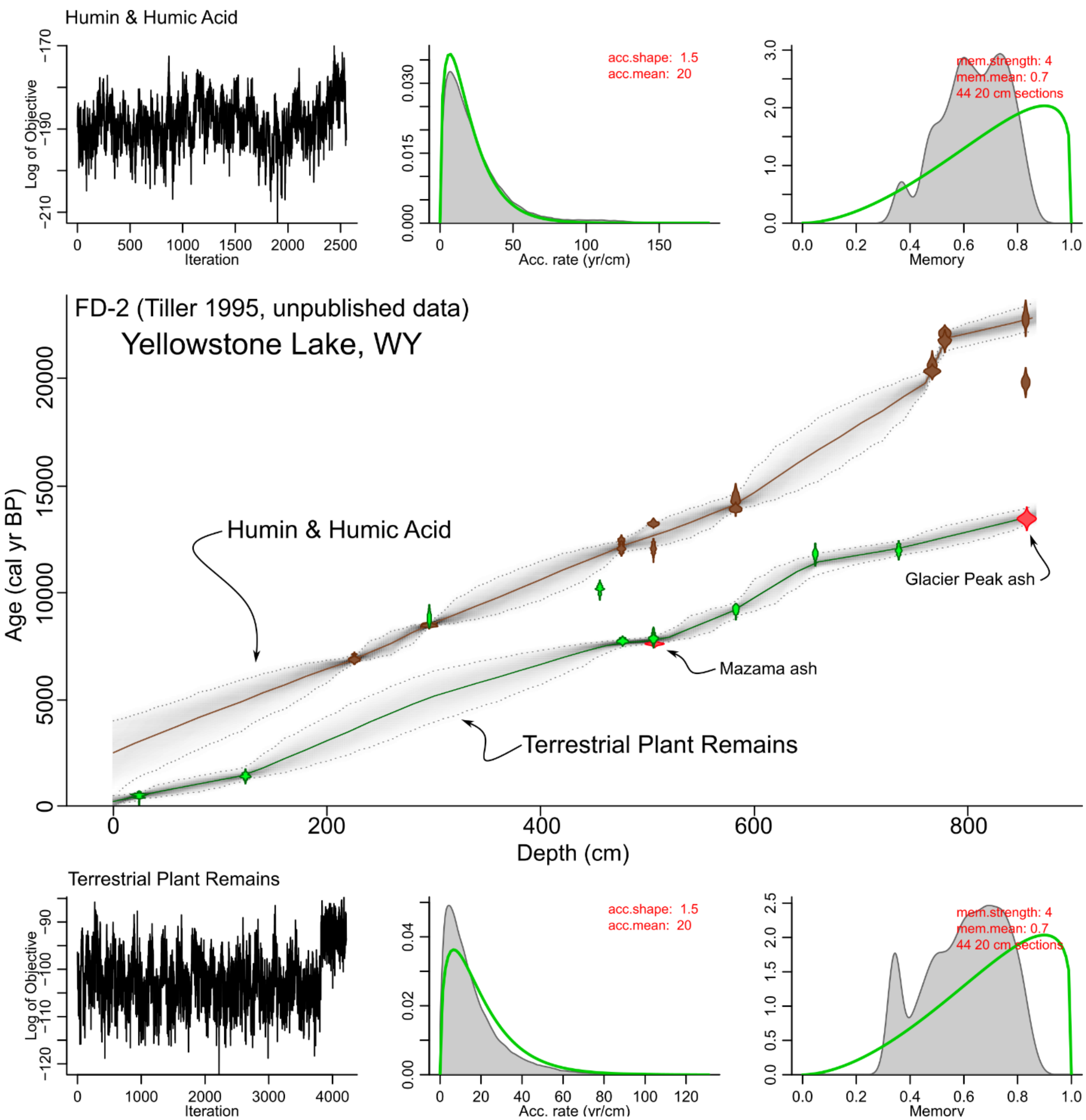

Figure 2.2: Bacon age-depth models for Yellowstone Lake (FD-2 from Tiller 1995) derived from bulk sediment components, humin and humic acid (brown), terrestrial plant remains (green; Tiller 1995), and ashes (red). Younger ash is Mazama (7682-7584 cal BP, 2σ range, Egan et al. 2015) and the older is Glacier Peak B or G (13410-13710 cal BP, 2σ range, Kuehn et al. 2009) as determined by petrographic analysis of Tiller (1995).

procedures (Bennett and Willis, 2001). Sediments were disaggregated and humic compounds removed with 0.9N KOH treatment (near-boiling hot bath, 2.5 min) and rinsed with distilled water, centrifuged, and decanted until the supernatant was clear. Large particles were wet sieved with distilled water through a 180-μm mesh. Carbonates were removed with 2.7N HCl treatment (near-boiling hot bath, until no effervescence was observed) and silicates were removed with 28.9N HF (near-boiling hot bath, 60 min). Acetolysis was foregone in favor of oxidation in 15.9N HNO_3 (near-boiling hot bath, 3 min) to remove cellulose while avoiding carbon-bearing acetate solutions. Samples were rinsed with distilled water, centrifuged, and decanted until the slurry was neutral. These samples are hereafter referred to as chemically concentrated pollen.

Paired bulk-sediment and picked-pollen concentrate samples also were collected from stratigraphic locations (in 1-cm intervals) where ages were known independently. Bulk-sediment and picked-pollen samples were collected at the sediment-water interface (core top) in the gravity cores (13A, 9A) where the true age was approximately the year of coring (~-67 cal BP). Further bulk-sediment and picked-pollen samples were collected from Kullenberg cores (2C, 5A) immediately above what is likely the Mazama ash (Tiller, 1995; Theriot et al., 2006). These tephra (2C, 5A), along with a new analysis of the younger (1995) tephra from core FD-2, were sampled and analyzed at the New Mexico Bureau of Geology and Mineral Resources on a Cameca SX-100 electron microprobe to confirm the geochemical correlation between the cores, and to the Mazama ash. Picked-pollen samples were obtained utilizing the maceration procedures described above and a modified pipetting procedure from Mensing and Southon (1999). Sieving with 90- and 38-μm mesh screens targeted *Pinus* pollen and further concentration was managed by picking with a micropipette under a stereomicroscope (63×

magnification). Pipette suction was gently produced by a syringe in place of the mouth. Identification under the stereomicroscope was generally only possible at the level of Pinaceae, so picked-pollen samples likely contained some mixture of *Pinus*, *Abies,* and *Picea*. It was not practical to count grains during the picking procedure, but resultant mass of C, 22-58 μg, was comparable to the yields of Mensing and Southon (1999).

Finally, to confirm that the carbon isotope composition of the pollen, like wood, reflects the atmospheric radiocarbon activity, modern pollen was collected from *Pinus contorta* trees in the Yellowstone Lake vicinity (Figure 1.1). Pollen (male) cones were collected from trees at three locations near Yellowstone Lake in June 2019: (1) upwind of Yellowstone Lake near the Riddle Lake Trailhead, (2) downwind of Yellowstone Lake near Cub Creek Pond, and (3) near Mud Volcano, where uptake of radiometrically old carbon has been previously documented in *Pinus contorta* tree rings ($F^{14}C$ up to 0.35 lower than NHZ1 post-bomb curve; Evans et al., 2010). Due to a cold, wet spring, pollen production was late, and samples collected in June 2019 were probably from the 2018 crop. Pollen was rinsed off of cones and sieved through 90- and 38-μm mesh screens to remove extraneous material and treated with Schulze solution (1:10 wt (g)/vol (mL) mixture $KClO_3$ in 15.9N HNO_3, near-boiling hot bath, 3 min) to remove extraneous organics (Doher, 1980). Samples were rinsed in distilled water, centrifuged, and decanted until the slurry was neutral.

AMS age determinations were made by the National Ocean Sciences AMS (NOSAMS) facility at the Woods Hole Oceanographic Institute. Traditional pretreatment was conducted only for terrestrial plant remains using a modified acid-base-acid method to remove non-structural carbon (de Vries and Barendsen, 1954) and bulk sediments were treated with 2.7N HCl

(McNichol et al., 1994). Pollen-concentrate samples were combusted without any further treatment at NOSAMS since previous concentration procedures made further pretreatment redundant. Pollen-concentrate samples were generally very small, <0.1 mg total sample mass. To preserve as much of the sample as possible, concentrates were shipped in dilute HCl in distilled water with subsequent filtering onto pre-baked quartz fiber filters, rinsed to neutral, dried, and combusted at 850 °C in sealed quartz tubes. Carbon yields from pollen concentrates ranged from 22 to 569 μg C. Radiocarbon results were blank corrected for the possible addition of contaminants during sample processing and AMS measurement. For samples that yielded <100 μg carbon, a mass-balance correction was made according to Roberts et al. (2019). For larger sample masses, the mass-dependent correction is relatively small, and an average large mass blank value from acetanilide samples (used as a home blank due to the unavailability of ^{14}C-free pollen material) measured concurrently with the unknown sample was used to correct the result. When samples were large enough, a split of CO_2 was sent to a stable mass spectrometer for $\delta^{13}C$ analysis to aid in the verification of results and identification of anachronous carbon sources including aquatic plants and carbonate rock.

Radiocarbon ages were calibrated with CALIB (version 7.1, Stuiver et al., 2019) utilizing the IntCal13 calibration curve (Reimer et al., 2013). Calibrated ages were further refined and interpreted in the context of stratigraphic depth through development of two age-depth models using Bacon software (rbacon version 2.3.9.1, Blaauw and Christen, 2011) based on chemically concentrated pollen and terrestrial plant remains. A priori assignment of mean sediment accumulation rate was set to 10 yr cm^{-1}, as suggested by Bacon and closely matching our data, but is somewhat faster than Holocene sediment accumulation rates estimated for other, deeper parts of Yellowstone Lake (~15 yr cm^{-1}, Tiller 1995; 17-10 yr cm^{-1}, Johnson et al., 2003). Thickness for spline calculation was set to 20 cm, above which the model diverged greatly from provided age controls. A priori parameters were held constant for age-depth models based on chemically concentrated pollen and terrestrial plant remains, and independent age controls were included in both models. Instantaneous deposits resulting from volcanic ashfall or hydrothermal explosions were relatively thin in this core (<5 cm) and not excised from the total core depth.

Results

Radiocarbon results

Calibrated radiocarbon ages for core 2C/13A are presented in Table 2.1, along with non-radiocarbon ages: the core top, a prominent charcoal peak from a large fire that occurred ca. 1700 CE (based on tree-ring analysis in the watershed; error assigned to ±10 years on the basis of two prominent decades of stand establishment; Romme and Despain, 1989; Higuera et al., 2010), and the geochemically fingerprinted Mazama ash (Table 2.2). All three lake-core tephra are geochemically identical to the Mazama ash (Jensen and Beaudoin, 2016) allowing for time to be correlated across Yellowstone lake. The age of the climactic Mt. Mazama eruption is well established in ice-core records (7777-7477 cal BP, 2σ range; Zdanowicz et al., 1999) and by thorough radiocarbon dating efforts (7682-7584 cal BP, 2σ range; Egan et al., 2015). One radiocarbon result from unidentified plant remains (OS-142084) was excluded from the terrestrial plant age-depth model, given its erroneously old age and a $\delta^{13}C$ value of -10.9 ‰, both of which are consistent with an aquatic plant fragment.

The age-depth models from chemically concentrated pollen and terrestrial plant remains diverge, except at the top of the core where closely spaced calendar ages enforce unity (Figure

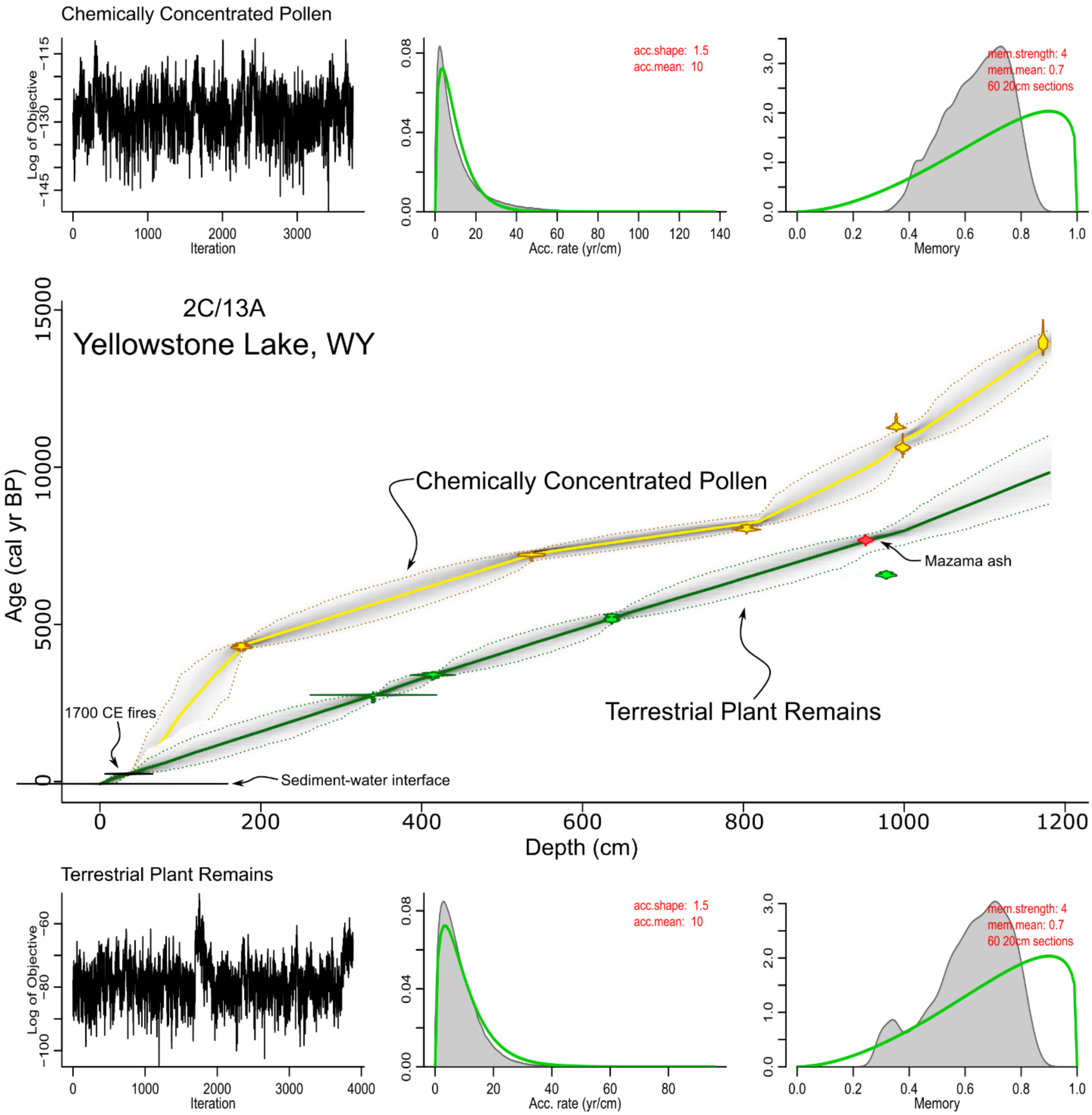

Figure 2.3: Bacon age-depth models for Yellowstone Lake (core 2C) derived from chemically concentrated pollen (yellow), terrestrial plant remains (green), the Mazama ash (red), and calendar ages of the coring date and a fire at 1700 CE.

2.3). Modelled median calibrated ages from pollen concentrates ranged from 1700 to 4300 years older than the modelled median calibrated ages from terrestrial plants. Ages from chemically concentrated pollen were internally consistent, with no ages falling outside the 2σ range of the age-depth model, but they too did not agree with the age of the Mazama ash. The Mazama ash age was rejected by Bacon as an outlier in the chemically concentrated pollen model. Terrestrial plant remain ages also were internally consistent, with only one age outside the 2σ range, and the age model aligned well with the age of the Mazama ash (Figure 2.3).

Paired bulk-sediment and picked-pollen sample ages were calibrated utilizing Intcal13 (Reimer et al., 2013) and plotted with CALIB (version 7.1, Stuiver et al., 2019, Figure 2.4). Bulk-sediment ages were 4600 and 6000 cal years too old ($F^{14}C$ 0.6017 ± 0.0019 and 0.5203 ± 0.0017) at the sediment-water interface and 5300 and 5400 cal years too old directly above Mazama ash ($F^{14}C$ 0.2524 ± 0.0016 and 0.2497 ± 0.0016). Picked-pollen samples offered an improvement, with ages that were 1900 and 2400 cal years too old at the sediment-water interface ($F^{14}C$ 0.7885 ± 0.0109 and 0.7505 ± 0.0164). Directly above the Mazama ash, the picked pollen age from 2C/13A (OS-142018) was 4300 cal years too old directly above the Mazama ash ($F^{14}C$ 0.2793 ± 0.0059), while the age from 5A/9A (OS-142221) was 1300 cal years too young ($F^{14}C$ 0.5021 ± 0.0083). The lower precision and resultant posterior distributions of picked-pollen ages were much wider than bulk-sediment ages, and understandably so, due to the larger uncertainties involved with small mass sample analysis.

Radiocarbon results from modern pollen from the Riddle Lake Trailhead, Cub Creek Pond, and Mud Volcano demonstrate virtually modern $F^{14}C$ values of 0.9903 ± 0.0019, 0.9940 ± 0.0022, and 0.9790 ± 0.0025, respectively (Figure 2.4). These $F^{14}C$ values were calibrated utilizing CALIBomb (Reimer and Reimer, 2004, Figure 2.4) with the NHZ1 post-bomb calibration (Hua et al., 2013) and IntCal13 pre-bomb calibration (Reimer et al., 2013).

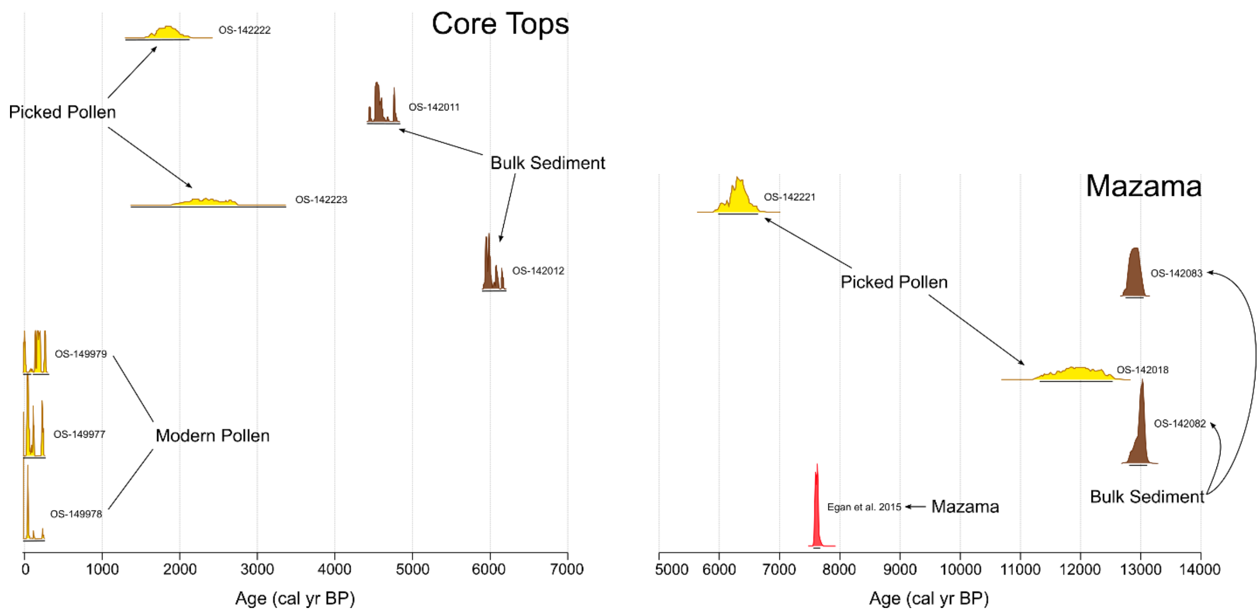

Figure 2.4: Probability density plots of dates from multiple materials at depths with known ages. Core top ages should be the approximate year of coring or pollen cone collection, -67 and -68 cal BP respectively. Samples were collected immediately above the Mazama ash, which was deposited at 7682-7584 cal BP (2σ range, Egan et al. 2015). All ages from Yellowstone Lake cores, except OS-142221, are erroneously old by thousands of years. Picked-pollen ages have wide age distributions owing to small sample sizes.

$\delta^{13}C$ results

Where samples were large enough, a split of CO_2 from combusted samples was analyzed for $\delta^{13}C$ as well as for radiocarbon, and the results were compared with existing $\delta^{13}C$ values obtained in earlier studies (Figure 2.5). Bulk sediments had less depleted $\delta^{13}C$ values than terrestrial plant remains, indicative of a non-terrestrial plant carbon source in the sediment. With the exception of one outlier, $\delta^{13}C$ values from terrestrial plant remains fell within the accepted range for terrestrial C_3 plants (Smith and Epsten, 1971). Chemically concentrated pollen $\delta^{13}C$ values were widely variable, however, with one outlier nearly at 0 ‰ VPDB. All $\delta^{13}C$ values from sediment core samples were less depleted than those from modern pollen cones, which were -31.0 ‰ VPDB on average. $\delta^{13}C$ values did also vary somewhat from site to site, but with

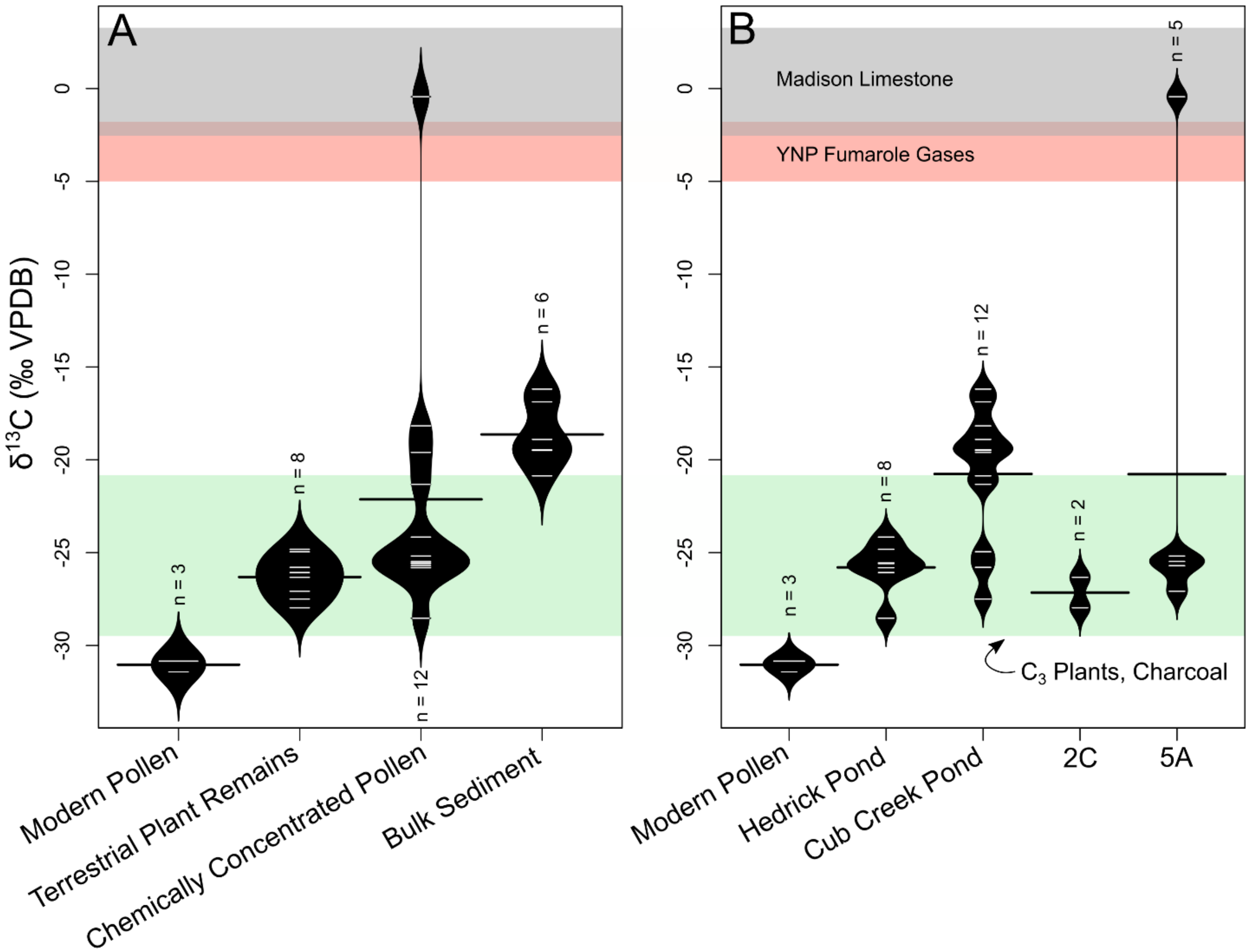

Figure 2.5: $\delta^{13}C$ values of radiocarbon materials are plotted using beanplot (Kampstra 2008) by material (A) and by site (B). C_3 plant and charcoal ranges are given by Smith and Epstein (1971). n is the number of samples included in each distribution. Yellowstone National Park (YNP) fumarole gas range taken from Craig (1963) and Werner and Brantley (2003) with Mississippian Madison Limestone range taken from Friedman (1970). Data from Hedrick Pond and Cub Creek Pond from Lu et al. (2017). Chemically concentrated pollen has a wide range of $\delta^{13}C$ values and the majority of least negative values come from areas near hydrothermal areas (Cub Creek Pond and Yellowstone Lake).

no apparent spatial pattern (Figure 2.5). Cub Creek Pond samples had the least depleted values (average -20.8 ‰ VPDB), with slightly more depleted values from 5A/9A (average -20.8 ‰

VPDB), Hedrick Pond (located 60 km south of Yellowstone Lake, 43.754° N, 110.590° W, elev. 2055 m.a.s.l.; average -25.8 ‰ VPDB), and 2C/13A (average -27.2 ‰ VPDB).

Discussion

Comparison of radiocarbon ages from Yellowstone Lake

In Yellowstone Lake, ages from chemically concentrated pollen were systematically and erroneously old, compared with ages established from terrestrial plant remains, tephrochronology, or the date of the sediment-surface interface (Figure 2.4). Chemically concentrated pollen ages from core 2C/13A were systematically older than terrestrial plant remains ages by up to 4300 cal years and disagree with the established age of the Mazama ash (7682-7584 cal BP, 2σ range; Egan et al., 2015) by 2300 cal years. Ages from strata of known age corroborate this finding, as picked Pinaceae pollen ages offered an improvement on bulk-sediment ages, but resultant ages remained too old by 1900 to 4300 cal years. These results are consistent with previous efforts at dating bulk sediments from Yellowstone Lake (Figure 2.2; Table 2.1) and bulk sediment and pollen concentrates from Cub Creek Pond (Whitlock, 1993; Lu et al., 2017). Ages from living *Pinus contorta* pollen are virtually modern by comparison (in equilibrium with atmospheric CO_2).

Carbon source of Yellowstone terrestrial pollen

Previous studies (referenced below) have reported erroneously old pollen ages in sediment cores and attributed the introduction of old carbon to: (1) laboratory processes; (2) incomplete removal of non-pollen materials during concentration procedures; (3) reworked pollen; and/or (4) enrichment of old CO_2 in source material. The likelihood of these explanations is explored below.

First, accidental contamination is a major concern in laboratories that prepare samples for AMS radiocarbon dating. Most laboratories contain potential sources of old carbon including sodium bicarbonate ($NaHCO_3$) and petrochemicals. $NaHCO_3$ is found in most pollen preparation fume hoods to neutralize surfaces exposed to caustic acids; however, it was not actively used in the fume hood during these analyses and would have been removed through subsequent acidification. Petrochemicals were not used as reagents in the pollen preparation laboratory. Definitively, additional studies that used the same pollen preparation environment and procedure have not reported difficulty with old ages from chemically concentrated pollen (Krause and Whitlock, 2013; Krause et al., 2015; Nanavati et al., 2019), making systematic laboratory contamination from old carbon or fractionation unlikely sources of error.

Second, old-carbon contamination from incomplete removal of non-pollen materials is commonly cited as an issue in procedures for concentrating pollen (Regnéll, 1992; Richardson and Hall, 1994), and sedimentological sources of old carbon exist in the vicinity. The Mississippian Madison Limestone, which is exposed in northern Yellowstone National Park outside the Caldera, produces near-zero $\delta^{13}C$ values (Figure 2.5; Friedman, 1970), but does not crop out near or upstream of Yellowstone Lake nor does any other significant carbonate formation (U.S. Geological Survey, 1972). Moreover, lake waters are relatively depleted in dissolved carbonate (<0.8 mM ΣCO_2, Balistrieri et al., 2007). The lake sediments from Yellowstone Lake themselves are not reported to contain carbonate mud (e.g. Tiller, 1995), contain < 1 wt% CaO (Shanks et al., 2007), and do not effervesce when submerged in hot 2.7N

HCl. Also, acidification treatments would remove most carbonates. Although our samples had no bituminous odor, we acknowledge that thermogenic hydrocarbons are found in several subaerial thermal areas of Yellowstone National Park (Love and Good, 1970; Clifton et al., 1990) and probably occur in hydrothermally altered sediments of Yellowstone Lake (Shanks et al., 2007). Core 2C/13A is not located near known hydrothermal vents (Figure 2.1); however, hydrocarbon contamination remains possible in core 5A/9A. Importantly, pollen ages remained erroneously old (with the exception of OS-142221) regardless of increasingly thorough concentration procedures through Schulze treatment and manual picking. Although chemically concentrated pollen ages were unilaterally more accurate than bulk-sediment ages, suggesting concentration procedures removed some old carbon, the calibrated ages of chemically concentrated and picked pollen were similar. The manually picked pollen probably produces the purest pollen sample currently possible, so erroneous ages in these samples probably reflect the age of the pollen grains with minimal sediment contaminants. Examination of picked pollen concentrates under a transmitted light microscope at 400× magnification confirmed the general absence of sediment contaminants. Remaining contaminant particles would have been too small to be detected under the stereomicroscope and insoluble in our chemical treatments.

Third, reworked pollen is suggested as a major source of old-carbon contamination in lacustrine settings where extensive old lacustrine deposits occur at the surface (Mensing and Southon, 1999; Zimmerman et al., 2019) or redeposition occurs from glacial melt (Neulieb et al., 2013; Zhang et al., 2017). There is no evidence of a Holocene glacial meltwater source in the Yellowstone Lake watershed. Given the size of the Yellowstone Lake depositional basin and the preponderance of pollen types that are produced in great abundance and distributed widely (e.g.

Pinus, *Artemisia*), a hypothetical ancient pollen source would need to be very large. Most unconsolidated surficial sediments were removed from the basin during repeated glacial episodes (Licciardi and Pierce, 2018). Remaining exposures of ancient lake sediments occur upstream (Baker, 1986) and downstream (Love et al., 2007), but are patchy and very small. Ancient shoreline facies also occur north of Yellowstone Lake (Pierce et al., 2007), but are situated upstream of the lake, probably too small to be the source area, and the coarse gravels and shallow-water depositional environments are not a good pollen preservation environment. Furthermore, pollen grains subjected to reworking should be observably broken and degraded under the light microscope (Tweddle and Edwards, 2010; Howarth et al., 2013), but pollen preservation was generally excellent in Yellowstone Lake as we observed that <1% of the pollen grains were unidentifiable and >50% of *Pinus* pollen had intact, distal membranes that allowed assignment to the subgeneric level under 400× magnification. Finally, dated terrestrial plant remains were clearly not out-of-sequence, and Holocene pollen spectra, dominated throughout core 2C by *Pinus* (>55%, <79%), are consistent with data from nearby sites within *Pinus contorta* forest (e.g. Baker, 1976; Whitlock, 1993; Whitlock et al., 1995; Theriot et al., 2006), further evidence against a significant component of reworked pollen.

Fourth, CO_2 vented from the Yellowstone Caldera is a somewhat unique source of old carbon in this region. Yellowstone Lake vents comprise a very active thermal area and account for an estimated 10% of the thermal water flux in Yellowstone National Park (Balistrieri et al., 2007); in addition, a small, subaerial thermal area exists ~1.5 km ESE of Cub Creek Pond (Vaughan et al., 2014). These areas potentially constitute a large source of old-carbon flux, although no estimates exist for the hydrothermal carbon budget of Yellowstone Lake, and the

Cub Creek Thermal Area is of unknown chemistry and considered potentially inactive (Vaughan et al., 2014). $\delta^{13}C$ values of pollen from Yellowstone Lake and nearby Cub Creek Pond (Lu et al., 2017) suggest an admixture of sources with less depleted $\delta^{13}C$ values than are typical for C_3 plants (Figure 2.5). Locally, fumarole gases produce the opposite end member of this admixture (Craig, 1963; Werner and Brantley, 2003). Large volumes of CO_2 are degassed from magmatic and pre-Tertiary basement sources at present, with daily, caldera-wide degassing estimated at 45 (± 16) kt primarily from acid-sulfate hydrothermal features (Werner and Brantley, 2003). Uptake of volcanically derived old CO_2 has been inferred elsewhere. For example, lake-sediment cores from volcanic lakes in Anatolia with bulk-sediment ages document reservoir effects of up to 14,000 years (Roberts et al., 2001; Jones, 2004). In other settings, uptake of old CO_2 through photosynthesis has been inferred in living plant tissue at sites near hydrothermal vents (Pasquier-Cardin et al., 1999; Cook et al., 2001; Evans et al., 2010; Lewicki and Hilley, 2014) and industrial areas (Baydoun et al., 2015), but generally do not occur more than 1 km away from the old-carbon source (Pasquier-Cardin et al., 1999; Evans et al., 2010; Baydoun et al., 2015). This observation is consistent with dates from modern pollen near Yellowstone Lake (Figure 2.4), which suggest minimal uptake of volcanic CO_2 through photosynthesis.

Potential sources for old-carbon contamination are narrowed by the fact that cone pollen collected in 2018 has the same $F^{14}C$ as the atmosphere and picked pollen from core tops is erroneously old. This limits the potential place of contamination to the water column or surficial lake sediments. However, it is unclear how hydrothermal carbon could be incorporated into pollen grains in either context, given that sporopollenins, which compose the chemically resistant coating of the pollen exine (outer wall), are “...probably the most resistant organic materials of direct biological origin found in nature...” (Brooks and Shaw, 1978). This hypothesis also is unsatisfactory given that old-carbon contamination of organic compounds by hydrothermal carbon apparently did not impact other terrestrial plant remains in the sediments.

Conclusions

Pollen concentrate ages are systematically older than terrestrial plant remains ages in Yellowstone Lake by 1700 to 4300 cal years and we can offer no clear explanation for this puzzlement. The most likely sources of old carbon are (1) CO_2 degassing from magmatic and pre-Tertiary basement sources, which may be incorporated into pollen grains in the water column or in surficial sediments; or (2) reworked pollen from older sediments. Neither explanation is fully adequate. In our consideration, further study of the radiocarbon signature of modern pollen from its production to its release, transport, deposition, and final burial in lake sediments is required to locate the source of old-carbon contamination. Such an investigation should include radiocarbon dating of modern pollen from the cone, pollen intercepted from the local atmosphere, pollen in the water column and carbon isotope analysis of the DOC in lake water. Experiments also may be employed in the laboratory to explore the possibility of incorporation of old carbon from artificially sourced CO_2 into pollen grains in an aqueous mixture. Future experiments also may examine the impact of individual steps in pollen concentration procedures for carbon contamination, obtain ^{14}C-free pollen concentrates as a more representative blank material, and utilize SEM microscopy to detect remaining contaminants associated with pollen grains.

With the current problem of old radiocarbon ages from pollen concentrates and the lack of other suitable materials for radiocarbon dating, we continue to be limited in our ability to produce quality age control for paleoenvironmental and geological reconstructions from Yellowstone Lake, Cub Creek Pond, and potentially other sites in the Yellowstone Caldera (e.g. Lewis Lake, glacial Yellowstone Lake). Current results underscore the necessity of careful consideration of carbon source—even in terrestrial plant remains and pollen concentrates—where reworked sediments or old-carbon degassing are possible.

Acknowledgements

This research was supported by NSF Grant No. 1515353 to C. Whitlock and sampling in Yellowstone National Park was conducted under permits YELL-SCI-0009 and YELL-SCI-5054. Coring efforts at Yellowstone Lake were aided by M. Baker, S.R. Brown, D. Conley, S.C. Fritz, C. Linder, L.A. Morgan, R. O'Grady, W.C. Shanks III, M.D. Shapley, R.A. Sohn, and three anonymous Yellowstone National Park rangers. This project was greatly improved through conversations with J. Southon and S.R.H. Zimmerman and thoughtful reviews of the manuscript came from D. McWethy, L.A. Morgan, D.A. Orme, and W.C. Shanks III.

Table 2.1: Yellowstone Lake and vicinity age controls

Accession No.[1] (Receipt No.)	Core Depth (cm)[2]/ Location	Material Dated[3]	C (µg)	$\delta^{13}C$ ‰ VPDB	Age ^{14}C	$F^{14}C$[4]	2σ cal BP age range (probability)[5]	Source[6]
FD-2								
C-5753	24.0	t. plant remains			430 ± 70	0.9479 ± 0.0082	307-552 (0.998), 614-616 (0.002)	Tiller 1995
C-5755	123.5	t. plant remains			1450 ± 100	0.8348 ± 0.0103	1179-1558 (1.000)	Tiller 1995
C-10034	225.5	humic acid			6060 ± 60	0.4703 ± 0.0035	6750-6767 (0.016), 6774-7030 (0.879), 7043-7070 (0.022), 7077-7086 (0.008), 7097-7156 (0.074)	This work
C-10035	225.5	humin			6030 ± 60	0.4721 ± 0.0035	6698-6700 (0.001), 6719-7022 (0.977), 7120-7152 (0.022)	This work
C-10048	295.5	t. plant remains			7950 ± 180	0.3717 ± 0.0082	8408-9289 (1.000)	Tiller 1995
C-10037	295.5	humic acid			7740 ± 60	0.3815 ± 0.0028	8410-8609 (0.991), 8618-8626 (0.009)	This work
C-10036	295.5	humin			7680 ± 60	0.3844 ± 0.0029	8389-8581 (1.000)	This work
C-5754	455.3	t. plant remains			9080 ± 100	0.3230 ± 0.0040	9915-10098 (0.149), 10110-10511 (0.851)	Tiller 1995
C-10039	475.5	humic acid			10460 ± 80	0.2720 ± 0.0027	12064-12596 (1.000)	This work
C-10040	475.5	humin			10280 ± 60	0.2781 ± 0.0021	11815-12244 (0.885), 12266-12383 (0.115)	This work
C-4977	476.6	t. plant remains			6290 ± 80	0.4570 ± 0.0045	7615-7879 (0.924), 7890-7931 (0.076)	Tiller 1995
C-10038	505.5	t. plant remains			7100 ± 210	0.4132 ± 0.0107	7580-8340 (1.000)	Tiller 1995
C-10047	505.5	t. plant remains			7060 ± 100	0.4152 ± 0.0051	7673-8051 (0.996), 8098-8102 (0.001), 8144-8149 (0.003)	Tiller 1995
C-9165	505.5	humic acid			11380 ± 80	0.2425 ± 0.0024	13079-13386 (1.000)	This work
C-9164	505.5	humin			10280 ± 90	0.2781 ± 0.0031	11651-11662 (0.003), 11705-12418 (0.997)	This work
	506.5	Mazama ash					7584-7682	Egan et al. 2015
C-4976	582.7	t. plant remains			8290 ± 120	0.3563 ± 0.0053	9010-9503 (0.997), 9511-9516 (0.003)	Tiller 1995
C-10042	582.5	humic acid			12350 ± 80	0.2149 ± 0.0021	14067-14830 (1.000)	This work
C-10041	582.5	humin			12050 ± 70	0.2231 ± 0.0019	13748-14088 (1.000)	This work
C-4974	657.0	t. plant remains			10200 ± 90	0.2809 ± 0.0031	11404-11568 (0.067), 11573-11576 (0.001), 11591-12189 (0.901), 12199-12237 (0.015), 12283-12301 (0.006), 12343-12376 (0.012)	Tiller 1995
C-4973	735.1	t. plant remains			10280 ± 80	0.2781 ± 0.0028	11757-12401 (1.000)	Tiller 1995

C-10044	766.5	humic acid			16850 ± 60	0.1228 ± 0.0009	20105-20523 (1.000)	This work
C-10043	766.5	humin			17090 ± 150	0.1191 ± 0.0022	20202-21013 (1.000)	This work
C-10046	778.3	humic acid			18240 ± 100	0.1032 ± 0.0013	21846-22366 (1.000)	This work
C-10045	778.3	humin			17950 ± 100	0.1070 ± 0.0013	21432-22027 (1.000)	This work
C-9162	854.0	humic acid			16420 ± 180	0.1295 ± 0.0029	19359-20279 (1.000)	This work
C-9163	854.0	humin			18900 ± 250	0.0951 ± 0.0029	22309-23445 (1.000)	This work
	855.0	Glacier Peak (B or G) ash					13410-13710 (1.000)	Kuehn et al. 2009
13A								
	0	core top					-67	
OS-142012 (153942)	1.0	bulk sediment	1559		5250 ± 25	0.5203 ± 0.0017	5928-6026 (0.729), 6047-6065 (0.029), 6077-6116 (0.160), 6152-6175 (0.082)	This work
OS-142223 (153938)	1.0	picked pollen	22		2310 ± 180	0.7505 ± 0.0164	1904-1907 (0.001), 1924-2755 (0.999)	This work
	12.0	1700 CE fire					240-260	Romme & Despain, 1989
2C								
OS-138757 (149875)	164.0	c.c. pollen	476		3860 ± 20	0.6185 ± 0.0016	4163-4166 (0.006), 4181-4198 (0.047), 4230-4407 (0.948)	This work
OS-135957 (147265)	328.0	t. plant remains	670	-26.3	2590 ± 20	0.7242 ± 0.0019	2723-2754 (1.000)	This work
OS-135958 (147266)	402.0	t. plant remains	1130	-28.0	3150 ± 25	0.6760 ± 0.0022	3272-3285 (0.038), 3339-3445 (0.962)	This work
OS-138692 (149876)	524.5	c.c. pollen	440		6280 ± 30	0.4574 ± 0.0017	7164-7263 (1.000)	This work
OS-136956 (147971)	624.0	t. plant remains	643		4510 ± 20	0.5707 ± 0.0016	5053-5190 (0.688), 5213-5296 (0.312)	This work
OS-142084 (153943)	755.0	t. plant remains	148	-10.9	9980 ± 45	0.2887 ± 0.0017	11259-11623 (0.985), 11675-11694 (0.015)	This work
OS-138693 (149877)	792.0	c.c. pollen	307		7220 ± 35	0.4068 ± 0.0018	7963-8072 (0.764), 8085-8158 (0.236)	This work
OS-142082 (153939)	934.5	bulk sediment	461		11150 ± 55	0.2497 ± 0.0016	12841-13112 (1.000)	This work
OS-142018 (153935)	934.5	picked pollen	58		10250 ± 170	0.2793 ± 0.0059	11348-11380 (0.011), 11386-12540 (0.989)	This work
	940.0	Mazama ash					7584-7682	Egan et al., 2015
OS-138622 (149869)	965.5	t. plant remains	190		5740 ± 30	0.4895 ± 0.0019	6453-6459 (0.012), 6462-6634 (0.988)	This work
OS-138700 (149878)	978.0	c.c. pollen	569		9870 ± 55	0.2928 ± 0.0019	11188-11405 (0.982), 11457-11465 (0.004), 11563-11593 (0.014)	This work
OS-138701 (149879)	986.0	c.c. pollen	248		9390 ± 50	0.3106 ± 0.0019	10500-10741 (1.000)	This work

OS-138866 (149880)	1160.5	c.c. pollen	545		12100 ± 110	0.2215 ± 0.0031	13639-13663 (0.004), 13707-14303 (0.996)	This work
9A								
	0	core top					-67	
OS-142011 (153941)	1.0	bulk sediment	2051		4080 ± 25	0.6017 ± 0.0019	4447-4470 (0.060), 4516-4644 (0.770), 4677-4692 (0.017), 4761-4800 (0.153)	This work
OS-142222 (153937)	1.0	picked pollen	34		1910 ± 110	0.7885 ± 0.0109	1571-1583 (0.006), 1598-2120 (0.994)	This work
5A								
OS-135959 (147267)	364.5	t. plant remains	730	-27.1	3760 ± 30	0.6261 ± 0.0022	3993-4039 (0.127), 4074-4184 (0.727), 4188-4192 (0.007), 4195-4235 (0.139)	This work
OS-138998 (149881)	533.5	c.c. pollen	202	-0.4	6140 ± 95	0.4654 ± 0.0054	6792-7254 (1.000)	This work
OS-138868 (149882)	540.5	c.c. pollen	411		6600 ± 45	0.4395 ± 0.0024	7433-7566 (1.000)	This work
OS-142083 (153940)	782.0	bulk sediment	405		11050 ± 50	0.2524 ± 0.0016	12779-13057 (1.000)	This work
OS-142221 (153936)	782.0	picked pollen	43		5530 ± 130	0.5021 ± 0.0083	5999-6568 (0.977), 6586-6627 (0.023)	This work
	783.0	Mazama ash					7584-7682	Egan et al., 2015
OS-139001 (149883)	814.0	c.c. pollen	243	-25.5	9060 ± 50	0.3236 ± 0.0021	10157-10299 (0.975), 10320-10343 (0.012), 10352-10374 (0.013)	This work
OS-139002 (149884)	823.5	c.c. pollen	303	-25.2	9100 ± 55	0.3222 ± 0.0021	10184-10409 (1.000)	This work
OS-138869 (149885)	837.0	c.c. pollen	413		9340 ± 70	0.3126 ± 0.0027	10297-10357 (0.047), 10369-10723 (0.953)	This work
OS-139116 (149886)	941.5	c.c. pollen	390	-25.7	9020 ± 50	0.3254 ± 0.0021	9936-9992 (0.070), 10008-10030 (0.017), 10035-10062 (0.027), 10128-10255 (0.886)	This work
Modern Pollen								
OS-149977 (160235)	Riddle Lk. TrlHd.	modern pollen	247	-30.8	80 ± 15	0.9903 ± 0.0019	-5 (0.003), 33-74 (0.556), 79-81 (0.004), 98-107 (0.023), 113-136 (0.170), 224-254 (0.243)	This work
OS-149978 (160236)	Cub Creek Pond	modern pollen	343	-31.4	50 ± 20	0.9940 ± 0.0022	-5 (0.024), 35-70 (0.835), 117-131 (0.056), 231-244 (0.081), 248-250 (0.004)	This work
OS-149979 (160237)	Mud Volcano	modern pollen	268	-30.8	170 ± 20	0.9790 ± 0.0025	-5-31 (0.214), 138-158 (0.111), 164-222 (0.492), 258-285 (0.182)	This work

[1] C-## (Chicago), OS-## (National Ocean Sciences Acceleratory Mass Spectrometry)
[2] Depths reported are tops of 1-cm intervals from which samples were collected
[3] c.c. pollen (chemically concentrated pollen), t. plant remains (terrestrial plant remains)

[4] FD-2 $F^{14}C$ back-calculated from measured ^{14}C age according to method of Reimer et al. (2004)
[5] Calibrated ranges calculated by CALIB and CALIBomb according to method described in text, parenthetical values relative area under probability distribution
[6] Source listed for lithological context (FD-2) or calendar age of event

Table 2.2: Summary of normalized[1] geochemical data from Yellowstone Lake Mazama ash samples compared with UA2832 of Jensen and Beaudoin (2016)

Sample	n[2]	P_2O_5	SiO_2	SO_2	TiO_2	Al_2O_3	MgO	CaO	MnO	FeO[3]	Na_2O	K_2O	F	Cl	Total	Analytical Total
2C	9	**0.07**	**72.77**	**0.01**	**0.45**	**14.22**	**0.43**	**1.64**	**0.05**	**2.00**	**5.25**	**2.84**	**0.10**	**0.17**	**100**	**99.09**
σ		*0.03*	*0.08*	*0.01*	*0.03*	*0.06*	*0.03*	*0.04*	*0.02*	*0.04*	*0.08*	*0.04*	*0.01*	*0.01*		*1.35*
5A	12	**0.06**	**72.78**	**0.02**	**0.42**	**14.20**	**0.43**	**1.64**	**0.06**	**2.03**	**5.28**	**2.79**	**0.11**	**0.19**	**100**	**97.33**
σ		*0.03*	*0.15*	*0.01*	*0.04*	*0.10*	*0.03*	*0.06*	*0.02*	*0.06*	*0.18*	*0.07*	*0.01*	*0.04*		*1.32*
FD-2	**9**	**0.08**	**72.87**	**0.01**	**0.41**	**14.25**	**0.42**	**1.62**	**0.05**	**1.99**	**5.24**	**2.77**	**0.11**	**0.19**		**97.56**
σ		*0.03*	*0.21*	*0.01*	*0.04*	*0.08*	*0.03*	*0.05*	*0.01*	*0.06*	*0.12*	*0.05*	*0.03*	*0.07*		*2.63*
UA2832	**21**		**72.84**		**0.44**	**14.73**	**0.47**	**1.64**	**0.05**	**2.01**	**4.88**	**2.77**		**0.18**	**100**	**96.97**
σ			*0.93*		*0.07*	*0.34*	*0.11*	*0.25*	*0.02*	*0.28*	*0.16*	*0.16*		*0.03*		

[1] Data has been normalized to 100% and the analytical total are presented for each sample. Oxidized reported as wt. %. Glass shards were analyzed on a Cameca SX100 with four WDS spectrometers an accelerating voltage of 15 kV and a probe current of 10 nA and a beam diameter of 20 microns were used. Count times = 20s except S = 30s, Cl = 40 and F = 60. Analytical precision from microprobe analyses is calculated by the standard deviation of replicate analyses of secondary standard VG568, are as follows (in wt.%): P_2O_5 ± 0.01, SiO_2 ± 0.23, SO_2 ± 0.01, TiO_2 ± 0.02, Al_2O_3 ± 0.08, MgO ± 0.01, CaO ± 0.01, MnO ± 0.02, FeO ± 0.06, Na_2O ± 0.23, K_2O ± 0.06, F ± 0.08, Cl ± 0.01.

[2] Number of analyses

[3] FeO total

CHAPTER THREE

MULTI-PROXY RECORD OF HOLOCENE PALEOENVIRONMENTAL CONDITIONS FROM YELLOWSTONE LAKE, WYOMING, USA

<u>Contribution of Authors and Co-Authors</u>

Manuscript in Chapter 3

Author: Christopher M. Schiller

Contribution: Participated in field work, conducted radiocarbon, pollen, and charcoal analyses, and contributed to the manuscript.

Co-Author: Rosine Cartier

Contribution: Conducted oxygen isotope analyses of diatoms and contributed to the manuscript.

Co-Author: Cathy Whitlock

Contribution: Provided funding and helped conceptualize and develop the manuscript.

Co-Author: Lisa A. Morgan

Contribution: Led lithological descriptions, advised on lithological interpretations, and contributed to the manuscript.

Manuscript Information

Christopher M. Schiller, Rosine Cartier, Cathy Whitlock, Lisa A. Morgan

Quaternary Science Reviews

Status of Manuscript:
__×__ Prepared for submission to a peer-reviewed journal
_____ Officially submitted to a peer-reviewed journal
_____ Accepted by a peer-reviewed journal
_____ Published in a peer-reviewed journal

Elsevier

CHAPTER THREE

MULTI-PROXY RECORD OF HOLOCENE PALEOENVIRONMENTAL CONDITIONS FROM YELLOWSTONE LAKE, WYOMING, USA

Abstract

Postglacial terrestrial and limnologic processes on the Yellowstone Plateau are strongly influenced by insolation-driven climate change. Relatively few studies have explored these impacts in central Yellowstone where widespread hydrothermal activity also may affect ecosystem development. We examined an 1174 cm-long Holocene (9876− -67 cal yr BP) sediment core from northern Yellowstone Lake to investigate regional paleoenvironmental evolution. Pollen, charcoal, and oxygen isotopes from diatom frustules were examined to explore past climate changes and their influence on ecosystem structure and function, as well as the impact of geologic forcing such as sub-lacustrine hydrothermal venting and hydrothermal explosions. The long-term, regional trends recorded in terrestrial proxy data for the last ~9880 years are consistent with decreasing summer insolation throughout the Holocene and a progressive change towards wetter and cooler conditions. This new multiproxy record from Yellowstone Lake matches other paleoecological records from the Yellowstone Plateau and highlights the close relationship between climate, hydrology, and ecological changes.

Introduction

Yellowstone Lake (44°30′N, 110°20′W; 2350 m elevation; Figure 3.1), in central Yellowstone National Park, is the largest alpine lake in North America (341 km^2, maximum depth ~131 m, Morgan et al., 2003). Located in the eastern part of the Yellowstone Plateau, the lake basin may date to the eruption of the Lava Creek Tuff *ca.* 631 ka (Christiansen, 2001; Matthews et al., 2015) and the margin of the Yellowstone Caldera crosses the southern portion of the lake and coincides with parts of the eastern shore of the lake (Morgan et al., 2007). Most of the lake floor is underlain by post-caldera rhyolite flows capped by glacial till and lake sediments representing as much as 200 ka of sedimentation (Otis et al., 1977; Johnson et al., 2003). A large glacier complex covered the watershed of Yellowstone Lake in late-Pinedale time until ca. 14 ka (Licciardi and Pierce, 2018). Basin morphology is the result of a combination of these factors, with dominantly volcanic controls to the north, including the 150 ka West Thumb Caldera, and glacial and fluvial controls evident to the south, including a paleo-canyon evident in the southeast arm, filled with lake sediment (Otis et al., 1977; Christiansen, 2001; Morgan et al., 2007). The lake has been influenced by an active hydrothermal system in the northern and West Thumb portions of the lake evidenced by heat flow studies (Morgan et al., 1977; Smith et al., 2009), with diverse hydrothermal features including active hydrothermal vent fields and large hydrothermal explosion craters and domes (Morgan et al., 2007, 2009). Yellowstone Lake sediments were examined in a previous paleoecological study (Theriot et al., 2006), including pollen and diatom analyses that provided environmental context for understanding the Holocene evolution of the endemic diatom *Stephanodiscus yellowstonensis*.

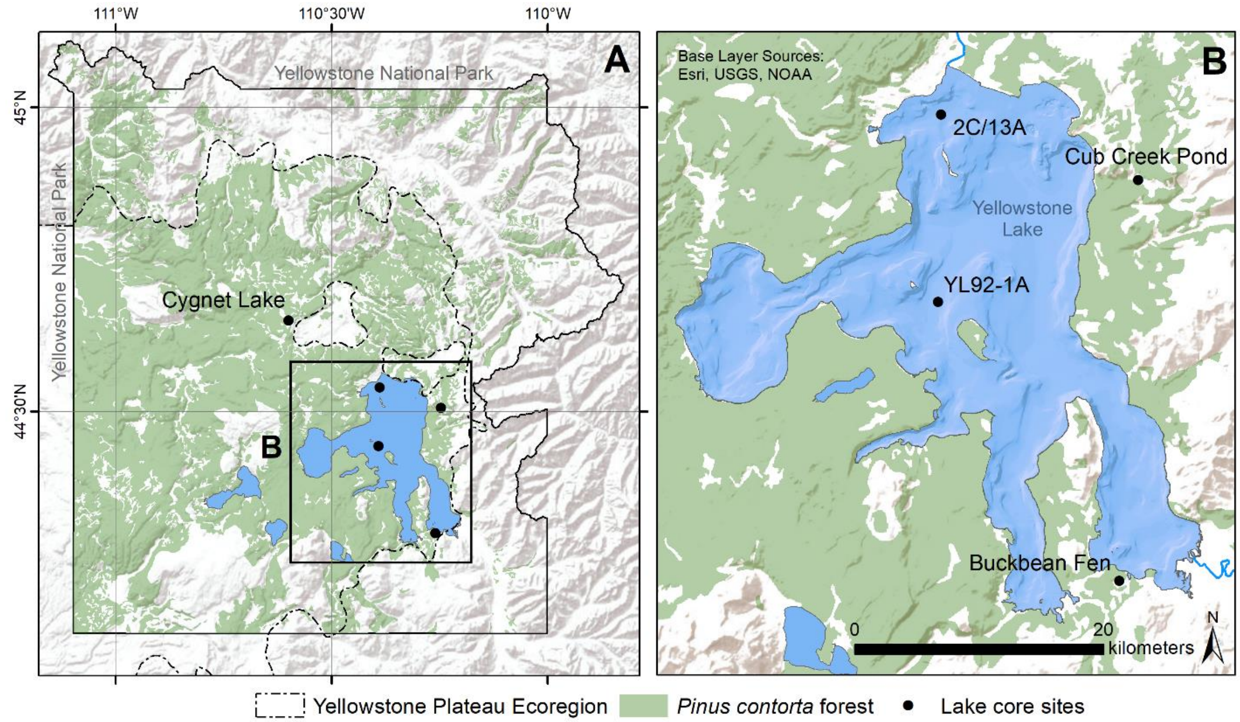

Figure 3.1: (A) Lake core sites in the Yellowstone Lake vicinity, Cygnet Lake (Whitlock, 1993), Cub Creek Pond (Waddington and Wright, 1974), and Buckbean Fen (Baker, 1976). (B) Core sites within Yellowstone Lake, FD-2 (Theriot et al., 2006) and 2C/13A (this study) are plotted with shaded bathymetry (Morgan et al., 2007b) and *Pinus contorta* forest extent (Despain, 1990).

The integration of new proxy data here allows for a more comprehensive understanding of paleoenvironmental conditions, such as past vegetation, fire, and lake hydrology.

The objective of this study is to better understand the Holocene hydroclimate, vegetation, and fire history of the Yellowstone Lake watershed and the role of past hydrothermal activity in shaping ecosystem dynamics. This chapter describes the analysis of a sediment core taken from the northern basin of Yellowstone Lake and its comparison with records from smaller lakes from and near the Yellowstone Lake watershed. We examined pollen, charcoal, and oxygen isotope composition of diatom frustules ($\delta^{18}O_{diatom}$) to answer the following questions: (1) What was the vegetation and fire response to changes in Holocene climate in the Yellowstone Lake watershed? (2) What was the influence of hydrothermal activity on Holocene-scale vegetation development?

Site description

Yellowstone Lake is located 600 km east of the Pacific Ocean and has a continental subarctic climate regime, under the influence of Arctic and Pacific air masses and, to a lesser degree, by warm, moist air originating from the Gulf of Mexico and subtropical Pacific during summer (Despain, 1987). Mean temperatures range from 13.7 (July) to -10.7 (January; 30-year normal, Arguez et al., 2010). The majority of winter precipitation is received from winter storm tracks funnelled through the low-elevation Snake River Plain (Bryson and Hare, 1974). Summers are relatively dry as a result of offshore subsidence produced by the northeastern Pacific subtropical high-pressure system and seasonal migration of the jet stream to higher latitudes (Mock, 1996), hence the term "summer-dry" (Whitlock and Bartlein, 1993). Nonetheless, spring and summer convective storms from the subtropical Pacific produce a precipitation balance that is somewhat equally distributed through the year. Precipitation ranges from 62.74 (May) to 29.97 mm (October, 30-year normals; Arguez et al., 2010).

The vegetation of the Yellowstone Lake watershed is controlled by a combination of soil characteristics and elevation. Most of the Yellowstone Plateau, to the north and west of Yellowstone Lake, is underlain by rhyolitic substrates which produce well-drained, nutrient-poor soils. As a result, the vegetation is dominated by dense *Pinus contorta* forest (Despain, 1990). On soils derived from andesite or sedimentary substrate to the south and east of Yellowstone Lake, vegetation consists of mixed conifer (*Abies lasiocarpa-Picea engelmannii-Pinus contorta* or *Pinus albicaulis*) forest (Despain, 1990). Steppe communities in Hayden and Pelican Valleys, underlain by proglacial lake sediments (Richmond, 1977), are dominated by *Artemisia* (*A. cana* and *A. tridentata*) (Despain, 1990). *Festuca idahoensis*, *Agropyron trachycaulum*, and a diverse suite of herbs grow in meadows in the andesitic Absaroka Range (Despain, 1990). Above ~2800 m elevation in the Absaroka Range, upper treeline is composed of *P. albicaulis* parkland or krummholz and, above ~2900 m elevation, is tundra (Despain, 1990). The fire regime of the subalpine forests is characterized by large, infrequent, and high-severity fires (Turner et al., 1994; Schoennagel et al., 2004). Charcoal data for the last two millennia suggest 2–5 fire episodes/1000 years at a *P. contorta* forest site (Millspaugh et al., 2000) and 6–13 fire episodes/1000 years at mixed conifer forest and parkland site just south of Yellowstone Lake (Whitlock et al., 2003). Two large fire episodes occurred in the Yellowstone Lake watershed, one in 1988 CE and in the decades from 1690 and 1710 CE (Romme and Despain, 1989).

Methods

A 1162 cm-long sediment core was retrieved with a Kullenberg sampler (Kelts et al., 1986) from 61 m water depth in northern Yellowstone Lake in September 2016 (44°32′21.37″N, 110°20′21.19″W; Figure 3.1; core YLAKE-YL16-2C-1K, hereafter 2C). An additional 54-cm-long core was recovered with a gravity corer in 2017, approximately 30 m from the 2C site (44°32′22.27″N, 110°23′21.08″W; Figure 3.1; core YLAKE-YL17-13A-1G, hereafter 13A), to recover the sediment-water interface. Cores were shipped to the LacCore facility at the University of Minnesota–Twin Cities for initial core description, subsampling, scanning for physical properties, and XRF geochemistry, and archiving. Initial core description included core splitting, scanning, and high-resolution photography. Kullenberg and gravity cores were correlated based on their charcoal stratigraphy (see *Charcoal results*). References to depth hereafter refer to depth in the 1174-cm-long 13A/2C composite core. For context, the lithological work of Morgan et al. (2019) will be described.

Age-depth model

Terrestrial plant remains were collected for accelerator mass spectrometry (AMS) radiocarbon dating. In addition, bulk sediment and pollen concentrates were collected for AMS dating, but most age determinations were rejected as erroneously old, probably as a result of contamination from reworked pollen or dead carbon from degassed magmatic or pre-Tertiary basement sources (Chapter 2). Additional age controls included the sediment-water interface from the gravity core (13A), a prominent charcoal peak attributed to a major fire episode *ca*. 1700 CE (Romme and Despain, 1989), and the 0.5-cm-thick Mazama ash identified chemically with electron microprobe analysis (Chapter 2). An additional siliciclastic unit was a thin (7 cm) hydrothermal explosion deposit (Morgan et al., 2019) in 2C and, relative to the uncertainty of the age-depth model, neither the ash or the explosion deposit were thick enough to remove from the composite depth in developing the age model. Radiometric ages determinations were converted to calendar ages with the IntCal13 calibration curve (Reimer et al., 2013) and modelled against depth using the software package Bacon (Blaauw and Christen, 2011) with the remaining six age controls. *A priori* assignment of mean sediment accumulation rate was set to 10 yr/cm, as suggested by Bacon and closely matching our data, but this rate is somewhat faster than Holocene sediment accumulation rates estimated for other cores from Yellowstone Lake (~15 yr/cm, Tiller, 1995; 17-10 yr/cm, Johnson et al., 2003). Thickness for spline calculation was set at 20 cm, above which the model diverged greatly from the age controls provided.

Pollen

Subsamples of 1 cm^3 at 1- to 24-cm intervals were prepared for pollen analysis following standard procedures (Bennett and Willis, 2001). A known concentration of *Lycopodium* tracer was added to each sample to calculate pollen concentration (grains/cm^3) and influx (grains/cm^2/yr). Residues were preserved and mounted in silicone oil. At least 300 pollen grains were identified at a minimum magnification of 400× and resolved to the lowest taxonomic level possible with the reference collection at Montana State University and published atlases (Hedberg, 1946; Bassett et al., 1978; Moore et al., 1991; Kapp et al., 2000). *Pinus* was identified to the subgeneric level when the distal membrane was intact and visible. *Pinus* subgen. *Strobus* was ascribed to *P. albicaulis*, which grows in the watershed. *P. flexilis*, which is more common at low elevations in the GYE, also may have been a contributor. *Pinus* subgen. *Pinus* was ascribed to *P. contorta*, given that *P. ponderosa* does not natively grow in the Yellowstone region (Dorn, 2001; Lesica, 2012). Cupressaceae pollen was ascribed to *Juniperus*-type and may represent either *J. communis*, *J. scopulorum*, or *J. horizontalis*. Degraded, crumpled, or otherwise unidentifiable pollen grains were classified as “Indeterminate”, whereas grains that could not be confidently identified were classified as “Unknown.” Vegetation reconstructions for the pollen assemblages was aided by a study of modern pollen assemblages from different vegetation types in the Yellowstone region (Iglesias et al., 2018). Due to the large lake surface area and the inflow of the Yellowstone River, a large tributary river entering the Southeast Arm of Yellowstone Lake, the pollen source area is large and the pollen record describes vegetation history at a regional scale (Jacobson and Bradshaw, 1981; Sugita, 1993).

Charcoal

Continuous subsamples (~2 cm^3) were collected for charcoal analysis at 1-cm increments from the entire composite core, providing a high-resolution analysis of fire activity. Charcoal particles >125 µm in diameter were analyzed as this size fraction registers local fire episodes (Whitlock and Millspaugh, 1996). Subsamples were disaggregated in 5% $Na_6[(PO_3)_6]$, treated with 5–10 wt/vol% NaOCl, washed gently through a sieve, and then counted with a stereomicroscope (Whitlock and Larsen, 2001). High-resolution records of charcoal accumulation rates are often separated into two components, a long-term trend, which represents the sum of regional charcoal production, charcoal redeposition, and sediment mixing (Whitlock and Larsen, 2001), and peaks, which represent local fire episodes (Whitlock and Millspaugh, 1996; Higuera et al., 2011). To accomplish this, we utilized CharAnalysis software (Higuera et al., 2009) to calculate charcoal accumulation rates (CHAR, particles/cm^2/yr), using the median sediment accumulation rate. The CHAR record was then decomposed into background charcoal accumulation rates (BCHAR), which is the long-term trend in biomass burning, and peaks, which represent fire episodes (one or more fires during the time span). BCHAR was calculated with a 500-year moving average (which kept the local signal-to-noise ratio index above 3 for the entire record). Charcoal peaks were flagged as significant if they registered above the 99th percentile of the local noise distribution of CHAR as defined by a Gaussian mixture model. This percentile was tuned to capture known, extremely large fire episodes (see charcoal results). Fire-episode frequency was then calculated as an average number of peaks per 100 years and peak magnitude was used as a proxy of fire-episode size (i.e., total area burned).

<u>Oxygen and hydrogen isotopes from diatom frustules</u>

Subsamples (~2 cm^3) for diatom isotope analysis were collected at 8-cm intervals through the core. Samples were prepared for isotope analysis following several cleaning steps to remove contaminants (Morley et al., 2004). Finally, samples were cleaned in 0.05 M sodium pyrophosphate ($Na_4P_2O_7$) and sieved through a 25 µm mesh screen to isolate *Stephanodiscus yellowstonensis*, thereby reducing potential biases due to different species' vital effects (Swann et al., 2007). The purity of samples was checked using a scanning electron microscope. Oxygen isotope analysis was performed at the National Environmental Isotope Facility, British Geological Survey (UK), for samples with sufficient material (~6 mg cleaned sample), using step-wise fluorination (Leng and Sloane, 2008). Liberated oxygen was converted to CO_2 through reaction with heated graphite (Clayton and Mayeda, 1963). Oxygen yields were monitored by comparison with the calculated theoretical yield for SiO_2. Resultant CO_2 samples were run on a dual inlet mass spectrometer. Oxygen isotope ratios are reported in standard delta notation ($\delta^{18}O_{diatom}$) as per mil (‰) deviations of the isotopic ratio ($^{18}O/^{16}O$) calibrated to the VSMOW (Vienna Standard Mean Ocean Water) scale using a within-run laboratory standard (BFC) calibrated against NBS 28. Analytical reproducibility of BFC was <0.4 ‰ (1σ) and for sample material standard deviation ranged from 0.01 to 0.54 ‰ based on 21 replicates.

Water samples from tributaries (n=17) and the lake (n=6) were collected in summer 2018 to determine the major factors influencing δD and $\delta^{18}O$ in lake waters. Water was collected in 60 mL dark glass bottles, fully filled to avoid air bubbles and light. Oxygen isotope ($\delta^{18}O$) measurements were made using the CO_2 equilibration method. Deuterium isotope (δD) measurements were made using an online chromium reduction method (Morrison et al., 2001).

Isotope measurements used internal standards calibrated against the international standards VSMOW2 and VSLAP2. Errors (1 SD) are typically +/– 0.05‰ for $\delta^{18}O$ and +/–1.0‰ for δD.

Results

Lithology and age-depth model

The 1174-cm-long core consists of variously well-laminated diatomaceous ooze with frequent black, sulfidic layers (Morgan et al., 2019). The stratigraphic section contained two siliciclastic deposits: (1) At 984-977 cm depth, normally graded sediments are present and are interpreted as originating from a sublacustrine hydrothermal explosion (Morgan et al., 2019); (2) At 933.5 cm depth, a 0.5 cm thick deposit of ash is attributed to the climactic Mount Mazama eruption (Chapter 2) at 7631 cal yr BP (median modelled age, 7584–7682 cal yr BP 2σ range, Egan et al., 2015).

Unfortunately, the lack of suitable radiocarbon materials, the small size of many samples, and the unreliability of radiocarbon dates from bulk sediments and pollen concentrates prevented development of a robust age model for this core (Chapter 2). The age-depth model for the 2C/13A core (Figure 3.2) was constructed using a subset of three calibrated macrofossil radiocarbon ages, the Mazama ash (Egan et al., 2015), the sediment-water interface (core top), and a peak in charcoal correlated to widespread fire at ca. 1700 CE (Romme and Despain, 1989; Table 3.1). Although no suitable materials for dating were found at the base of the 2C/13A core, the model produced an extrapolated basal age of 9880 cal yr BP. *Pinus*-dominated pollen spectra at 1174 cm depth (9880 cal yr BP; see *Pollen and charcoal* results) are consistent with a Holocene age for the record (Whitlock, 1993; Iglesias et al., 2018). The average sediment accumulation rate for the core was calculated at 8.4 years/cm, or a sedimentation rate of 0.119

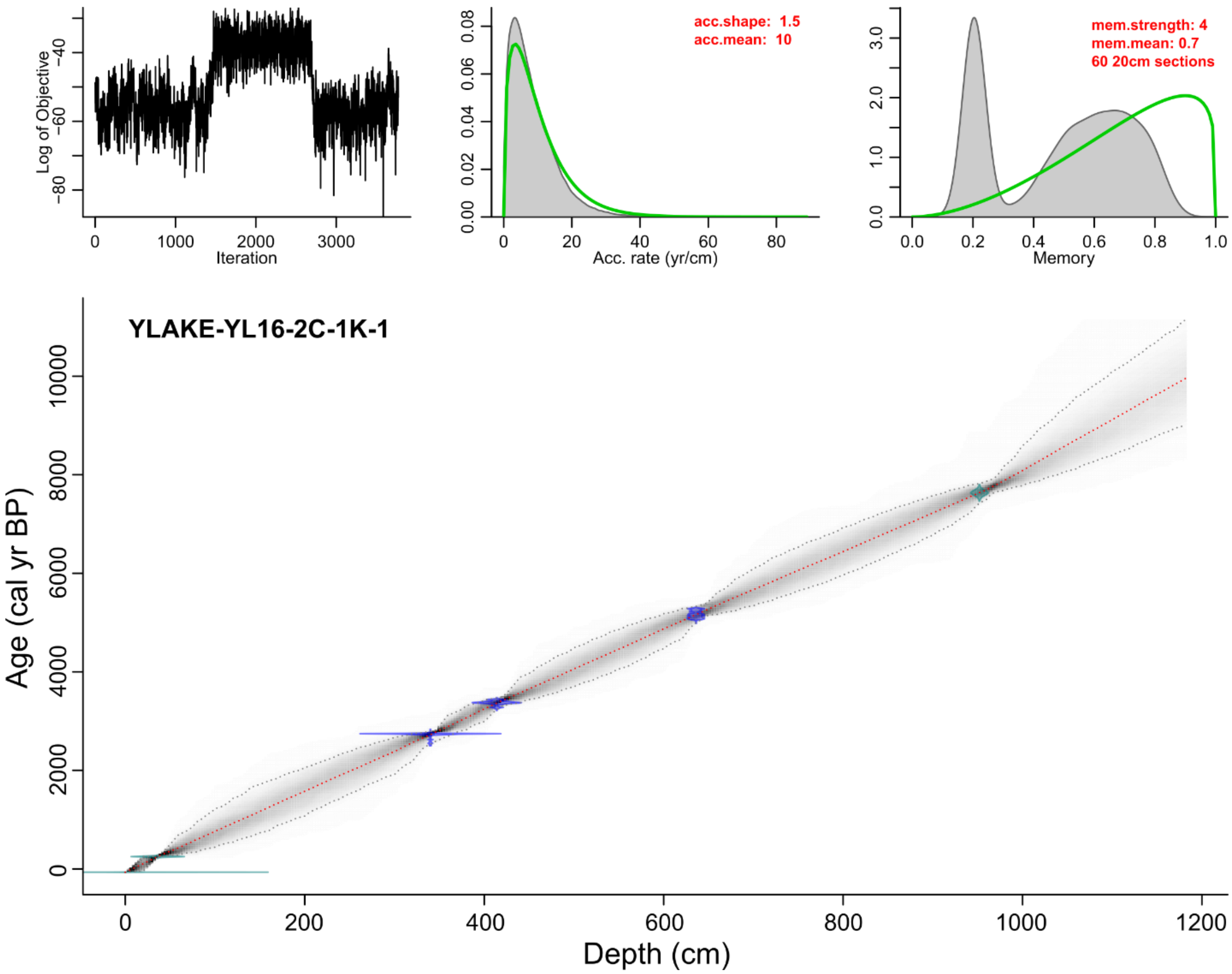

Figure 3.2: Age-depth model for the composite 2C/13A Yellowstone Lake core. Red line is the median probability age from all run age-depth iterations, representing the best point estimate of age for any given depth. Gray point cloud represents age model probability and contains a 95% confidence interval (dashed lines). Iteration history (left inset), prior and posterior densities of the mean accumulation rate (middle inset), and prior and posterior of the memory (right inset).

cm/year. The resultant model had wide error ranges for age estimates and also fails to capture likely sedimentation rate changes associated with Holocene episodes of graben movement documented in previous seismic surveys (Johnson et al., 2003).

Table 3.1. 2C/13A age controls

Accession No.	Core depth, cm (core)	Material dated	$\delta^{13}C$, ‰ VPDB	Age ^{14}C	2σ cal age range (probability)
	0 (13A)	core top			-67
	12.0 (13A/2C)	1700 CE fire			240-260[2]
OS-135957	328.0 (2C)	terrestrial plant fragment	-26.33	2590 ± 20	2723-2754 (1.000)
OS-135958	400.0 (2C)	wood	-27.97	3150 ± 25	3272-3285 (0.038), 3339-3445 (0.962)
OS-136956	621.5 (2C)	wood		4510 ± 20	5053-5190 (0.688), 5213-5296 (0.312)
OS-142084[1]	750.0 (2C)	aquatic plant fragment	-10.86	9980 ± 45	11259-11623 (0.985), 11675-11694 (0.015)
	933.5 (2C)	Mazama ash			7584-7682[3]
OS-138622[1]	964.0 (2C)	wood		5740 ± 30	6453-6459 (0.012), 6462-6634 (0.988)

[1]Age rejected by Bacon model
[2]Romme and Despain (1989)
[3]Egan et al. (2015)

Pollen and charcoal

Pollen and charcoal data in the 2C core were divided into two zones based on visual inspection of pollen spectra and CHAR (Figure 3.3):

Zone YL-P1 (1174–719 cm depth; 9880–5800 cal yr BP) was dominated by *Pinus* (55–77%), except immediately above the Mazama ash where *Pinus* values declined to 48%. Most identifiable *Pinus* grains were *P. contorta*-type, with low to moderate amounts of *P. albicaulis*-type (3-36% of *Pinus*). *Picea* (<5%), *Abies* (<3%), *Pseudotsuga* (<1%), *Juniperus*-type (<2%), and *Salix* (<2%) were present in small proportions. Shrub and herbaceous steppe taxa, including *Artemisia* (10–24%), Poaceae (1–4%), and Amaranthaceae (2–8%), constituted another major component, along with trace abundance of xerophytic pollen types (<1%), including *Sarcobatus* and *Ephedra viridis*-type. The xerophytic taxa do not grow locally, consistent with a significant

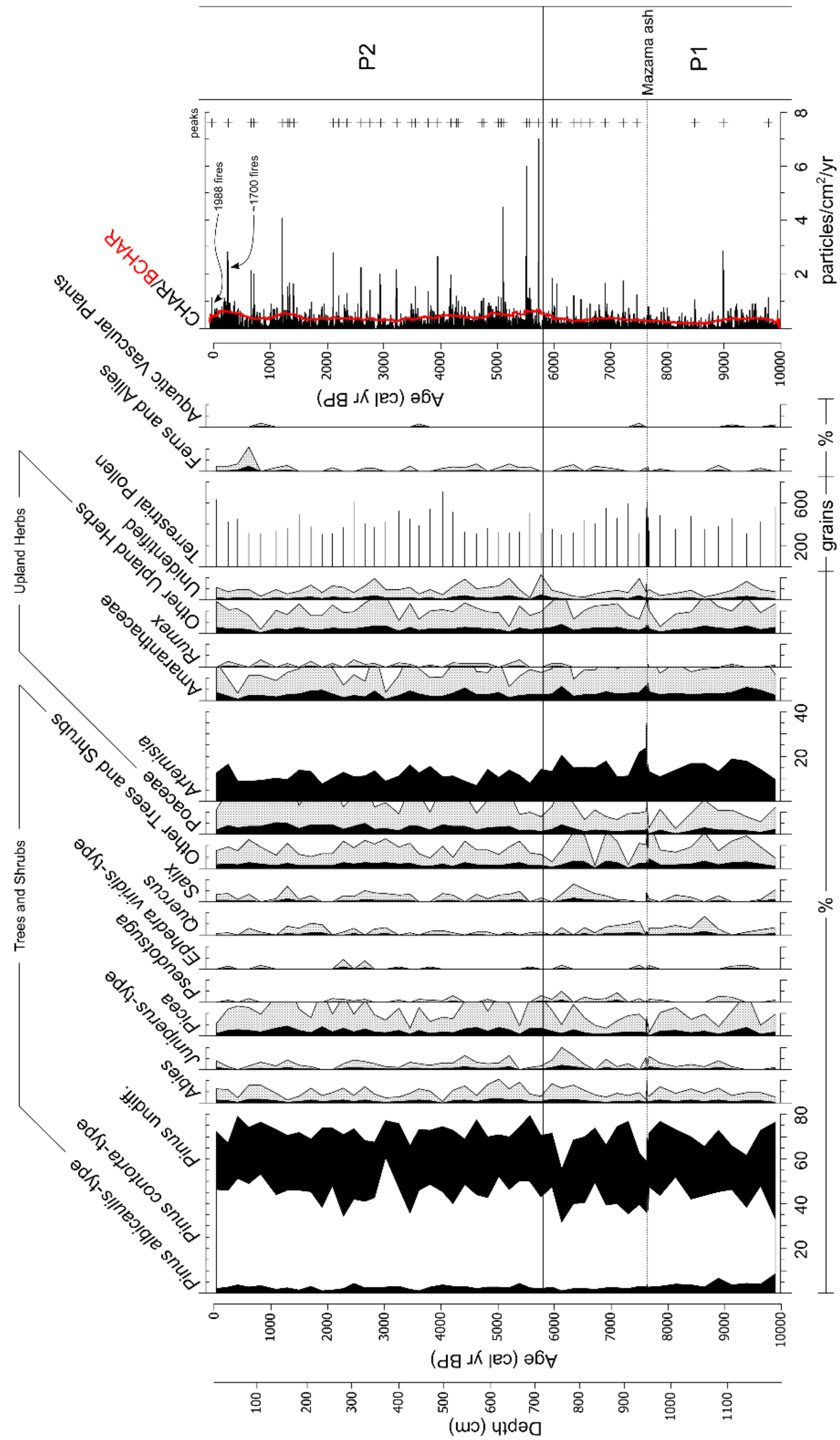

Figure 3.3: Percentage diagram of important pollen types (>1%) and CHAR/BCHAR plotted by age. Gray pollen plots are 5× exaggeration.

regional component in the pollen spectra. CHAR (mean 0.3 particles/cm^2/yr) was generally steady. Fire frequency (2.7 peaks/1000 years) and peak magnitude (mean peak magnitude 6.9 particles/cm^2/yr) were smaller than the more recent interval (Figure 3.3).

Zone YL-P2 (719–0 cm depth; 5800– -67 cal yr BP) was characterized by slightly higher percentages of *Pinus* (66–79%) and a lower proportion of *P. albicaulis*-type (2–11% of *Pinus*) than Zone YL-P1. Other tree taxa remained present in low percentages, including *Picea* (<5%), *Abies* (<3%), *Pseudotsuga* (<1%), *Juniperus*-type (<2%), and *Salix* (<2%). Steppe taxa, including *Artemisia* (7–16%) and Amaranthaceae (1–6%), decreased in abundance. Poaceae percentages (2–5%) increased somewhat, and *Rumex*, while rare or not detected in the previous period, was consistently detected in trace amounts (<1%). CHAR (0.4 particles/cm^2/yr) was modestly higher than Zone YL-P1. Fire episodes were more frequent than before (5.1 peaks/1000 years) and peak magnitudes were higher (mean peak magnitude 13.8 particles/cm^2/yr) (Figure 3.3).

A distinct charcoal peak was present in the Kullenberg core (2C) at 24 cm core depth and the gravity core (13A) at 36 cm depth, with charcoal concentrations of 37 and 39 particles/cm^3, respectively. Dendrochronological and charcoal data suggest only two large fire episodes in the last few centuries in the region established, the 1988 CE fires and ~1700 CE fires (1690–1710 CE, Romme and Despain, 1989; Higuera et al., 2010). The depth of this peak seems too great to be attributed to the 1988 fires, and an overlying peak is evident in the gravity core at 3 cm core depth, likely representing the 1988 fires. A peak at 24 cm core depth in the Kullenberg core and at 36 cm core depth in the gravity core is attributed to the ~1700 CE fire episode. We use this charcoal peak to correlate the two cores.

Isotopes in diatoms and water samples (Cartier, unpublished data)

In August 2018, mean $\delta^{18}O$ in the main tributaries entering the lake was −18 ‰, and the Yellowstone River inlet was −17.7 ‰. Lake-surface water in 2018 from different locations had mean $\delta^{18}O_{water}$ of −15.7 ‰, and mean $\delta^{18}O$ at the Yellowstone River outlet was −15.9 ‰. $\delta^{18}O_{water}$ values in surface waters of the Southeast Arm are lower because of the inflowing Yellowstone River waters in 1997-1999 that had $\delta^{18}O_{water}$ of -19.6 to -18.1 (Balistrieri et al., 2007). A snow sample taken in 2018 had a $\delta^{18}O_{water}$ value of −24.8 ‰.

The average $\delta^{18}O_{diatom}$ for the entire sediment core was 25.8 ‰ (s.d. = 0.66 ‰), with a minimum value of 24.2 ‰ at 5360 cal yr BP and a maximum value of 27.01 ‰ at 8700 cal yr BP (Fig. 4). The total variance was 2.9 ‰. Oxygen isotope data show a general, time-transgressive record from high $\delta^{18}O_{diatom}$ values at the beginning of the record, ~26.5 ‰, to lower $\delta^{18}O_{diatom}$ values to the present. $\delta^{18}O$ in the lake surface water was −15.7 ‰ in different locations, and mean $\delta^{18}O$ at the outlet was −15.9 ‰ (in 2018). $\delta^{18}O$ values in surface waters of the Southeast Arm were lower, because of its proximity to the Yellowstone River inlet (Balistrieri et al., 2007). $\delta^{18}O$ in a snow sample was −24.8 ‰. Lake water is well mixed, and a similar degree of influence of evaporation on isotopic composition was observed in 1998/1999 (Balistrieri et al., 2007) and in 2018 (Cartier, *unpublished data*), with a slope of 5.

Discussion

The climate history of the Yellowstone region is the result of slow changes in the seasonal cycle of insolation that, in turn, led to changes in the strength and location of atmospheric circulation features. The complex topographic landscape of the region creates sharp differences between the precipitation regimes in Yellowstone at present and these regimes were affected directly and indirectly by changes in the seasonal cycle of insolation through time (Whitlock and Bartlein, 1993). In the early Holocene, the climate of the Yellowstone Plateau was dominated by warmer summers and a strengthened northeastern Pacific subtropical high-pressure system, which created conditions that were effectively drier than present (here and elsewhere the comparative "present" is a reference to the mean 20th century) (Bartlein et al., 1998). During the middle Holocene, the influence of the subtropical high weakened, and conditions became progressively cooler and wetter (Bartlein et al., 1998), but still warmer and effectively drier than present (Diffenbaugh et al., 2006). In the late Holocene, cooling and wetting trends continued to the present (Bartlein et al., 1998). The northern margin of the Yellowstone Plateau is and was more influenced by summer precipitation, and summers may have become wetter than present in the early Holocene, as a result of strengthened monsoonal circulation (Whitlock and Bartlein, 1993).

To interpret biological proxy data from Yellowstone Lake, we compare core 2C/13A datasets with well-documented changes in the seasonal cycle of insolation, reconstructed with the 44.5 °N model solution (Laskar et al., 2004) and with Holocene climate changes inferred from paleoclimate model simulations (Bartlein et al., 1998; Diffenbaugh et al., 2006). For consistency with forthcoming publications (Brown et al. *in prep*), the Yellowstone Lake vegetation and hydroclimate reconstruction is broken into three periods based on diatom (Brown, 2019) and lithological data, as well as data detailed here: (1) early Holocene (9880–6300 cal yr BP), (2) middle Holocene (6300–3000 cal yr BP), and (3) late Holocene (3000– -67 cal yr BP). The regional pollen record from Yellowstone Lake is compared with three published records from nearby, smaller lakes from the rhyolite region where *Pinus contorta* forests dominate today

(Cygnet Lake; Table 3.2) and from the andesitic region where mixed *Pinus-Abies-Picea* forest occurs (Cub Creek Pond, Buckbean Fen, Table 3.2).

Table 3.2. Paleoecological sites used in regional/local vegetation comparison

Site	Location	Elevation, m.a.s.l.	Modern vegetation	Source
Cygnet Lake	44°23′N 110°22′W	2530	*P. contorta* forest	Whitlock, 1993
Cub Creek Pond	44°30′N 110°15′W	2511	*Pinus-Abies-Picea* forest	Waddington and Wright, 1974
Buckbean Fen	44°18′N 110°22′W	2367	*Pinus-Abies-Picea* forest	Baker, 1976

Interpretation of stratigraphic $\delta^{18}O_{diatom}$ data

The diatom species selected for isotopic analysis, *Stephanodiscus yellowstonensis,* typically blooms in late June and develops large populations during summer (Theriot et al., 2006). The $\delta^{18}O_{diatom}$ record represents average $\delta^{18}O_{water}$ after snowmelt and during the ice-free season. Possible controls on the oxygen isotope values of diatoms ($\delta^{18}O_{diatom}$) include water temperature at the time and place of diatom growth and oxygen isotope composition of lake water ($\delta^{18}O_{water}$). Lake water $\delta^{18}O_{water}$, in turn, is influenced by climate through changes in (1) temperature, (2) evaporation, and (3) lake water balance and precipitation (Leng and Barker, 2006). We interpret changes in the $\delta^{18}O_{diatom}$ record as variations in lake water evaporation, driven by temperature, and to a lesser degree winter and spring precipitation relative to summer precipitation. Our reasoning is as follows: Although temperature may have driven the observed trend, but the range of variability in $\delta^{18}O_{diatom}$ of 2.9 ‰ would imply a change in lake-water temperature of 14–15 °C on average, which is unlikely on Holocene timescales (Shuman and Marsicek, 2016).

The second influence is surface water evaporation. Present-day lake waters are enriched in heavy isotopes in comparison to tributaries, precipitation, and snow, as a result of evaporation during summer. The effects of evaporation in 1998/1999 and in 2018, produced a $\delta^{18}O$-δD trajectory with a slope of 5 (Balistrieri et al., 2007; Cartier, *unpublished data*). With an estimated water residence time of 12 years (Balistrieri et al., 2007), the impact of snowmelt, which lowers $\delta^{18}O$, is strongest for surface waters close to the major inflow. The isotopic values at the coring site for 2C near the outlet likely reflects the composition of waters in the northern part of Yellowstone Lake that are isotopically heavier as a result of surface-water evaporation while water flows through the lake basin from the Southeast Arm inlet.

The third influence is the isotopic composition of the Yellowstone River, which delivers around 70% of annual water inflow (data from 1997 and 1998; Balistrieri et al., 2007). Interannual changes in Yellowstone River discharge will influence the lake water's isotopic signature. Because most precipitation at Yellowstone Lake occurs as snowfall, the lake-water balance is primarily affected by the isotopic composition of snowmelt. Modern winter and spring precipitation derives mainly from northern Pacific storm systems (Despain, 1987), whereas during summer, warmer subtropical moisture sources deliver higher $\delta^{18}O$ (Anderson et al., 2016).

Early Holocene (9880–6300 cal yr BP, 1174–777 cm depth)

The early Holocene experienced significantly increased summer insolation in the Northern Hemisphere (~493 W/m^2) (Figure 3.4; Laskar et al., 2004). Enhanced summer insolation was responsible for warmer, drier summers than the 20th century average in the

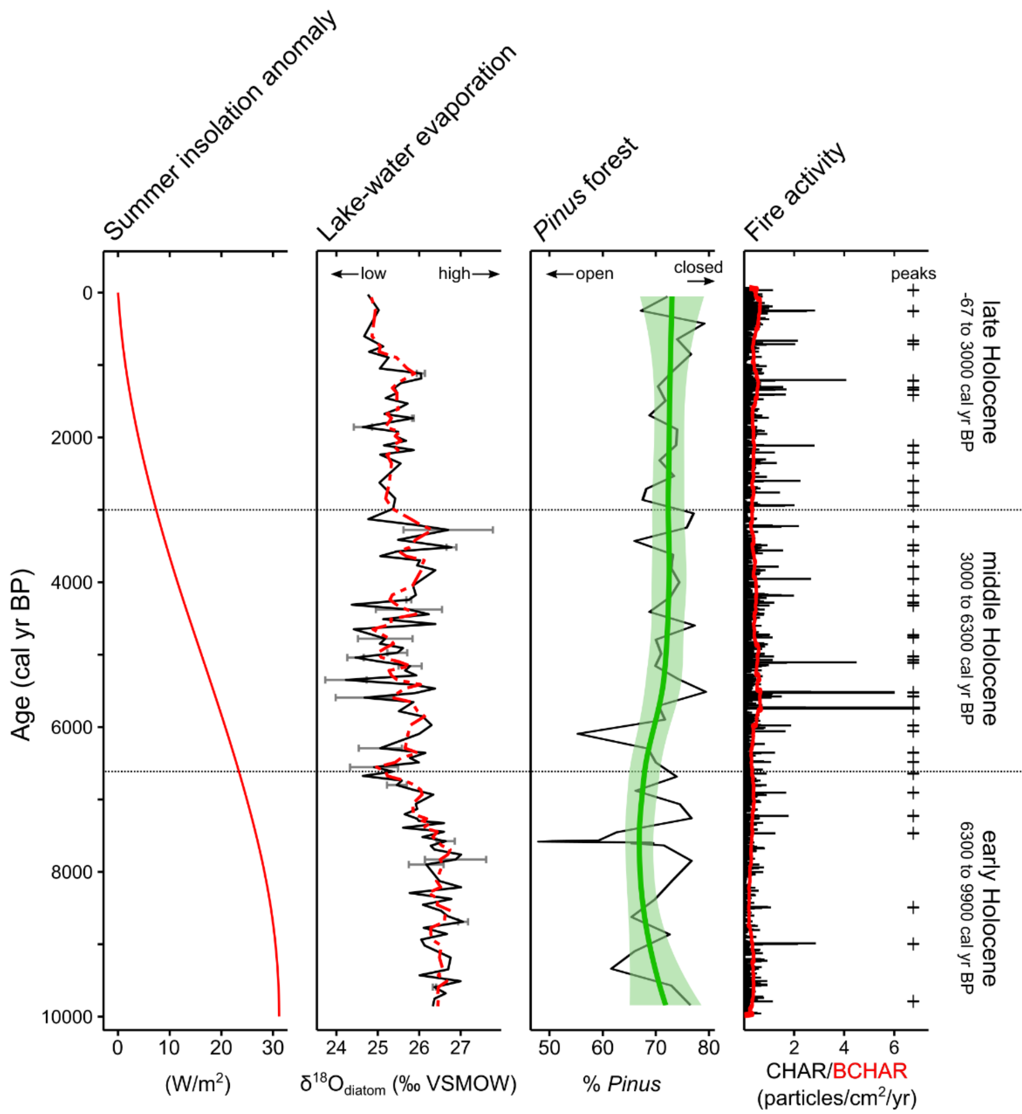

Figure 3.4: Summer insolation anomaly (44.5°N solution; Laskar et al., 2004) compared with $\delta^{18}O_{diatom}$ (Cartier, *unpublished data*), percent *Pinus* pollen (lowess smoother in green to emphasize long-term trends, with 2σ standard error), and charcoal from the Yellowstone 2C/13A juxtaposed to illustrate the importance of Holocene insolation changes on ecological development.

Yellowstone Lake watershed (Whitlock and Bartlein, 1993), driven by a strengthened northeastern Pacific subtropical high-pressure system (Bartlein et al., 1998).

The abundance of *Pinus contorta*-type pollen in early Holocene (Zone YL-P1) sediments at Yellowstone Lake falls within the range of modern pollen samples from *P. contorta* forests in the Yellowstone region (~55-95%, Iglesias et al., 2018). *P. albicaulis*-type pollen is also more abundant in the early Holocene (Zone P1), consistent with an expansion of *P. albicaulis* or *P. flexilis* from 12,00–7000 cal yr BP in the Yellowstone region (Iglesias et al., 2015). Indicators of steppe vegetation, including *Artemisia*, Poaceae, and Amaranthaceae, were not abundant at this time. However, a single sample immediately above the Mazama ash was dominated by *Artemisia* pollen and is attributed to brief proliferation of steppe vegetation following ash deposition (Schiller et al., 2020). Theriot et al. (2006), examining core YL92-1A (Figure 3.1), inferred increased riparian area at 7000 cal yr BP from *Salix* pollen, but we did not observe a marked increase of riparian taxa in our data. *P. contorta* was the dominant tree at the rhyolitic site (Whitlock, 1993) and the non-rhyolitic sites (Waddington and Wright, 1974; Baker, 1976), with only minor components of other conifers (Figure 3.5). At all sites, the percentage of *Pinus* pollen was lower in the early Holocene than later periods (Figure 3.5), evident despite a sedimentary discontinuity at Buckbean Fen (Baker, 1976). The Yellowstone Lake pollen record thus provides a good depiction of the vegetation trends at a regional scale.

Low fire-episode frequency with small CHAR peak magnitudes suggest fire events were comparatively infrequent and small or distant (relative to YL-P2, Figure 3.3). Significant charcoal peaks in a large lake likely represent large fires. For example, charcoal data from a short core taken from the West Thumb of Yellowstone Lake revealed a prominent charcoal peak only from the 1988 Yellowstone Fires, where as much as 40% of the Park burned, whereas smaller lakes in the watershed showed larger peaks from other, local fire episodes (Millspaugh and Whitlock, 1995).

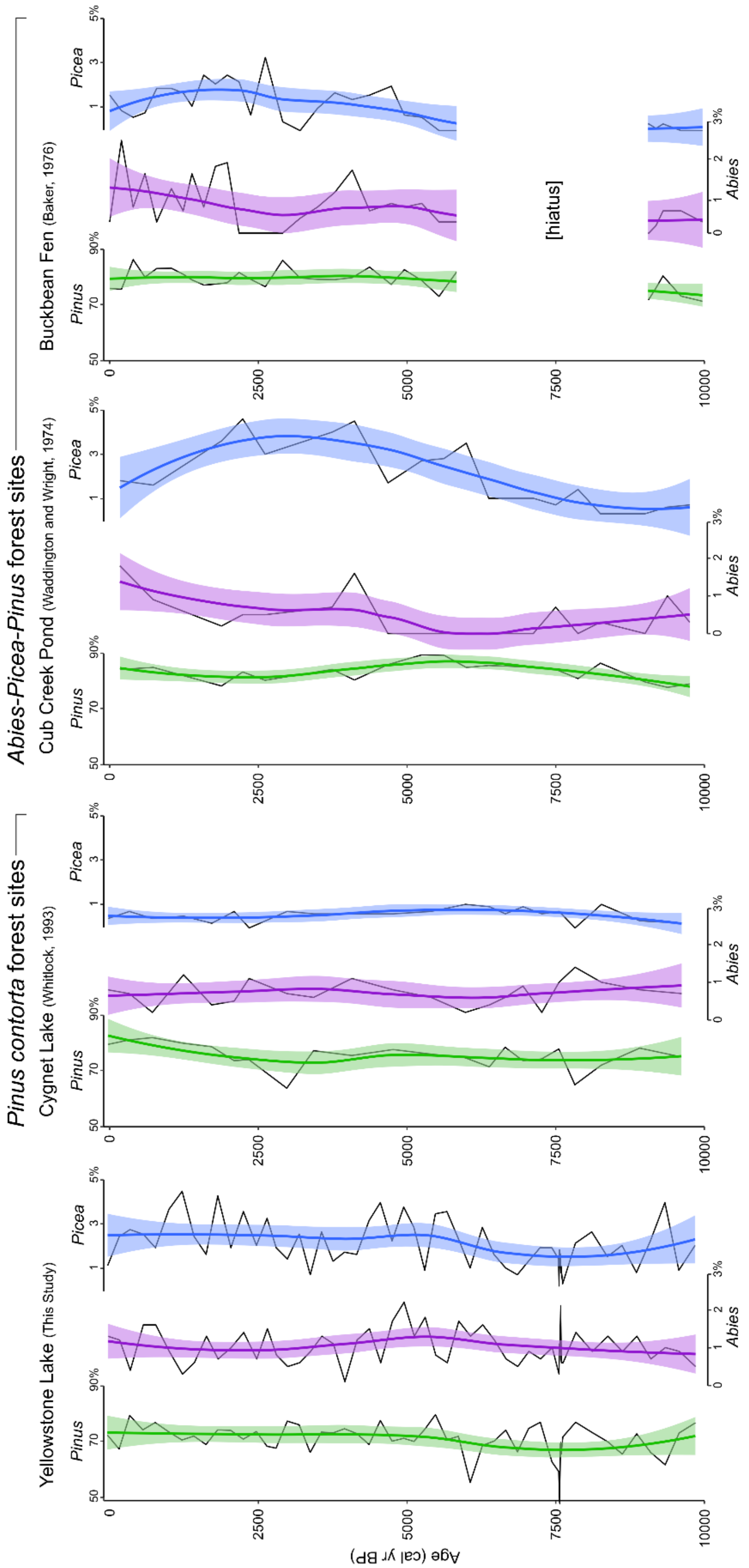

Figure 3.5: Major conifer pollen percentages from Yellowstone Lake (this study), Cygnet Lake (Whitlock, 1993), Cub Creek Pond (Waddington and Wright, 1974), and Buckbean Fen (Baker, 1976). Data are not available for Buckbean Fen from 9000 to 5900 cal yr BP due to a sedimentary discontinuity (Baker, 1976). Lowess smoother applied to each data set to emphasize long-term trends with 2σ standard error range.

High $\delta^{18}O_{diatom}$ values during this period (Figure 3.4), particularly from 9880 to 7500 cal yr BP (1174–928 cm depth), are attributed to greater lake-water evaporation rates than present and/or reduced inflow linked to decreased winter/spring precipitation and/or increased summer thunderstorms with ^{18}O-enriched precipitation (Anderson et al., 2016). These results are consistent with $\delta^{18}O$ on endogenic carbonates at Bison Lake, Colorado, where positive anomalies were associated with a precipitation regime dominated by rain rather than snow (Anderson, 2011).

The 2C/13A core contains one hydrothermal explosion deposit at 984-977 cm depth (Morgan et al., 2019) and geological studies suggest at least three large (>100 m crater diameter) hydrothermal explosions occurred in or near the northern basin of Yellowstone Lake in the Holocene (Muffler et al., 1971; Richmond, 1977; Morgan et al., 2003, 2009; Pierce et al., 2007). Pollen data from another Yellowstone Lake core suggest that the early Holocene event may have led to a brief decline in conifers that lasted decades or less, but otherwise it had no lasting impact on the vegetation (Schiller et al., 2020, Chapter 5). The hydrothermal explosion also was not associated with Holocene-scale vegetation changes or modifications of lake water balance evidenced from $\delta^{18}O_{diatom}$ data in the 2C/13A core.

In summary, the Yellowstone Lake data indicate warmer, drier summers than present, consistent with a clear response to enhanced summer insolation in the early Holocene. *Pinus contorta* forests were relatively open, regionally, possibly the result of summer drought. Infrequent large fires recorded at Yellowstone Lake contrast with more frequent local fires at Cygnet Lake (Millspaugh et al., 2000). $\delta^{18}O_{diatom}$ values from this interval suggest higher-than-present lake-water evaporation in summer and/or reduced winter to spring precipitation.

Middle Holocene (6300–3000 cal yr BP, 777–366 cm depth)

The middle Holocene was characterized by declining summer insolation (~480 W/m^2; Figure 3.4; Laskar et al., 2004). The attendant weakening of the northeastern Pacific subtropical high pressure system resulted in summers that were cooler and effectively wetter before (Whitlock and Bartlein, 1993), although still warmer and drier than today (Bartlein et al., 1998; Diffenbaugh et al., 2006).

Pinus pollen percentages increased in Zone YL-P2 (Figure 3.3) and at other sites in the Yellowstone Lake vicinity (Figure 3.5), suggesting increased forest density in the middle Holocene (Iglesias et al., 2018; Iglesias and Whitlock, 2020). Since *Pinus* pollen in all of these records is dominantly *P. contorta*-type, we infer increased closure or extent of *P. contorta* forest on the landscape. The increase in *Pinus* came at the expense of steppe taxa, Poaceae, *Artemisia*, and Amaranthaceae. Cygnet Lake (Whitlock, 1993) registered slightly increased *Pinus* pollen percentages at this time, with negligible amounts of *Abies* and *Picea* pollen (Figure 3.5). Cub Creek Pond (Waddington and Wright, 1974) and Buckbean Fen (Baker, 1976), located on andesitic substrate, documented increasing percentages of *Pinus*, *Abies*, and *Picea* as mixed *Pinus-Abies-Picea* forests became established at these sites after *ca.* 5000 cal yr BP (Figure 3.5). The regional Yellowstone Lake record reflects both components, with increased percentages of all three conifer taxa.

The Yellowstone Lake record suggests an increase in large fire episodes, reflecting greater area burned, higher fire severity, or closer fire proximity (Figure 3.3). Today, closed *Pinus contorta* forests support infrequent high-severity fires (Pfister and Daubenmire, 1975), and we assume this regime was established based on both the large charcoal peaks and abundance of *P. contorta* pollen.

After a peak at *ca.* 6000 cal yr BP, $\delta^{18}O_{diatom}$ values were lower (Figure 3.4) from 5800 to 4500 cal yr BP, suggesting less lake-water evaporation than before, with the possible contribution of increased inflow of low $\delta^{18}O$ water from snowmelt. A general trend towards increased winter precipitation and decreased summer temperatures is evident in the regional synthesis of Shuman and Marsicek (2016). Between 4500 and 3000 cal yr BP, $\delta^{18}O_{diatom}$ values departed from this trend (Figure 3.4) and increased to values similar to those in the early Holocene. This excursion suggests a renewed period of high evaporation, reduced snowmelt, and/or precipitation from subtropical vapor sources with higher $\delta^{18}O$ content.

To summarize, our records indicate a response to the attenuation of summer insolation during the middle Holocene. Lake-water evaporation was reduced and/or snowmelt increased. Forests in the watershed became more closed or extensive, supporting larger fire episodes than in the early Holocene.

<u>Late Holocene (3000– -67 cal yr BP, 366–0 cm depth)</u>

Summer insolation values declined to their present low levels in the last three millennia (Figure 3.4; Laskar et al., 2004), leading to the establishment of the present climate of relatively cool, effectively wet conditions (Whitlock and Bartlein, 1993).

The vegetation and fire dynamics in the Yellowstone Lake watershed appeared to remain relatively unchanged from the middle Holocene, evidenced by the lack of pollen and charcoal trends (Figure 3.4). In the late Holocene, Cygnet Lake (Whitlock, 1993) documents the highest *Pinus* pollen percentages of that record near the present day, while other conifer pollen remained nearly absent (Figure 3.5). *Pinus* pollen percentages declined somewhat at the same time at Cub Creek Pond (Waddington and Wright, 1974) and remained steady at Buckbean Fen (Baker,

1976) as those forests became more densely populated by *Abies lasiocarpa* and *Picea engelmannii* (Figure 3.5). Pollen percentages at Yellowstone Lake remained relatively unchanged in the late Holocene at Yellowstone Lake reflecting the fact that *Pinus* became more abundant on rhyolitic substrates and less abundant, increasingly locally replaced by *A. lasiocarpa* and *P. engelmannii*, on andesitic substrates. In other words, diverging trends in *Pinus* pollen abundance in different parts of the Yellowstone Lake vicinity resulted in a regional pollen record that displayed little change.

Uppermost charcoal peaks may be correlated in this interval with modern fire observations and dendroecological stand-establishment data. These correlations suggest that these fire episodes burned 100,000s of hectares in the Yellowstone Lake watershed (Romme and Despain, 1989; Tinker et al., 2003), including the 1988 CE fires, which burned approximately 400,000 ha in Yellowstone National Park (Schullery, 1989). These extremely large events are recorded in the West Thumb of Yellowstone Lake and in small lakes in the region, along with smaller fire episodes that affected individual sites (Millspaugh and Whitlock, 1995). This further suggests that charcoal peaks registered in Yellowstone Lake sediments represent extremely large fire episodes.

$\delta^{18}O_{diatom}$ at Yellowstone Lake decreased from 3000 to 1200 cal yr BP, indicating less lake-water evaporation and/or increased winter precipitation, broadly consistent with cooler conditions and Neoglacial glacial advances (3500–1300 cal yr BP) throughout the Rocky Mountain region (Menounos et al., 2009). $\delta^{18}O_{diatom}$ values were slightly higher at *ca.* 2000 cal yr BP (242 cm depth) than before, suggesting a brief hydroclimatic reversal, and this event is also registered as an interval of dry summers and winters at Crevice Lake (Whitlock et al., 2012).

Another shift to lower $\delta^{18}O_{diatom}$ values indicating less lake-water evaporation and/or increased winter precipitation, occurred after ca. 1000 cal yr BP (125 cm depth) during the Little Ice Age (1550–1850 CE, Viau et al., 2012). Cooler conditions in the Rocky Mountain region is also evidenced by Neoglacial glacial advances (3500–1300 cal yr BP) at high elevations in the Canadian Rockies (Menounos et al., 2009).

The late Holocene was characterized by relatively low lake water evaporation and/or increasing snowmelt as a result of wetter winters and cooler summers. Extensive, dense *Pinus contorta* forest dominated on rhyolitic substrates as they did for the last 11,500 cal years (Iglesias et al., 2018), while *Abies lasiocarpa* and *Picea engelmannii* became more abundant on andesitic substrates.

Conclusions

Pollen, charcoal, and oxygen isotope data provide new information about the Holocene history of the Yellowstone Lake watershed. The records show the strong influence of the seasonal cycle of insolation in governing the region's vegetation, fire, and hydrological history, while more local hydrothermal events had little impact. Specifically, our results show:

- Presence of a more open or less extensive forest in the watershed with small, frequent fires in the early Holocene (9880–6300 cal yr BP) during a time of warmer and effectively drier conditions (relative to the 20th century average); isotopic evidence suggests higher lake-water evaporation in summer and/or reduced snow fall in winter or spring.
- Establishment of a more closed or extensive *Pinus contorta* forest in the region, with the establishment of *Pinus-Abies-Picea* forest on andesitic substrates, and larger fire episodes

in the middle Holocene (6300–3000 cal yr BP). This vegetation change co-occurs with isotopic evidence for greater lake-water evaporation in summer and/or increased snowmelt.

- Further closure or increasingly extensive *Pinus contorta* forest in the late Holocene (3000– -67 cal yr BP) on rhyolitic substrate was contemporaneous with increased abundance of *Abies lasiocarpa* and *Picea engelmannii* on andesitic substrate, at the expense of *Pinus*, creating the illusion of steady-state vegetation in the Yellowstone Lake regional record. This vegetation supported by infrequent but large fires as summers became cooler and effectively wetter; synchronous with isotopic evidence for reduced evaporation and/or increased snowmelt.

Acknowledgements

This research was supported by the National Science Foundation's Integrated Earth Systems program 1391 EAR-1516361, NSF Grant No. 1515353 (C. Whitlock), 1515377 (S.C. Fritz), the Swedish Research Council (D.J. Conley), and The Royal Physiographic Society in Lund (to both R. Cartier and P. Zahajská). The research was conducted under Yellowstone National Park research permits YELL-2016-SCI-7018 and YELL-2016-SCI-5054. Yellowstone Lake coring was aided by M. Baker, C. Linder, R. O'Grady, M. Shapley, R. Sohn, and Yellowstone National Park rangers. LacCore provided coring infrastructure, laboratory space for core splitting, subsampling, and analyses including magnetic susceptibility. We thank K. Ljung for his help in the analysis of the organic matter and C. Alwmark for the observations with the SEM at Lund University.

CHAPTER FOUR

HOLOCENE GEO-ECOLOGICAL EVOLUTION IN LOWER GEYSER BASIN, YELLOWSTONE NATIONAL PARK

Contribution of Authors and Co-Authors

Manuscript in Chapter 4

Author: Christopher M. Schiller

Contribution: Conceived of project, led field work, conducted lab work (except diatom and biogenic silica analyses), and led manuscript preparation.

Co-Author: Cathy Whitlock

Contribution: Provided funding and guided the development of the manuscript.

Co-Author: Sabrina R. Brown

Contribution: Conducted analysis of diatoms.

Co-Author: Petra Zahajská

Contribution: Conducted analysis of biogenic silica content of sediments.

Manuscript Information

Christopher M. Schiller, Cathy Whitlock, Sabrina R. Brown, Petra Zahajská

Geological Society of America Bulletin

Status of Manuscript:
__×__ Prepared for submission to a peer-reviewed journal
_____ Officially submitted to a peer-reviewed journal
_____ Accepted by a peer-reviewed journal
_____ Published in a peer-reviewed journal

The Geological Society of America

CHAPTER FOUR

HOLOCENE GEO-ECOLOGICAL EVOLUTION IN LOWER GEYSER BASIN, YELLOWSTONE NATIONAL PARK

Abstract

Changes in climate and fire regimes have long been recognized to drive the postglacial vegetation history of the Yellowstone Plateau (e.g. Chapter 3). However, the impacts of locally dramatic, but widespread, processes such as hydrothermal activity are less well studied. A multi-proxy data set from Goose Lake in Lower Geyser Basin allows for an examination of Holocene hydrothermal history and its impact on terrestrial and limnic ecological development. From 10,300 to 3800 cal yr BP, hydrothermal fluids discharged directly into Goose Lake, as evidenced by the deposition of arsenic-rich sediment, fluorite mud, and relatively heavy $\delta^{13}C_{sediment}$ values. Hydrothermal discharge impacted limnic ecology, allowing diatoms and coccal algae adapted to extreme, warm conditions to thrive; by contrast, surrounding *Pinus contorta* forests and fire were little affected, responding chiefly to soil constraints and regional climate trends. At 3800 cal yr BP, basin-wide hydrothermal activity was abruptly reorganized, leading to a cessation of hydrothermal activity at Goose Lake. Diatoms and coccal algae responded to new lake conditions, shifting towards an oligotrophic assemblage more typical of nonhydrothermal sites. Expansion of hydrothermal activity elsewhere in the basin led to a more open landscape with less extensive *Pinus contorta* forest than before and diminished fire activity. The modern, predominantly treeless vegetation of Lower Geyser Basin ecosystem, thus, developed in close conjunction with the shifting distribution of hydrothermal activity. Lake sediments from Goose

Lake provide a unique opportunity to reconstruct both the development of hydrothermal landscapes as well as the ecological response.

Introduction

The Yellowstone Plateau Volcanic Field hosts among the largest and most diverse continental hydrothermal fields on Earth (Hurwitz and Lowenstern, 2014). More than 10,000 thermal features, including thermal pools, frying pans, fumaroles, mud pots, and geysers (Hurwitz and Lowenstern, 2014), are found in the volcanic field, concentrated within the 631 ka Yellowstone Caldera (Vaughan et al., 2014). Thermal areas occupy more than 48 km^2 in Yellowstone National Park (Vaughan et al., 2014) and present-day hydrothermal basins have been active since at least the Pinedale Glaciation (Muffler et al., 1971, 1982; Sturchio et al., 1994; Pierce et al., 2007; Morgan et al., 2009). In Yellowstone National Park's thermal areas, hydrothermal processes directly cause plant mortality and stunt tree growth through heated soils (White et al., 1988; Lowenstern et al., 2003) and contact with hot, mineral-saturated fluids (Pitt and Hutchinson, 1982; Channing and Edwards, 2003). Paleoecological data suggest short-lived damage to past vegetation from large hydrothermal explosions (Schiller et al., 2020) and varied impacts to limnobiota (Brown, 2019). The long-term consequences of hydrothermal activity on the ecological development of thermal areas are unknown.

Here, we focus on the ecological history of Lower Geyser Basin (LGB), the largest thermal basin on the Yellowstone Plateau (topographic area ~25 km^2, active hydrothermal area ~14 km^2, Vaughan et al., 2014). Within LGB lies a series of small lakes in close proximity to active thermal features. This juxtaposition enables the use of lake sediment records to examine past hydrothermal activity and ecosystem responses. A 10,300 year-long sediment core from the

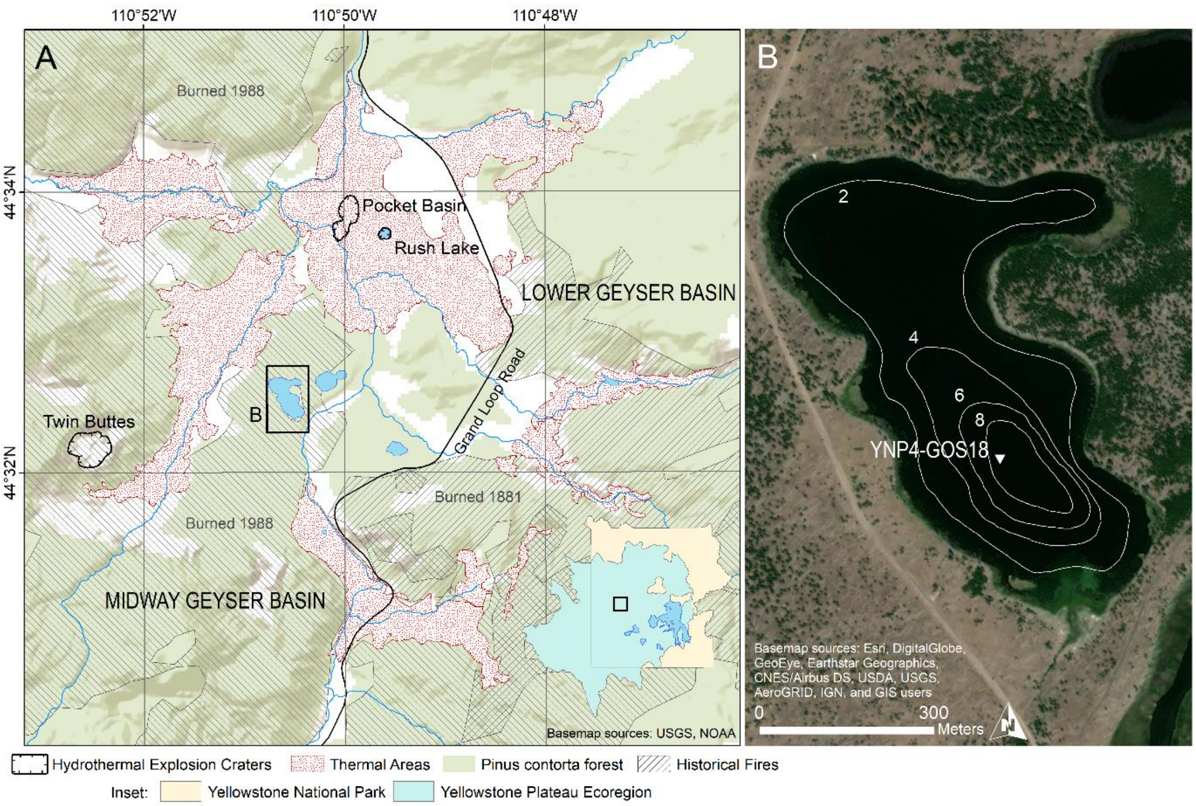

Figure 4.1: Location of Goose Lake. (A) Location of Goose Lake within Lower Geyser Basin with active thermal areas (red and dotted, Vaughan et al., 2014), large hydrothermal explosion craters (black basin outlines, Morgan et al., 2009), pre-1988 CE extent of *Pinus contorta*-dominated forest (green, Despain, 1990), and the extent of historical fires (back and hashed, H.L. Williams personal communication 2020). Evidence of hydrothermal activity is pervasive in the Goose Lake vicinity, although the lake is not situated adjacent to any active thermal features. (B) Location of YNP4-GOS18 cores within the deepest part of Goose Lake. Bathymetry (m) modified from Arnold and Sharpe (1967).

largest of the LGB lakes, Goose Lake (44.54°N, 110.84°W, 2196 m.a.s.l., 13.8 ha), was studied to address the following questions: (1) What is the history of hydrothermal activity at Goose Lake, as registered in the lake-sediment archive? (2) What is the role of climate, hydrothermal activity, and fire in shaping the LGB geo-ecosystem during the Holocene, including its vegetation and limnologic history relative to other locations in the Yellowstone Plateau ecoregion?

Site Description

Lower Geyser Basin (LGB) is a large, predominantly treeless basin (Figure 4.1), and its thermal features have chiefly neutral and alkaline chemistry, with fewer acidic features (Hurwitz and Lowenstern, 2014). The area was covered by the Yellowstone Glacier Complex during the Pinedale Glaciation (locally 22-13 ka, Licciardi and Pierce, 2018). Although the timing of ice retreat in the vicinity of LGB is poorly constrained by absolute ages, the area was probably ice-free after ~14 ka based on correlation with recessional moraines in northern Yellowstone (Licciardi and Pierce, 2008) and the basal ages of nearby lake-sediment cores (Whitlock, 1993). LGB hydrothermal activity has occurred since the late Pinedale time, as evidenced by thick hydrothermal deposits interbedded with glacial outwash in drilled cores (Bargar and Beeson, 1981), hydrothermal explosion deposits containing inferred proglacial lake sediments (Muffler et al., 1971), and silica-cemented kame deposits at several localities (Bargar and Beeson, 1981, 1985; Muffler et al., 1982). Evidence of present and past hydrothermal activity is pervasive throughout the Goose Lake area, including vast flats of sinter, hydrothermal mud, and diatom ooze (Muffler et al., 1982), but the lake itself is ~280 m from the nearest active thermal features along Fairy Creek to the west (Figure 4.1). Several large (>100 m diameter) hydrothermal explosion craters are known from LGB as well, including those at Twin Buttes, Pocket Basin, and Rush Lake (Muffler et al., 1971; Morgan et al., 2009).

LGB lies within the Yellowstone Plateau ecoregion, which is characterized by abundant rhyolitic substrate and *Pinus contorta* (Figure 4.1). LGB is surrounded by rhyolitic lava flows (Waldrop and Pierce, 1975), which weather to nutrient-poor, well-drained soils that support *P. contorta* forest (Despain, 1990). *P. contorta* forest first established on the Yellowstone Plateau *ca.* 11 ka and the composition of the forest has changed little since then due to the edaphic constraints of rhyolite (Whitlock, 1993; Iglesias et al., 2018). Within LGB, dense *P. contorta* forests grow where thermal activity is not active and meadows with *Artemisia* are present on nearby slopes. The vegetation was extensively burned in 1988 including the margins of Goose Lake (H.L. Williams *personal communication* 2020). Grassland grows in thermally active flats and dominated by diminutive grasses like *Puccinellia nuttalliana* and *Dichanthelium acuminatum* that are well adapted to heated, salt-rich soils (Despain, 1990). The dynamic relationship between hydrothermal activity and vegetation in LGB is further illustrated by so-called "bobby-sox" trees, which were killed by hot, mineral-saturated water and bear distinctive white, silica-impregnated wood at their base, following death.

Goose Lake (0.14 km^2) has a small inlet in the southwest (< 1 cfs, Arnold and Sharpe, 1967) and no surface outlet. Lake bathymetry reveals a broad, shallow bench, comprising up to 80% of the lake bottom, and a maximum depth of 9.5 m (Figure 4.1; Arnold and Sharpe, 1967). The lake may have formed from past hydrothermal processes (Bauer, 1962) or as a late-Pinedale kettle hole, given that it is surrounded by sandy gravel deposits (Waldrop and Pierce, 1975) interpreted as Pinedale glacial outwash (Muffler et al., 1982). A recent rise in lake level is evidenced by the presence of dead, submerged pines along the shore. *Typha latifolia*, *Scirpus*, and *Carex* grow around the margin and *Nuphar luteum*, *Potomogeton spp*, *Myriophyllum spp*, and *Polygonum amphibium* are present as aquatics. In an early sampling, water temperatures ranged from 20.8°C at the surface in July to 11.6°C at the base of the hypolimnion and pH was 8.1 (Arnold and Sharpe, 1967). Previous paleoecological study of Goose Lake includes an examination of diatoms as they relate to fish introductions (Shaw Chraïbi, 2016) and an analysis of charcoal abundance in the surface sediments following the 1988 fires (Whitlock and Millspaugh, 1996).

Methods

Field Sampling

A series of sediment cores was collected from an anchored platform in the deepest part of Goose Lake (YNP4-GOS18, 44.54135°N, 110.84237°W, 8.86 m water depth, Figure 4.1) in June 2018, with a modified Livingstone sampler (Wright et al., 1984). Cores 1A (564 cm long), 1B (100 cm long), and 1D (793 cm long) were extruded, described, and wrapped before being transported from the field. Uppermost sediments were recovered with a gravity sampler to retrieve the sediment-water interface, and this short core (20 cm long) was extruded in the field at 1-cm resolution and samples were placed in whirlpak bags before transport to the lab.

Laboratory Analyses

Chronology Age control was provided by accelerator mass spectrometry (AMS) radiocarbon dating of 15 charcoal samples. Prior to submission, samples were isolated and cleaned of extraneous material with a dissecting needle and distilled water under a stereomicroscope and pretreated with acid-base-acid washes. Additional age control was also provided by the age of the sediment-water interface and from tephrochronology.

Lithology and Geochemistry Cores were correlated by depth and Cores 1A and 1D were correlated based on lithostratigraphy, particularly a distinctive, dark ash layer (Figure 4.2). The

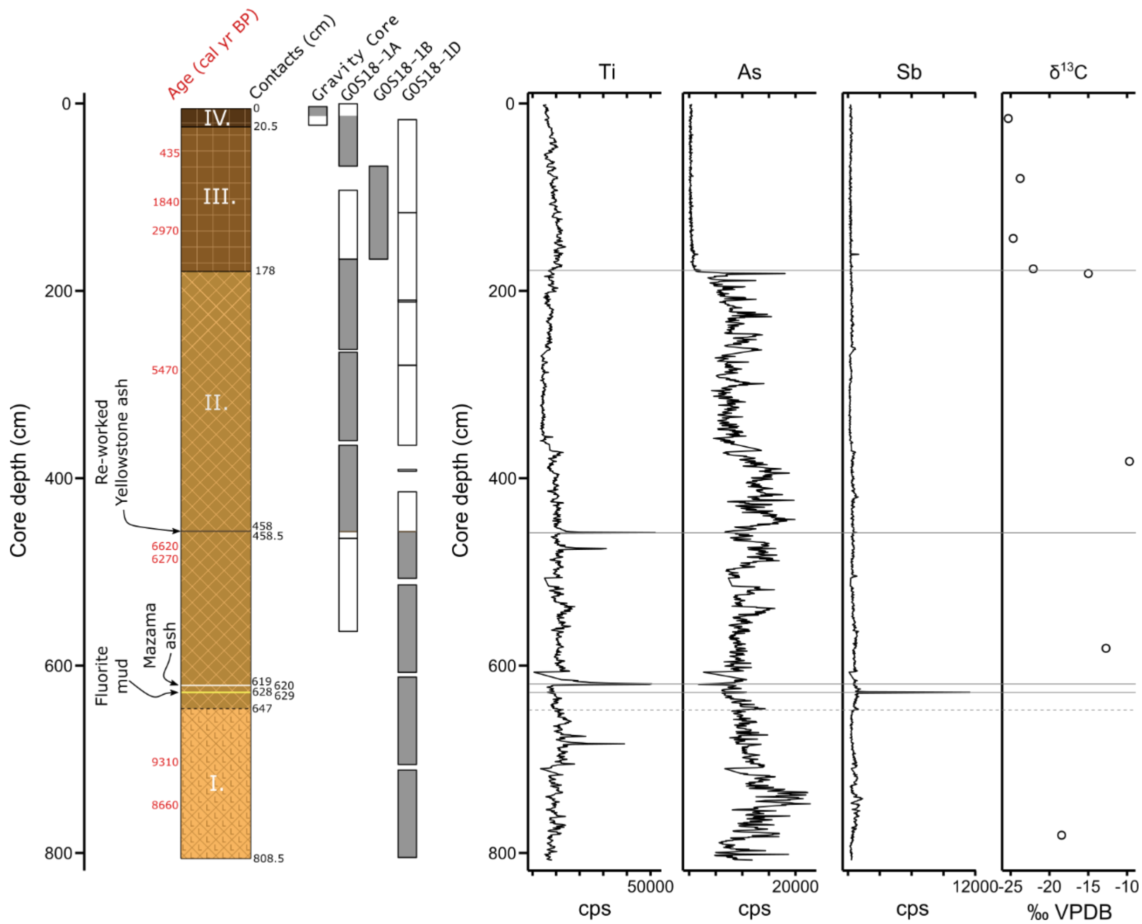

Figure 4.2: Lithology and geochemistry of composite Goose Lake core. The stratigraphy may be divided into: I. Indistinctly laminated diatomaceous ooze with clay; II. Laminated diatomaceous ooze with sapropel and minor, fragmental plant remains, punctuated by fluorite mud (629 to 628 cm depth), the Mazama ash (620 to 619 cm depth), and a reworked ash of probable Yellowstone provenance (458.5 to 458 cm depth); III. Thinly bedded diatom ooze with sapropel; and IV. Massive diatomaceous sapropel with high water content. Below 178 cm depth, sediments are enriched in As, have heavy $\delta^{13}C_{sediment}$ values, and are depleted in BSi. The fluorite mud is enriched in antimony, while other autochthonous deposits are expectantly rich in titanium. The diagram of the composite core is given. Most correlations between drives were made on the basis of cored depth, except the correlation between GOS18-1A and GOS18-1D, which was made with the re-worked Yellowstone ash.

composite core was 808.5 cm long, and subsequent information uses the depth of the composite core. Cores were longitudinally split, imaged, and measured every 0.5 cm for physical parameters (magnetic susceptibility, color, reflectance, density, profile) at the National

Lacustrine Core Facility (LacCore, University of Minnesota-Twin Cities) and kept under refrigeration except when being sampled or analyzed. Sediments were classified by composition and texture according to the scheme of Schnurrenberger et al. (2003). Volcanic ash deposits were further characterized by mineralogy and texture to identify their source. Measurements also were made every 0.5 cm for bulk geochemistry and X-radiographs produced from X-ray fluorescence (XRF) at the Large Lakes Observatory (LLO, University of Minnesota-Duluth). A section of the core with unusual bulk geochemistry (high antimony, Figure 4.3) was also analyzed for grain texture (SEM), elemental composition (SEM-EDS), and mineralogy (XRD) to help ascertain hydrothermal provenance at the Image and Chemical Analysis Laboratory (ICAL, Montana State University). In addition, $\delta^{13}C$ measurements were made from bulk sediments at the Reston U.S. Geological Survey Stable Isotope Laboratory to help ascertain sedimentary carbon provenance.

Pollen Analysis Subsamples of 0.5 cm^3 were prepared for pollen analysis at intervals of 3 to 16.5 cm depth in the core, with highest sampling resolution in close proximity to ash deposits to explore potential impacts of ash falls on vegetation history. Preparation followed standard procedures (Bennett and Willis, 2001). A known concentration of *Lycopodium* spores was added as a spike to calculate pollen concentration (grains/cm^3) and influx (grains/cm^2/year). Residues were preserved and mounted in silicone oil. At least 300 terrestrial pollen grains and spores were identified at a minimum of 400× magnification and resolved to the lowest possible taxonomic level with relevant atlases (Hedberg, 1946; Moore et al., 1991; Kapp et al., 2000) and the modern reference collection at Montana State University. Coccal algae palynomorphs were enumerated from synchronous transects of pollen slides.

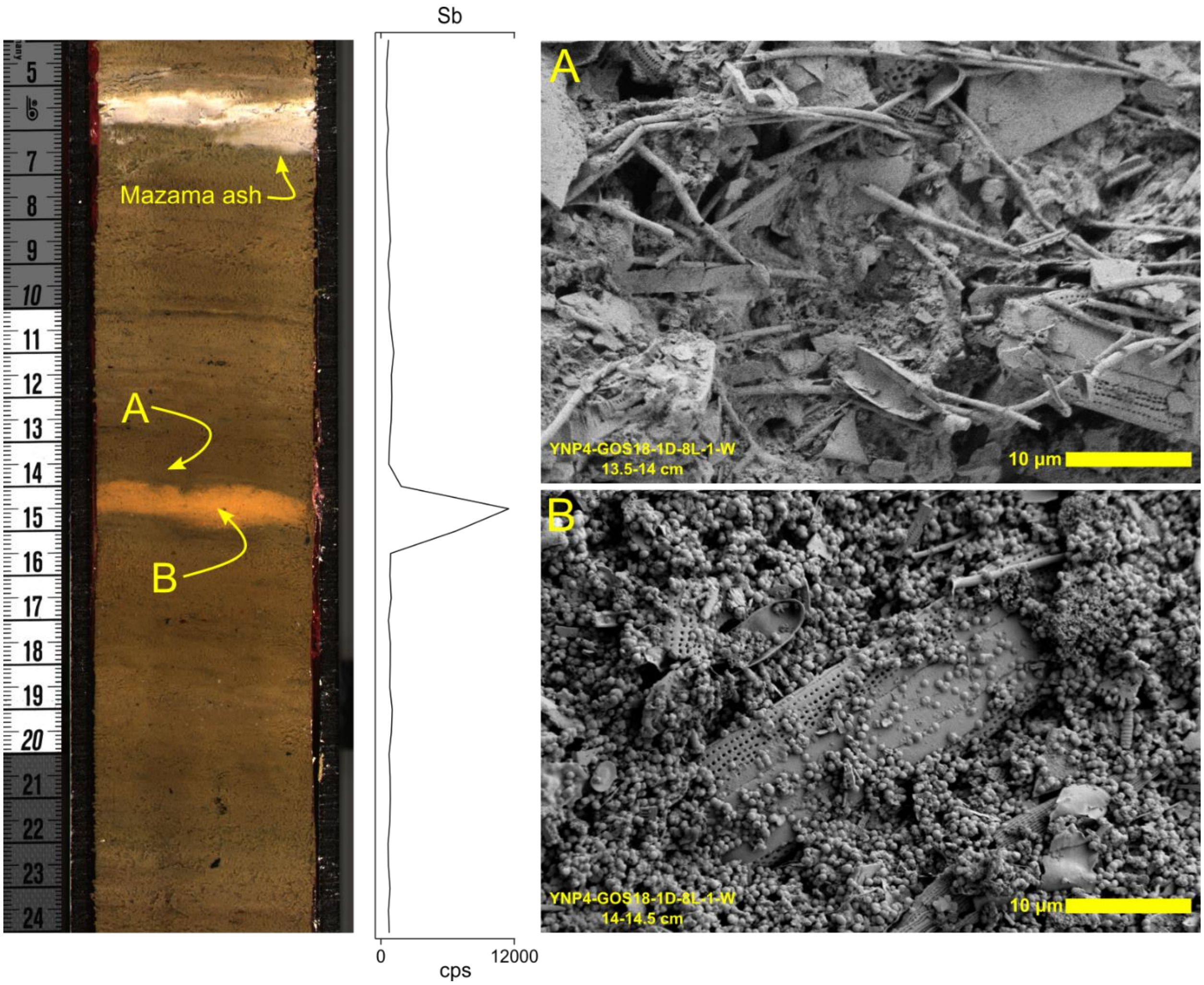

Figure 4.3: Lithology and geochemistry of fluorite mud occurring at 628-629 cm depth in the composite core. (A) SEM image of sediment immediately above contact with fluorite mud, showing abundant diatom frustules, sponge spicules, and fine-grained clays and organics. (B) SEM image of fluorite mud with 81 wt% fluorite. Note large diatoms in a matrix of fluorite spherules.

Pinus grains were identified to subgenus for grains with observably intact distal membranes. *Pinus* subgen. *Pinus* (diploxylon type, psilate distal membrane) was attributed to *P. contorta*, on the grounds that *P. ponderosa* does not presently grow on the Yellowstone Plateau (Arno, 1979). *Pinus* subgen. *Strobus* (haploxylon type, verrucate distal membrane) was attributed to *P. albicaulis*-type, which may include *P. flexilis* that occurs at lower elevations in northern Yellowstone National Park. Cupressaceae grains are assigned to *Juniperus*-type based on the fact that only *J. communis*, *J. horizontalis*, and *J. scopulorum* grow in the region. Percentage of terrestrial pollen was calculated with a denominator of total terrestrial pollen, and aquatic pollen and spores were analyzed as a percent of total pollen and spores. Coccal algae were identified to the genus level (Jankovská and Komárek, 2000) and were analyzed as influx (NISP (number of individuals specimens) /cm^2/yr) given their great abundance. Attribution of pollen assemblages to present-day vegetation types was aided by comparison to modern pollen assemblages from the Yellowstone region (Baker, 1976; Whitlock, 1993; Iglesias et al., 2018).

Charcoal Analysis Subsamples of ~2 cm^3 were collected for charcoal analysis at 0.5-cm intervals for the entire composite core to reconstruct fire history. Charcoal particles >125 μm in diameter were extracted and counted according to standard methodology to analyze long-term trends in charcoal as well as local fire episodes (Whitlock and Millspaugh, 1996; Whitlock and Larsen, 2001). Charcoal accumulation rates (CHAR, particles/cm^2/year) were calculated with CharAnalysis software for MatLab (Higuera et al., 2009) and were interpreted as an indicator of fire activity or overall, time-averaged biomass burned. The CHAR record then was decomposed into background charcoal accumulation rates (BCHAR), the long-term trend in CHAR, and peaks. BCHAR was calculated with a 500-year lowess smoother (which minimized the sum of the median signal to noise index and the goodness of fit value), robust to outliers. Charcoal peaks were considered “significant” fire episodes if they registered above the 99th percentile of the local noise distribution of CHAR as defined by a Gaussian mixture model. Peaks were considered “insignificant” if they registered between the 95th and 99th percentile.

CHAR represents overall, time-averaged biomass burned. That record is decomposed into BCHAR, which reflects a combination of regional fire, secondarily transported charcoal, and sediment mixing, and peaks, which represent fire episodes, individual fires or series of fires in close succession and within the duration of the charcoal peak (Higuera et al., 2009, 2011). Charcoal peaks in Yellowstone Plateau *Pinus contorta* forest sites have previous been found to most accurately represent fire episodes within 1.2–3.0 km of the lake (Higuera et al., 2010). Greater (or lesser) peak magnitude is interpreted as greater biomass burned through increased fire size or severity. Peak detection was improved by comparison with the dates of historical fires in 1988 and 1881 CE based on historical records (H.L. Williams *personal communication* 2020).

Diatom Analysis Diatom subsamples of ~0.5 cm^3 volume were collected from the core, ensuring a sample at least every 500 cal years of the age-depth model. Treatment consisted of a wash with 30 wt/vol% hydrogen peroxide to remove organic matter (Battarbee et al., 2001), and the residue was mounted in Naphrax optical adhesive. Diatom valves were identified to species using taxonomic resources relevant to the Northern Rocky Mountains (Bahls, 2005; Spaulding and Edlund, 2016) and general references (Patrick and Reimer, 1975). A total of 300 diatom valves were enumerated per slide and analyzed as a percent of the diatom sum. Lake conditions were inferred from the diatom community based on species-level autecology.

Results

Chronology

The Goose Lake age-depth model was based on 15 of the 22 AMS radiocarbon ages, the age of the sediment-water interface, and Mazama ash (Figure 4.4). Radiocarbon ages were calibrated

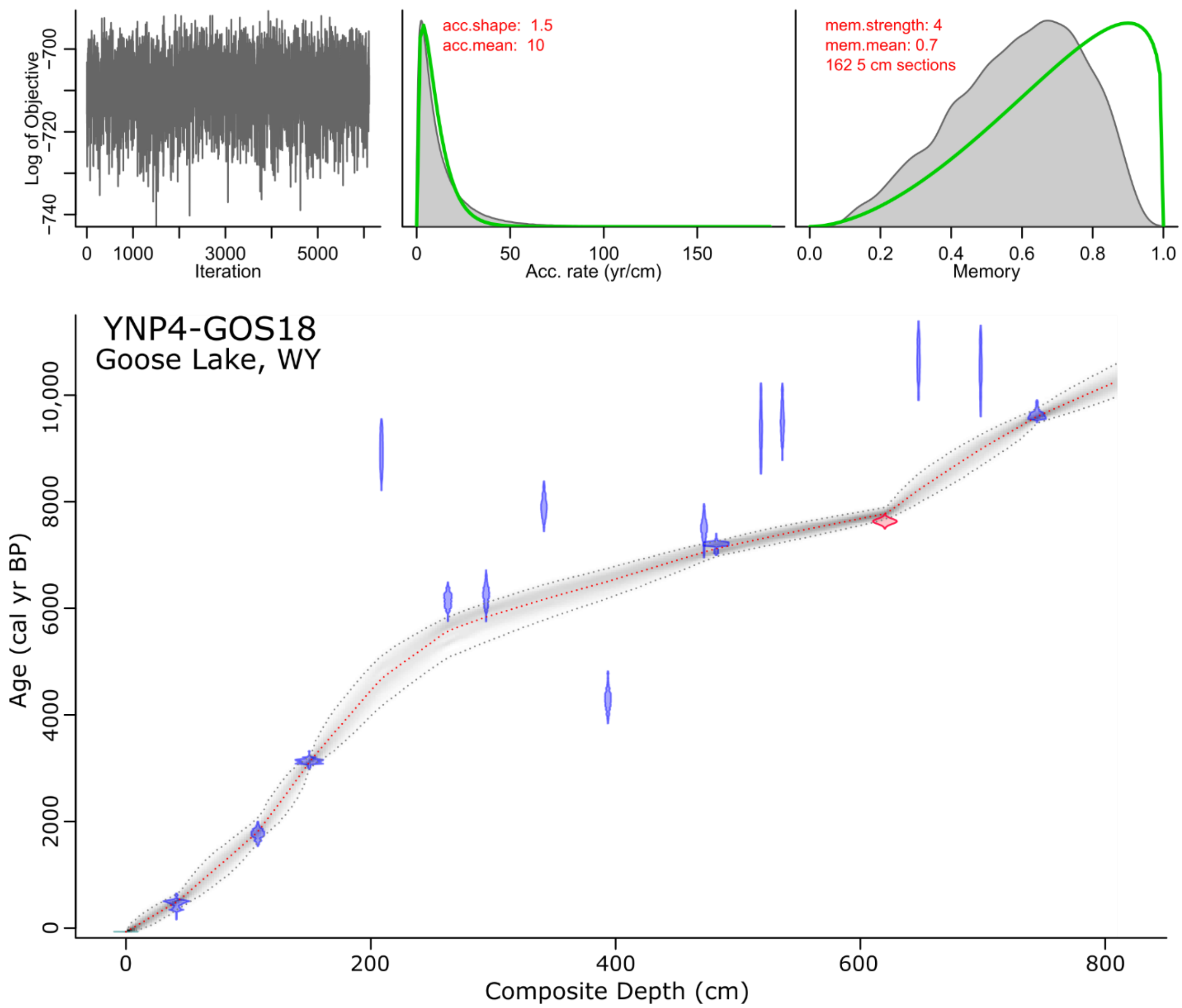

Figure 4.4: Bacon age-depth model for Goose Lake core. Red line is the median probability age from all run age-depth iterations, representing the best point estimate of age for any given depth which is used for remaining plots. Gray point cloud represents age model probability and contains a 95% confidence interval (dashed lines). Iteration history (left inset), prior and posterior densities of the mean accumulation rate (middle inset), and prior and posterior of the memory (right inset).

with the IntCal13 calibration curve (Reimer et al., 2013). A preliminary chronology suggested that some of the radiocarbon-dated samples were anomalously old. On the assumption that: (1) sediment accumulated over time without reversals and (2) the age of Mazama ash was most secure, we took a Bayesian approach to enforce a monotonic model. We constrained accumulation rates to positive values by setting a prior distribution for sediment deposition time with a mean of 10 years/cm^{-1} and a shape of 1.5 (Blaauw and Christen, 2011). Reversals in radiocarbon ages were addressed by using Student's t-distributions with heavier tails for our

Table 4.1. Goose Lake age determinations

Accession No.[1]	Core/Depth (cm)	Material Dated	Age ^{14}C	2σ cal Age Range (Probability)[2]
	0.0	Core Top		-68
OS-144345	41.25	charcoal	435 ± 55	316–399 (0.227), 422–545 (0.773)
OS-144559	107.75	charcoal	1840 ± 65	1609–1902 (0.989), 1910–1923 (0.011)
OS-144382	149.75	charcoal	2970 ± 20	3071–3185 (0.931), 3190–3209 (0.069)
OS-146794*	208.75	charcoal	8050 ± 340	8171–9709 (0.998), 9716–9735 (0.002)
OS-146796	263.0	charcoal	5390 ± 140	5893–6478 (1.000)
OS-144560	294.25	charcoal	5470 ± 150	5919–6565 (0.996), 6591–6600 (0.004)
OS-146789*	341.5	charcoal	7070 ± 190	7575–8218 (0.974), 8240–8305 (0.026)
OS-144561*	393.75	charcoal	3870 ± 120	3923–4614 (0.994), 4766–4784 (0.006)
OS-146790	472.25	charcoal	6620 ± 190	7160–7867 (0.993), 7899–7924 (0.007)
OS-146813	482.25	charcoal	6270 ± 35	7029–7043 (0.010), 7070–7077 (0.005), 7087–7111 (0.015), 7155–7272 (0.971)
OS-146791*	518.75	charcoal	8390 ± 330	8560–10,197 (1.000)
OS-146792*	536.25	charcoal	8500 ± 230	8989–10,192 (1.000)
	620.0	Mazama ash		7584–7682
OS-146793*	647.5	charcoal	9400 ± 290	9763–11,407 (0.993), 11,450–11472 (0.002), 11,557–11,597 (0.004)
OS-146795*	698.25	charcoal	9310 ± 330	9552–11,362 (0.998), 11,374–11,391 (0.002)
OS-146814	744.25	charcoal	8660 ± 50	9531–9744 (1.000)

[1]Measured at NOSAMS Laboratory at the Woods Hole Oceanographic Institution
[2]Calibrated age ranges calculated with CALIB ver. 7.1 according to method described in text
*Age outside of 95% range of final age-depth model, not used in final age model

calibrated ages (t_a = 3, t_b = 4) than for the ages of the tephra (t_a = 33, t_b = 44) (Christen and Perez, 2009). This approach allowed us to inform the model that the ages of the known tephra were more precise than other ages and increase their influence on the chronology accordingly (Blaauw et al., 2018). Finally, we used splines to model depth from the explicitly combined probability distribution of all ages (Blaauw and Christen, 2011).

Age reversals were present in the core below 178 cm depth, and seven radiocarbon dates were rejected by the Bacon model. All but OS-144561 were interpreted as erroneously old. The cause of these erroneously old ages is not clear, but old-carbon contamination from lake-sediment samples has been described in Yellowstone Lake (Chapter 2). It is likely that these samples contained old carbon sourced from either reworked sediment, volcanic CO_2 incorporated into plants during photosynthesis (Evans et al., 2010) or gases in the water column/surficial sediments (Chapter 2).

To address the uncertainty of point estimates of age from the age-depth model, median calibrated ages with standard deviations greater than 100 years are rounded to the nearest 100 cal years. The extrapolated age-depth model suggests a basal core age of 10,300 cal yr BP. A Holocene age is consistent with the fact that the basal pollen spectra were dominated by *Pinus contorta*-type, which was first abundant in Yellowstone Plateau pollen records after *ca.* 11,500 cal yr BP (Whitlock, 1993; Theriot et al., 2006). The age-depth model also suggests the presence of two changes in sediment accumulation rate. Sediment accumulation rates sharply increased between 4000 and 6000 cal yr BP, correlating with the lithological contact between Unit II and III at 647 cm depth. The slower sediment accumulation rate following Mazama ash deposition is probably an artifact of the Bacon model and the high confidence placed on the age of the

Mazama ash and the high influence of the basal radiocarbon date. Pre-Mazama ages were retained as they produce the best whole-core age-depth model, but age-dependent calculations from that interval are less certain the rest of the record.

Lithology and Geochemistry

Unit I (808.5–647 cm depth; 10,300–8200 cal yr BP) consisted of light olive-brown (2.5Y 5/3), indistinctly laminated diatomaceous ooze with clay (Figure 4.2). Diatoms and sponge spicules were dominant in smear slides. Diatoms were mostly intact. Peaks in sediment titanium were associated with lenses of inorganic clay and arsenic was relatively abundant throughout the interval. $\delta^{13}C$ value of bulk sediment was measured at -18.43 ‰ VPDB.

Unit II (647–178 cm depth; 8200–3800 cal yr BP) consisted of laminated diatomaceous ooze with sapropel and minor fragmental plant remains (Figure 4.2). Diatoms and sponge spicules were dominant in smear slides. Laminations were alternately grayish-brown (2.5Y 5/2), dark reddish-brown (5YR 3/2), and gray (GLEY1 5/N). Titanium peaks were associated with allochthonous deposits, included ashes and inorganic clay layers and arsenic was abundant throughout the unit. $\delta^{13}C$ values averaged -12.47 ‰ VPDB. An orange, inorganic clay was noted in the composite core at 628–629 cm depth (7900 cal yr BP; Figure 4.3). XRD analysis showed that it consisted of 81.1 wt. % fluorite (fluorite mud) and SEM-EDS measurements indicated abundant calcium and fluorine. Remaining weight fraction consisted of silica. SEM photomicrographs revealed diatom frustules and sponge spicules in a matrix of fluorite spherules (~0.5 μm matrix grain size, Figure 4.3). The fluorite mud was notably enriched in Sb relative to the other Goose Lake sediments, indicated by XRF (Figure 4.3).

Two ash deposits were noted in the composite core at 620–619 and 458.5–458 cm depth (Figure 4.2). The lower ash was white and composed dominantly of glass (~100%, much of which is pumiceous, grain size ~250–50 μm) with trace occurrence of plagioclase, mica (unknown green probably phyllosilicate), and quartz. Its color, abundant pumiceous glass fragments, and fine to very-fine sand grain size are consistent with the Mazama ash (Kittleman, 1973; Sarna-Wojcicki et al., 1983; Tiller, 1995). Presence of quartz is established with just a few grains, which may have been reworked. Hypersthene and hornblende, which characterize Mazama ash deposits elsewhere in the western North America (Kittleman, 1973; Sarna-Wojcicki et al., 1983; Tiller 1995), were not observed. The upper ash was dark colored and contaminated with a mixed composition of organic lacustrine material, reworked minerogenic sediment, and ash. The allochthonous fraction was composed chiefly of quartz (~60%) and glass (~40%, grain size <50 μm) with trace (<1%) occurrence of plagioclase, potassium feldspar, and clinopyroxene. Felsic mineral abundance (quartz, potassium feldspar) and limnic component suggest a local, rhyolitic source that was reworked and redeposited into Goose Lake.

Unit III (178–20.5 cm depth; 3800–200 cal yr BP) consisted of dark olive-brown (2.5Y 3/3), thinly bedded diatom ooze with sapropel (Figure 4.2), containing highly fragmented diatom frustules and chrysophytes. $\delta^{13}C$ values were considerably lower, -23.05 ‰ VPDB on average.

Unit IV (20.5–0 cm depth; 200– -68 cal yr BP) consisted of very dark grayish-brown (2.5Y 3/2), massive diatomaceous sapropel with high water content (Figure 4.2). Diatom frustules remained relatively intact and $\delta^{13}C$ values were similar to the previous interval, -25.30 ‰ VPDB.

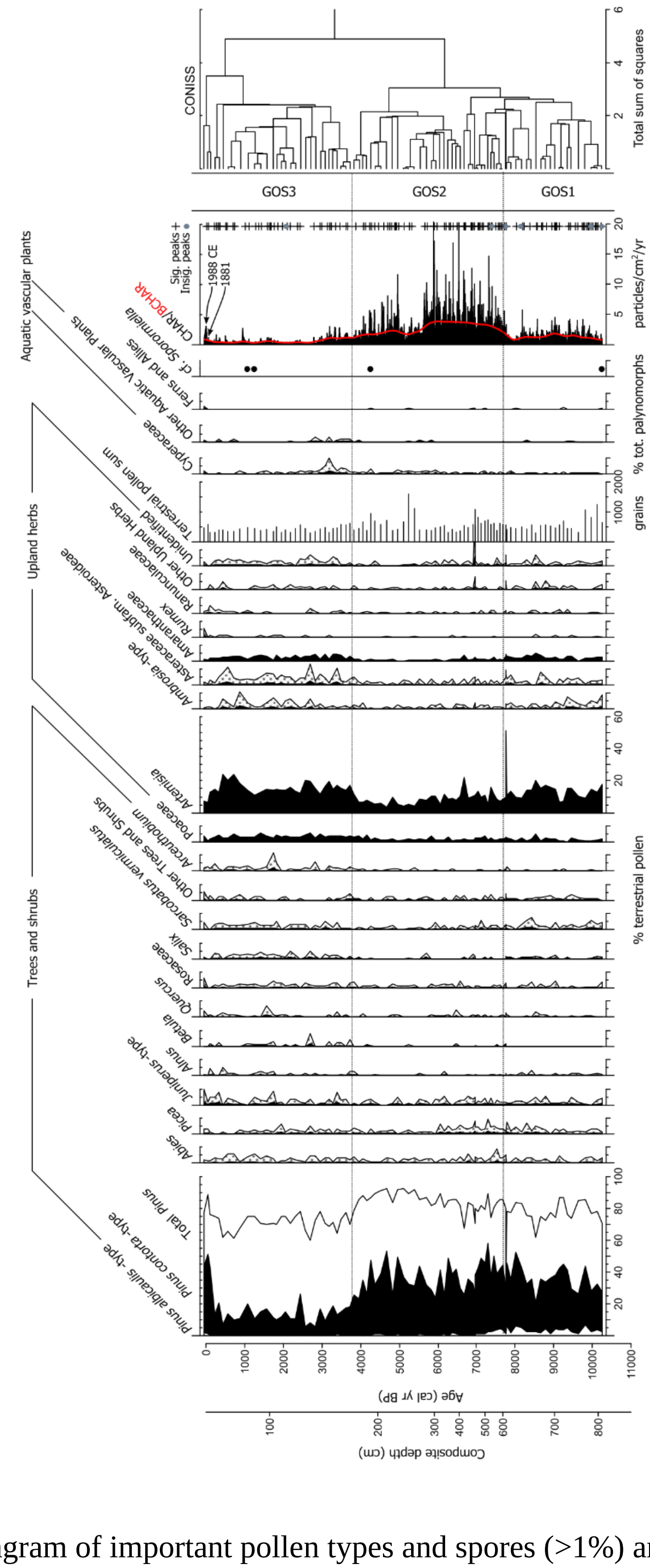

Figure 4.5. Percentage diagram of important pollen types and spores (>1%) and charcoal data (CHAR and BCHAR). Where present, curve exaggeration is 5×. Zone delineation is supported by CONISS dendrogram constructed with percentage data from terrestrial pollen.

Biological Proxies

The pollen data from Goose Lake were divided into three zones, based on transitions readily apparent with visual inspection and supported by CONISS (Figure 4.5, Grimm, 1987). These zones also defined changes in the charcoal and diatom records and were used as a framework for all biological proxy data.

Zone GOS1 (808.5–618 cm depth, 10,300–7800 cal yr BP) *Pinus* dominated the pollen spectra (77%, excluding a sample immediately above the Mazama ash) (Figure 4.5), most was assigned to *P. contorta*-type (81% of *Pinus* grains identifiable to subgeneric level). *Artemisia* (<13%), Amaranthaceae (<3%), and Poaceae (<2%) pollen were present in smaller proportions in Zone GOS1. A pollen sample immediately above the Mazama ash consisted of more *Artemisia* (51%) than *Pinus* (34%) and was the only sample of the record where the sum of nonarboreal pollen exceed arboreal pollen types, suggesting a brief (<8 years) vegetation change following ashfall. CHAR (mean 1.4 particles/cm^2/yr) was generally low (Figure 4.5), although the uppermost CHAR values were probably artificially deflated due to the rapid increase in sediment accumulation time noted above (Figure 4.4). Mean fire frequency reached its highest values of the record (14 episodes/1000 years).

The diatom record was dominated by *Cyclotella meneghiniana* (28%) and *Diatoma moniliformis* (21%) with lesser amounts of *Navicula wildii* (12%), *Amphora copulata* (9%), *Gomphonema gracile* (7%), and *Achnanthidium minutissimum* (7%). The lower portion of this zone was dominated solely by *C. meneghiniana* (Figure 4.6), but by mid-zone, *C. meneghiniana* abundance decreased and *D. moniliformis* and *N. wildii* co-dominated. *Botryococcus* (89,981 NISP/cm^2/yr) dominated the coccal algae assemblage with few *Pediastrum* (56 NISP/cm^2/yr).

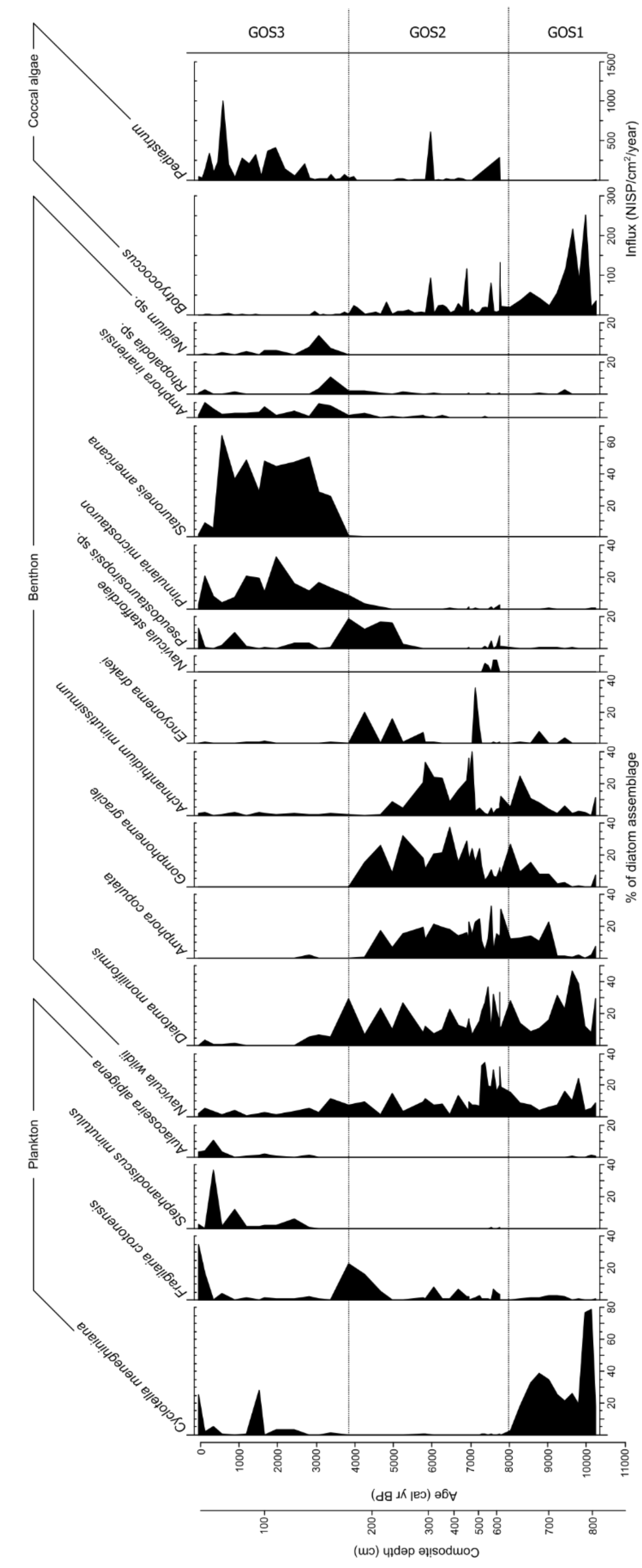

Figure 4.6: Percentage diagram of important diatom types and coccal algae.

Zone GOS2 (618–178 cm depth, 7750–3800 cal yr BP) Percentages of *Pinus* percentages increased in Zone GOS2 with the abundance reaching 84% at the top of the zone (Figure 4.5). *P. contorta*-type accounted for 93% of identifiable *Pinus*. Increased *Pinus* percentages came at the expense of upland herb taxa, with lower abundances of *Artemisia* (<9%), Amaranthaceae (<2%), and Poaceae (<2%) than before. A horizon rich in degraded, indeterminate herbaceous pollen grains (457.5 cm depth, 6950 cal yr BP) was associated with the reworked Yellowstone ash at 458 depth, and likely redeposited during the same geomorphic or climatic event. CHAR (mean 3.5 particles/cm^2/yr) substantially increased compared to Zone GOS1 (Figure 4.5). Mean fire frequency was somewhat lower than before (13 episodes/1000 years).

The diatom record shows a loss of *Cyclotella meneghiniana* and continued abundance of *Diatoma moniliformis* (17%), *Gomphonema gracile* (17%), *Amphora copulata* (16%), *Navicula wildii* (13%), and *Achnanthidium minutissimum* (12%) (Figure 4.6). Additionally, the upper part of this zone (225–178 cm depth, 4970–3960 cal yr BP) contained a peak in *Encyonema yellowstonianum* (9%) and synchronous increase in *Pseudostaurosiropsis* sp. (16%). The coccal algae assemblage consisted of *Botryococcus* (20,211 NISP/cm2/yr) and Pediastrum (3167 NISP/cm2/yr). Pediastrum assemblage was dominated by *P.* cf. *boryanum* var. *longicorne* with low numbers of *P. integrum*.

Zone GOS3 (178–0 cm depth, 3800– -68 cal yr BP) Zone GOS3 was characterized by less *Pinus* than before (72%). Total *Pinus* continued to be dominated by *P. contorta*-type (95% of identifiable *Pinus*) (Figure 4.5). Major upland herb taxa concurrently increased in abundance, including *Artemisia* (<16%), Amaranthaceae (<3%), and Poaceae (<4%). Other upland herb types were rare, but consistently detected in Zone GOS3, including *Ambrosia*-type (<1%) and

Asteraceae subfam. Asteroideae (<1%). Riparian shrubs *Alnus* (<1%), *Betula* (<1%), and *Salix* (<1%) also reached their highest abundances of the record. *Arceuthobium* (<1%) was consistently detected for the first time in Zone GOS3. CHAR (mean 9.6 particles/cm^2/yr) was at the lowest values of the record (Figure 4.5). Mean fire frequency also substantially declined (to 10 episodes/1000 years). The median calibrated ages from the two uppermost CHAR peaks (1988–1948 CE, 1903 CE) correlate well with fires in 1988 and 1881 within LGB (W.H. Williams *personal communication* 2020).

The Zone GOS3 diatom assemblage was dramatically different than previous zones and dominated by *Stephanodiscus minutulus* (5%), *Pinnularia microstauron* (14%), and *Stauroneis americana* (31%) (Figure 4.6). Additionally, diatom abundance was lower in this zone compared to previous ones, whereas chryophyte cysts were more abundant. The coccal algae assemblage was dominated by *Pediastrum* (15,294 NISP/cm^2/yr) with a lesser amount of *Botryococcus* (1880 NISP/cm^2/yr). As in Zone GOS2, the *Pediastrum* assemblage was dominated by *P.* cf. *boryanum* var. *longicorne* with subordinate numbers of *P. integrum*.

DISCUSSION

We consider LGB to represent a geo-ecosystem, given the close interrelationship between physical geological processes and ecological processes. Changes to climate, hydrology, and geology affect the terrestrial and limnological components of this ecosystem. The geochemical and lithological data from Goose Lake present primary evidence for changes in hydrothermal activity at Goose Lake and the pollen, charcoal, and diatom records describe basin-wide vegetation and limnological changes for comparisons with other sites on the Yellowstone Plateau.

Past hydrothermal activity at Goose Lake

Hydrothermal discharge impacted Goose Lake core from *ca.*10,300 cal yr BP to 3800 cal yr BP, based on geochemical and lithologic data. Arsenic is abundant in lithological units I and II, which date to this period, and is present in sediments of hydrothermal provenance elsewhere on the Yellowstone Plateau (Morgan et al., 2009) as well as in present-day hydrothermal fluids in LGB (Stauffer and Thompson, 1984; McCleskey et al., 2005; Ball et al., 2006). In addition, the deposition of antimony-rich fluorite mud at ca. 7900 cal yr BP (619–618 cm depth), albeit for a short period, also points to a hydrothermal provenance, inasmuch as fluorite is a common accessory mineral in rhyolite flows that underlie Goose Lake (Bargar and Beeson, 1981), and fluorine (Bargar et al., 1973) and antimony (Stauffer and Thompson, 1984) are abundant in geothermal waters from LGB. Lithologic units I and II also have less negative $\delta^{13}C$ values from bulk sediment (-18.43– -9.7 ‰ VPDB) than overlying units, possibly pointing to an admixture of hydrothermally degassed C (near 0 ‰ VPDB), which is less negative than terrestrial vegetation (Craig, 1963; Werner and Brantley, 2003). In addition, the lighter color and more distinct lamination (Figure 4.2) of sediments, especially in unit II, suggest frequently shifting limnological conditions, as might be produced by varying levels of hydrothermal discharge.

Hydrothermal activity ceased abruptly at *ca.* 3800 cal yr BP for unknown reasons. Rapid, widespread changes in hydrothermal activity have been known to occur on the Yellowstone Plateau as a result of earthquakes (Marler and White, 1975; Pitt and Hutchinson, 1982) or ground deformation (Vaughan et al., 2020). The 1959 Hebgen Lake Earthquake (M 7.1, epicenter about 40 km from the LGB's thermal areas), for example, caused many existing thermal features to erupt vigorously, creating new thermal features (notably Seismic Geyser) and causing the dormancy of others (Marler and White, 1975). A similar geologic event at *ca.* 3800 cal yr BP may have extinguished the hydrothermal feature(s) at Goose Lake.

Development of the LGB geo-ecosystem within a regional context

To determine if past hydrothermal activity influenced the ecosystem development of LGB, we compare the proxy data at Goose Lake with three other paleoecological records from the Yellowstone Plateau. We assume that if sites broadly show concurrent changes in the past, a regional forcing, such as climate, was the likeliest, most parsimonious cause. When a vegetation or fire regime change occurred only at one site, the forcing is attributed to local drivers, such as shifts in fire or hydrothermal activity. Pollen data suggest that the Yellowstone Plateau supported forests dominated by *Pinus contorta* for the last 11,000 cal years, and we use percent *Pinus* pollen as an indicator of forest closure or extent. To evaluate vegetation change across sites, the records at Goose Lake with those at sites that lack significant surficial hydrothermal activity: Cygnet Lake (Whitlock, 1993; Millspaugh et al., 2000), Loon Lake (Whitlock et al., 1995), and Yellowstone Lake (Chapter 3, Table 2). The vegetation and size of Cygnet Lake is most comparable to Goose Lake, to it is used as the primary source of vegetation comparison in the following synthesis (Figure 4.7) Goose Lake charcoal record was compared with the charcoal record at Cygnet Lake (Millspaugh et al., 2000). CharAnalysis was conducted for Cygnet Lake charcoal data in the same manner as Goose Lake, except BCHAR values were calculated with the use of a 700-year lowess smoother (which minimized the sum of the median signal to noise index and the goodness of fit value), robust to outliers.

Table 4.2. Paleoecological sites within *Pinus contorta* forest

Site	Location	Elevation (m.a.s.l.)	Modern vegetation	Source
Loon Lake	44.11°N 110.94°W	1968	*P. contorta* forest	Whitlock et al., 1995*
Cygnet Lake	44.39N 110.36W	2530	*P. contorta forest*	Whitlock, 1993*; Millspaugh et al., 2000†
Yellowstone Lake	44.5°N 110.3°W	2350	Forest-meadow mosaic with abundant *P. contorta*	Brown et al., *in prep**

*Source of pollen data, †source of charcoal data

<u>Holocene climate history of the Yellowstone Plateau</u> The Holocene climate history was strongly influenced by slow variations in the seasonal cycle of insolation, which led to a summer insolation maximum in the Northern Hemisphere at *ca.* 11 ka and a steady decline in summer insolation thereafter (Laskar et al., 2004). The Yellowstone Plateau has a summer-dry precipitation regime (*sensu* Whitlock and Bartlein, 1993), and the summer insolation maximum (summer anomaly up to ~30 W/m^2 at 44.5°N; Laskar et al., 2004) in this region resulted in warmer conditions than present (i.e., 20th century average) on the Yellowstone Plateau and effectively drier conditions as a result of the expansion and strengthening of the northeastern Pacific subtropical high-pressure system (Whitlock and Bartlein, 1993; Bartlein et al., 1998). In the middle and late Holocene, summers on the Yellowstone Plateau became cooler and effectively wetter than before, due to declining summer insolation and the attendant weakening of the northeastern Pacific subtropical high, leading to the establishment of present climate (hereafter "present" in this context refers to the mid-20th century average) (Whitlock and Bartlein, 1993; Bartlein et al., 1998).

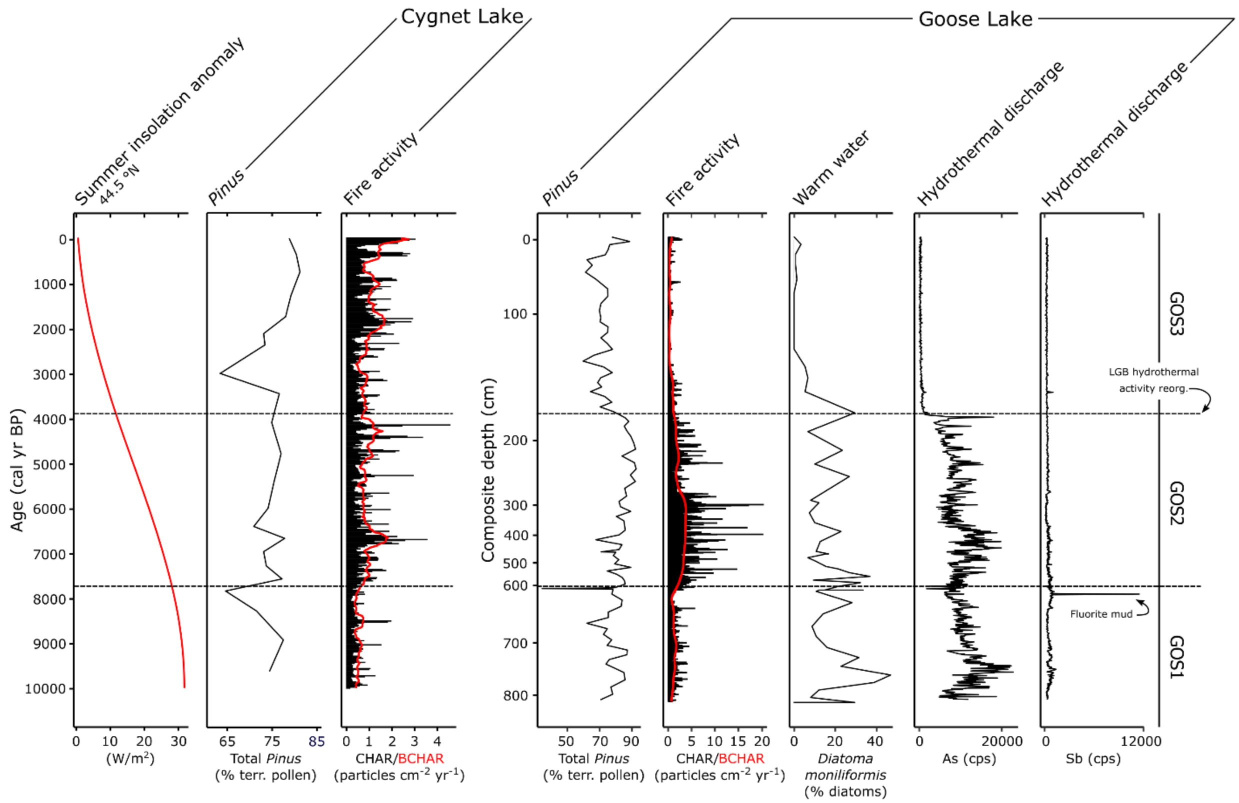

Figure 4.7. Synthesis plot of proxy data from the Goose Lake composite core. Seasonal insolation anomaly calculated for 44.5°N (Laskar et al., 2004). *Pinus* pollen percentages (Whitlock, 1993) and CHAR (Millspaugh et al., 2000) are plotted for Cygnet Lake, which is a nearby site that does not feature any hydrothermal activity.

<u>Early Holocene (GOS1, >10,300–7800 cal yr BP)</u> Pollen records from Cygnet Lake, Loon Lake, and Yellowstone Lake indicate that the *Pinus contorta* forest was relatively open or less extensive, compared with the Holocene-long average, as evidenced by the low *Pinus* percentages (Whitlock, 1993; Whitlock et al., 1995; Chapter 3, Figure 4.7). The landscape at Goose Lake was similarly open, as evidenced by comparatively low percentages of *Pinus* (77%) and relatively high abundance of shrub and herb pollen, largely from *Artemisia*, Poaceae, and Amaranthaceae. The deposition of Mazama ash at 7630 cal yr BP (Egan et al., 2015) led to a short-term proliferation of *Artemisia*, as indicated by the spike in *Artemisia* pollen percentages

immediately above the ash. This spike is attributed to short-lived mulching effects of volcanic ash on the landscape (Schiller et al., 2020).

The charcoal record from Cygnet Lake shows that fire activity was generally low in the early Holocene, evidenced by the CHAR of the record (mean CHAR 0.53 particles/cm^2/yr). Fire activity at Goose Lake was similarly low in this period, compared with the rest of the record (mean CHAR 1.35 particles/cm^2/yr). This period at Goose Lake had the highest fire frequency of the record (14.45 episodes/1000 years) with relatively small charcoal peak magnitudes, suggesting that fire episodes were frequent, small and/or of low severity in the early Holocene. This fire regime may have helped to maintain relatively open vegetation at Goose Lake.

The diatom assemblage of GOS1 indicates that Goose Lake was shallower than at present with oligotrophic to mesotrophic conditions at Goose Lake. *Cyclotella meneghiniana*, *Amphora copulata*, and *Achnanthidium minutissimum* are favored by oligotrophic to mesotrophic conditions (Parsons et al., 2006; Salm et al., 2009; Saros and Anderson, 2015). *C. meneghiniana* populations are abundant in well-mixed or relatively shallow lakes (Reynolds, 1980), blooming in response to influxes of nitrogen and phosphorous (Salm et al., 2009). The presence of *Diatoma moniliformis* is consistent with water temperatures greater than 10–15°C (Pniewski and Sylwestrzak, 2018) and/or harsh conditions, inasmuch as the species is found in nuclear power-plant cooling channels today (Potapova and Snoeijs, 1997). Another benthic species, *Navicula wildii*, prefers neutral to moderate alkalinity (Bahls, 2012), and *Achnanthidium minutissimum* is present in a wide variety of pH conditions (Ponader and Potapova, 2007). *Gomphonema gracile* is a cosmopolitan benthic species. The diatom assemblage, along with the preservation of diatoms and palynomorphs, which are destroyed under strongly alkaline conditions, indicates that the water pH was neutral to somewhat alkaline, similar to that of most LGB hydrothermal features today (Vaughan et al., 2014). The dominance of *C. meneghiniana* from 10,300 to 9800 cal yr BP suggests an initial period of high nutrient input, and the later abundance of low-nutrient specialist *A. copulata* implies decreasing nutrient availability after 9420 cal yr BP.

Botryococcus was abundant in Goose Lake in the early Holocene, while *Pediastrum* was nearly absent, an assemblage often interpreted as evidence of extremely cold, oligotrophic, or acidic waters (Jankovská and Komárek, 2000). Those conditions seem unlikely at this time at Goose Lake, in light of the diatom assemblage, which suggests neutral to alkaline water chemistry, and inferred warm, dry conditions (Whitlock and Bartlein, 1993). A non-climate explanation for abundant *Botryococcus* may be high levels of arsenic. Modern waterways contaminated by anthropogenic arsenic have abundant *Botryococcus*, with little to no *Pediastrum* (Meeinkuirt et al., 2008). *B. braunii* has, in fact, shown some promise as a bioremediator of environmental arsenic (Onalo et al., 2014; Podder and Majumder, 2016). Taken together, the diatom and coccal algae assemblages indicate warm, somewhat alkaline, and arsenic-rich conditions associated with hydrothermal discharge into Goose Lake.

In summary, the early-Holocene vegetation history at Goose Lake resembled that of the Yellowstone Plateau as a whole, with relatively open *Pinus contorta* forest or expanded non-forested vegetation with frequent fires during a time of warm, dry climate during the summer insolation maximum. Within LGB, there is no evidence that hydrothermal activity altered the upland vegetation to a large extent during the early Holocene. Nonetheless, hydrothermal waters discharged directly into Goose Lake, as the geochemical and lithological characteristics of the sediments and limnobiotic communities indicate.

Middle Holocene (GOS2, 7750–3800 cal yr BP) Pollen percentage records from Cygnet Lake, Loon Lake, and Yellowstone Lake suggest that *P. contorta* forest became more closed or extensive region-wide in the middle Holocene (Whitlock, 1993; Whitlock et al., 1995; Chapter 3, Figure 4.7). At Goose Lake, *P. contorta* forest became similarly closed or extensive through this period, as *Pinus* percentages increased (up to 84%) at the expense of those of non-forested taxa (Figure 4.5).

The charcoal record suggests that fire activity increased at Cygnet Lake in this period (mean CHAR 0.96 particles/cm^2/yr, Figure 4.7). This increase in fire activity is coupled with particularly extreme (large or severe) fire episodes, evidenced by high charcoal peak magnitudes at Cygnet Lake (Millspaugh et al., 2000) and Yellowstone Lake (Brown et al., *in prep*). Peak magnitude data, coupled with more frequent fire episodes at Cygnet Lake in this interval as summer insolation rose (Millspaugh et al., 2000), allows one to infer that Yellowstone Plateau fire episodes in the middle Holocene were larger/more severe and less frequent than the early Holocene. Charcoal levels at Goose Lake were higher than the early Holocene (mean CHAR 3.45 particles/cm^2/yr), indicative of enhanced fire activity similar to regional trends. Charcoal peak frequency indicate fewer fire episodes than before (mean 13.23 episodes/1000 years) and increased mean CHAR together suggest that fires were less frequent than in the early Holocene, but probably larger or more severe (Figure 4.5), similar to inferences from other sites in the region.

The middle Holocene diatom assemblage at Goose Lake is similar to that of the early Holocene, except for the conspicuous absence of *Cyclotella meneghiniana*. The dominance of benthic taxa suggests a hydrologic change, but it is unclear whether water level was higher or lower than before given the broad, flat bathymetry of Goose Lake (Figure 4.1). Persistence of species with warm-water preferences (*Diatoma moniliformis*) and wide pH tolerance ranges (*Achnanthidiuim minutissimum*, *Navicula wildii*, and *Pseudostaurosiropsis* sp., Ciniglia et al., 2007) indicates that the diatom assemblage continued to be influenced by hydrothermal inputs through this period. Low nutrient availability is indicated by *A. minutissimum* and *Amphora copulata*. Peaks of *Encyonema yellowstonianum* and *Pseudostaurosiropsis* sp., both colonial tube-forming taxa, suggest periods of enhanced turbidity (Krammer, 1997; Ciniglia et al., 2007). *Botryococcus* and *Pediastrum* both occur in this interval, suggesting improved limnic conditions for *Pediastrum* growth.

During the middle Holocene, the vegetation history at Goose Lake continued to resemble that of other sites on the Yellowstone Plateau, with increasingly closed or extensive *Pinus contorta* forest and greater fire activity during a time of increasingly cool, effectively wet summers, based on pollen and charcoal data. Geochemical and limnobiotic proxies indicate a sustained hydrothermal influence at Goose Lake. Other local scale factors were important for the diatom community as well, including shifts in lake level and enhanced turbidity.

<u>Late Holocene (GOS3, 3800 cal yr BP–present)</u> *Pinus* percentage data from Cygnet Lake, Loon Lake, and Yellowstone Lake suggest continued expansion of *Pinus contorta* (Figure 4.7). At Goose Lake, a decline in *Pinus* forest closure or extent was evidenced by decreased *Pinus* and increased *Artemisia*, Poaceae, and Amaranthaceae pollen percentages, diverging from the regional, composite trend (Figures 4.5, 4.7). This shift marks the establishment of present-day open vegetation in LGB. *Artemisia* and Amaranthaceae are not abundant in present-day local vegetation, and their high pollen percentages after *ca.* 3800 cal yr BP may come from long-

distance sources in the Snake River Plain as the vegetation in LGB opened. Both *Artemisia* and Amaranthaceae are prolific pollen producers and their long-distance transport from low elevation, semiarid regions has been documented in modern pollen studies in the region (Fall, 1992). Moreover, up to 30% *Artemisia* pollen is found in modern pollen samples from all vegetation types in the Yellowstone region (Iglesias et al., 2018), illustrative of its broad dispersal capacity. Steady but low amounts of *Alnus* (<1%), *Betula* (<1%), and *Salix* (<1%) pollen in the late Holocene (Figure 4.5) suggest the presence of riparian areas and wet meadows Goose Lake.

Charcoal levels continued to increase at Cygnet Lake (mean CHAR 1.08 particles/cm2/yr, Figure 4.7), evidence of increased fire activity. In contrast, fire activity (mean CHAR 9.64 particles/cm^2/yr) declined at Goose Lake suggesting a more open landscape with less fuel biomass. Fire episodes, evidenced by charcoal peaks, were also less frequent than before at Goose Lake (9.64 episodes/1000 years, Figure 4.5).

The late-Holocene diatom assemblage at Goose Lake is starkly different from previous periods and suggest that the water column was better mixed with relatively low conductivity. The dominant taxa were *Stephanodiscus minutulus, Pinnularia microstauron,* and *Stauroneis americana*. *S. minutulus* is a planktic, high-phosphorous specialist with low nitrogen and silica requirements that blooms in early spring during isothermal mixing (Lynn et al., 2000; Interlandi et al., 2003; Theriot et al., 2006). *P. microstauron* is a benthic species that favors oligotrophic, oxygen-rich waters with low conductivity (Krammer, 2000). *S. americana* is benthic, preferring wetlands with low to moderate conductivity (Vijver et al., 2005). *Pediastrum* dominated the coccal algae assemblage at Goose lake in this interval, probably growing along the shallow margins of Goose Lake despite oligotrophic conditions (Jankovská and Komárek, 2000).

In summary, abrupt reorganization of hydrothermal activity in LGB at ca. 3800 cal yr BP had a profound impact on the vegetation of LGB and the limnobiota at Goose Lake (Figure 4.7). The Goose Lake pollen record diverged from other records at 3800 cal yr BP, showing evidence of an open or contracted forest at a time when forests were becoming more closed elsewhere on the Yellowstone Plateau. The development of more-open vegetation may mark the time when a broad sinter flat developed in LGB, creating an open landscape with less extensive *Pinus contorta* forest. The diatom taxa that thrived in warm, thermally influenced waters declined and *Botryococcus*-dominated coccal algae assemblage was fully replaced by *Pediastrum*. A shift in hydrothermal activity away from the lake and the creation of broad hydrothermal flats, seems the likely cause for these biotic changes at Goose Lake and the abiotic changes inferred from lithology and geochemistry.

Conclusions

The Goose Lake study suggests that LGB experienced a marked shift in hydrothermal activity during the last *ca.* 10,300 years that affected the terrestrial and aquatic ecosystems, based on the following observations:

1. Hydrothermal fluids discharged directly into Goose Lake prior *ca.* 3800 cal yr BP and had little influence on the upland basin vegetation. In the early and Middle Holocene, the *Pinus contorta* forest of LGB became increasingly closed and fire activity was generally high. Limnic conditions were impacted by hydrothermal discharge, evident

in diatom and coccal algae communities adapted to extreme, warm, and potentially somewhat alkaline conditions.

2. An abrupt reorganization of hydrothermal activity in LGB occurred at ca. 3800 cal yr BP, when hydrothermal waters no longer fed directly into Goose Lake. A seismic event may have triggered this shift in basin hydrothermal activity, just as recent earthquakes and deformation have done.
3. At *ca.* 3800 cal yr BP, hydrothermal activity became more extensive in LGB, leading to expansion of non-forested vegetation. The late Holocene vegetation and fire history at Goose Lake diverges from other sites on the Yellowstone Plateau reflecting the development of the modern, treeless hydrothermal flat.

This study of landscape evolution from an active hydrothermal landscape complements existing studies, which have studied the age of thermal features from direct radiometric dating (Marler, 1956; Lowenstern et al., 2016). The Goose Lake record provides more holistic information on the evolution of a hydrothermal landscape, including the impact of hydrothermal activity on surrounding terrestrial and limnic ecosystems. Building upon past investigations of hydrothermal activity on the Yellowstone Plateau (Pitt and Hutchinson, 1982; White et al., 1988; Vaughan et al., 2020), the Goose Lake record indicates that vegetation development was governed by a combination of regional climatic and local geologic forcings.

Acknowledgements

This research was supported by the National Science Foundation (1515353 to C. Whitlock) as part of the HD-YLAKE project, and a research fellowship from the Montana Institute on Ecosystems to C.M. Schiller. Field work was conducted under Yellowstone National Park permit

YELL-2018-SCI-0009. Goose Lake coring was aided by A. Carlson, R.E. Gresswell, N.E. Kichas, and W.P. Nanavati. We are indebted to J.A. Eggers, B. Hosseini, D.W. Mogk, and E. Roehm for laboratory assistance. S.C. Fritz provided helpful feedback on diatom interpretations. This work was performed in part at the Montana Nanotechnology Facility, a member of the National Nanotechnology Coordinated Infrastructure (NNCI), which is supported by the NSF Grant No. ECCS-1542210.

CHAPTER FIVE

VEGETATION RESPONSES TO QUATERNARY VOLCANIC AND HYDROTHERMAL DISTURBANCES IN THE NORTHERN ROCKY MOUNTAINS AND GREATER YELLOWSTONE ECOSYSTEM

Contribution of Authors and Co-Authors

Manuscript in Chapter 5

Author: Christopher M. Schiller

Contribution: Led field work at Cub Creek Pond and Goose Lake, conducted new pollen analyses at Cub Creek Pond, Goose Lake, and Yellowstone Lake, completed statistics, and led manuscript development.

Co-Author: Cathy Whitlock

Contribution: Provided funding and conceived of and edited the manuscript.

Co-Author: Mio Alt

Contribution: Contributed new pollen analyses at Twin Lakes, MT and contributed to the manuscript.

Co-Author: Lisa A. Morgan

Contribution: Provided lithological descriptions and edited the manuscript.

Manuscript Information

Christopher M. Schiller, Cathy Whitlock, Mio Alt, Lisa A. Morgan

Palaeogeography, Palaeoclimatology, Plaeoecology

Status of Manuscript:
_____ Prepared for submission to a peer-reviewed journal
_____ Officially submitted to a peer-reviewed journal
_____ Accepted by a peer-reviewed journal
__×__ Published in a peer-reviewed journal

Elsevier
Vol. 559, p. 109859
https://doi.org/10.1016/j.palaeo.2020.109859

CHAPTER FIVE

VEGETATION RESPONSES TO QUATERNARY VOLCANIC AND HYDROTHERMAL DISTURBANCES IN THE NORTHERN ROCKY MOUNTAINS AND GREATER YELLOWSTONE ECOSYSTEM

Abstract

Volcanic and hydrothermal processes produce disturbances by diverse mechanisms and ecological responses are varied. New and published pollen records from the Northern Rocky Mountains and Greater Yellowstone Ecosystem document the response of vegetation to three different types of volcanic and hydrothermal disturbances: (1) Pleistocene rhyolite lava flows in the central Greater Yellowstone Ecosystem created infertile landscapes that have shaped vegetation since rhyolite emplacement. Nutrient-poor, well-drained soils that developed on these flows supported low-diversity grassland during late-glacial time and *Pinus contorta* forests in interglacial periods. (2) Ash layers from eruptions of Pacific Northwest stratovolcanoes are commonly preserved in lake-sediment records in the Northern Rocky Mountains, and associated pollen records show enhancement of steppe vegetation for years to decades. (3) Local hydrothermal explosions have resulted in vegetation changes in hydrothermal areas that indicate tree mortality following deposition of explosion debris, followed by recovery in years. Thus, the type and duration of the vegetation response to volcanic and hydrothermal disturbances is highly contextual and governed by the antecedent plant communities and the magnitude and mechanism of the volcanic or hydrothermal disturbance. Vegetation resilience varied between disturbances,

ranging from enduring ecosystem parameter changes to short-lived state changes in resilient plant communities.

Introduction

Plant succession following volcanic disturbances may be chiefly primary and long lasting in places where soil and antecedent vegetation are destroyed, such as after lava flows (Clarkson and Clarkson, 1983; del Moral and Grishin, 1999 and citations therein), pyroclastic flows, and lahars. Faster, secondary succession processes may occur following less destructive ashfall (Antos and Zobel, 1985, 1986; Lees and Neall, 1993; Martin et al., 2009; Chaneton et al., 2014) and scorch (Winner and Casadevall, 1983; Seymour et al., 1983). Hydrothermal disturbances, triggered by hot water circulating in the subsurface above a magma chamber at depth, may cause localized plant death or stunted growth by heating soils (White et al., 1988; Lowenstern et al., 2003) and releasing hot, silica- or calcium carbonate-saturated fluids or gases (CO_2, H_2S, or steam) on the landscape (Miller and Cooper, 1969; Pitt and Hutchinson, 1982; Bryan, 1995), potentially through intratissue deposition of minerals (Channing and Edwards, 2003). A more extreme form of hydrothermal disturbance, large hydrothermal explosions, creating large (>100-m diameter) craters, may inundate areas as much as 30 km^2 (Morgan et al., 2009) and potentially bury vegetation with excavated rock debris and mud deposits up to several meters thick (Browne and Lawless, 2001; Morgan et al., 2009). Similar to other types of ecological disturbances, such as fire, herbivory, and pathogen outbreaks, volcanic and hydrothermal disturbances vary by size, severity, and frequency, which shapes their impact on terrestrial vegetation. In particular, volcanic and hydrothermal processes are complex disturbances that impact the landscape through multiple mechanisms and the recovery can be short term or last for millennia (del Moral and Grishin, 1999 and citations therein).

Volcanic and hydrothermal disturbances have occurred through geologic time, yet their impacts on terrestrial plant communities are not well understood in many settings. We consider three types of these disturbances in the Northern U.S. Rocky Mountains (NRM) and Greater Yellowstone Ecosystem (GYE) (Figure 5.1): (1) extensive rhyolite lava flows from the Yellowstone Plateau Volcanic Field (Christiansen, 2001); (2) ashfall from Cascades stratovolcanoes, located about 500 to 800 km to the west, particularly the eruption of Mount Mazama in southwestern Oregon; and (3) postglacial hydrothermal explosions within the Yellowstone Caldera. We draw upon new and published paleoecological data from the NRM and GYE that reveal the vegetation response to different types of volcanic and hydrothermal disturbances. Furthermore, we hypothesize whether vegetation communities recover from such disturbances or whether they are permanently transformed by the event. This information helps us develop a conceptual framework for understanding the resilience of plant communities to volcanic and hydrothermal disturbances of different magnitude and duration. Documented impacts of these volcanic and hydrothermal disturbances suggest that vegetation resilience may have varied greatly between them.

The first example focuses on the most recent cycle of caldera-forming volcanism in the GYE, which produced extensive lava flows and ignimbrites starting ~1.3 Ma until ~70 ka (Christiansen, 2001; Wotzlaw et al., 2015). The composition of these volcanic rocks is dominated by rhyolite, with estimates of 6500 km^3 of rhyolite and 250 km^3 of basalt; no intermediate volcanic rocks are recognized (Christiansen, 2001). *Pinus contorta* dominates

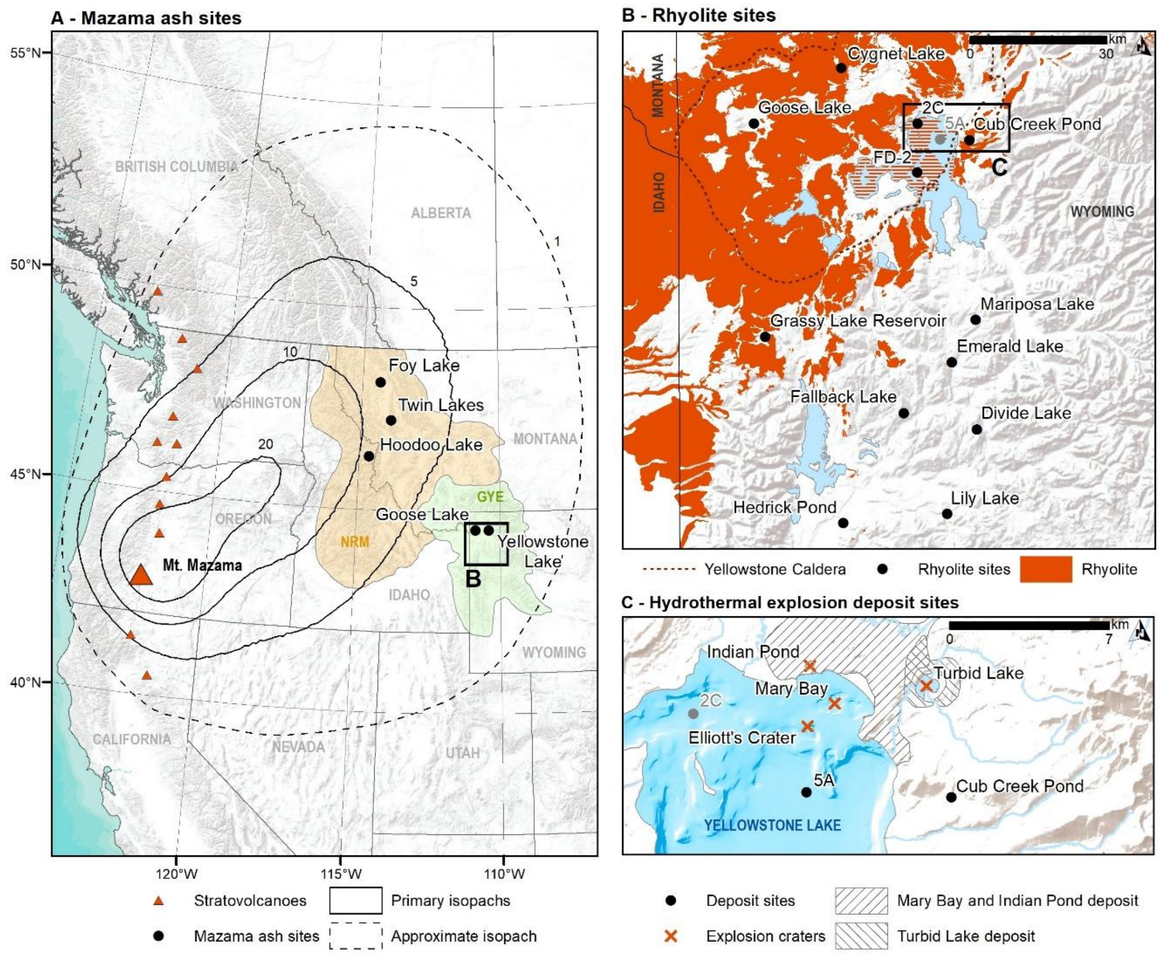

Figure 5.1: (A) Northern Rocky Mountains (NRM, orange) and Greater Yellowstone Ecosystem (GYE, green) sites used in the Mazama ash comparison, with primary deposition isopach of Buckland et al. (2020). 20-, 10-, and 5-cm isopachs are well-constrained with 45 sampled localities, but the 1-cm isopach is considered approximate due to a paucity of sites (Buckland et al. 2020). NRM sites are generally characterized by thicker Mazama ash deposits than GYE sites. (B) GYE lake sediment sites used in the comparison of postglacial vegetation histories on rhyolitic and non-rhyolitic substrates, with the mapped extent of rhyolite (Bond et al. 1978; Green et al. 1994; Green et al. 1999; Christiansen 2001) and the margin of the Yellowstone Caldera as mapped by Christiansen (2001), modified within Yellowstone Lake by Morgan et al. (2003; 2007) (dotted line). (C) Sites with hydrothermal explosion deposits with a high-resolution bathymetric map of northern Yellowstone Lake with large (>100 m diameter) sublacustrine and subaerial hydrothermal explosion craters indicated (Morgan et al. 2007; Morgan et al. 2009). Areas of Mary Bay and Turbid Lake hydrothermal explosion breccia deposits are plotted as mapped by Christiansen (2001) and modified by Morgan et al. (2009). Sites situated in the mapped extent of an inset, but not used for the labelled comparison, are included in gray.

forests on rhyolitic substrates (Despain, 1990; Figure 5.1) as the soils are too nutrient poor and well drained to support most of the region's conifer taxa (Despain, 1990; Anderson and Romme, 1991). Pollen records from sites on rhyolite have demonstrated the continued presence *P. contorta* forest since at least 11,500 cal yr BP (Whitlock, 1993; Theriot et al., 2006). Those records allow for analysis of edaphic controls on the sensitivity of vegetation to postglacial climate change.

The second example describes the ecological consequences of the climactic eruption of Mount Mazama (7682–7584 cal yr BP, 2σ range, Egan et al., 2015), which was the most explosive eruption in North America during the Holocene (Sarna-Wojcicki et al., 1983). Its ashfall had the greatest depositional extent of any Holocene eruption in the United States (Sarna-Wojcicki et al., 1983) covering, conservatively, over 1.7 million km^2 (Sarna-Wojcicki et al.; Mullineaux, 1974; Matz, 1987; Egan et al., 2015; Buckland et al., 2020; Figure 5.1), not including distal cryptotephra. Depth of ash deposited in lake sediments varies even over relatively short distances, although ash thickness is inflated by reworking in many cases (Buckland et al., 2020). In the NRM and GYE, Mazama ash usually is observed as a single layer, with thicknesses varying from 0.5 cm on the Yellowstone Plateau (Tiller, 1995; Morgan et al., 2019) to 50 cm or more in extreme western Montana (Brunelle et al., 2005). Ash thickness is commonly considered the dominant factor influencing ashfall impacts (Lawrence and Ripple, 2000; Payne and Egan, 2019). Importantly, deposits at NRM sites with more than ~10 cm of ash documented may be overthickened from reworking, based on the typical thicknesses in the isopach map of Buckland et al. (2020). Although the impacts to Cascade Range forests have been described in pollen studies (Hansen, 1942a, 1942b; Long et al., 2011, 2014; Egan et al., 2016), distal impacts in the NRM are only occasionally noted (Mehringer et al., 1977b; Mack et al., 1978; Brant, 1980; Mack et al., 1983; Power et al., 2011; Alt et al., 2018). Several of these studies note a short-lived increase in the percentage of *Artemisia* pollen and a decrease in *Pinus* pollen (Mehringer et al., 1977b; Mack et al., 1978; Brant, 1980; Power et al., 2011; Alt et al., 2018), although the interpretation of these data is not clear. Ecological impacts of ash deposition in the GYE have not been reported.

The third example examines the influence of hydrothermal explosions, which are rapid ejections of water, steam, mud, and rock fragments that are triggered by sudden drops in confining pressure and subsequent rapid generation (flashing) of steam (Smith and McKibbin, 1997; Browne and Lawless, 2001; Morgan et al., 2009). Explosion debris may be ejected to heights of tens to hundreds of meters in the most extreme cases (Morgan et al., 2009). At least 24 explosions, mostly small and producing crater diameters <10 m, have been observed in the central GYE since the 1881 explosions of Excelsior Geyser in Midway Geyser Basin (Whittlesey, 1990; Lowenstern et al., 2005; Christiansen et al., 2007). Current estimates are that a small hydrothermal explosion occurs on the Yellowstone Plateau every two years, on average (Lowenstern et al., 2005; Christiansen et al., 2007). Large hydrothermal explosion craters, defined as those with diameters exceeding 100 m, may occur at frequencies of 200-700 years (Christiansen et al., 2007; Morgan et al., 2009) and are scattered across the postglacial landscape of the Yellowstone Caldera. The larger explosion events deposited explosion debris covering areas of 0.1-5 km^2 in the past (Morgan et al., 2009). At least twenty of these large craters have been documented (Morgan et al., 2009). The largest documented explosion crater in the world is the 13.0-ka Mary Bay explosion crater (Browne and Lawless, 2001); the debris covered a ~30 km^2 area mapped with brecciated rock and mud 3 to 4 km from its crater rim (Morgan et al., 2009). While most historical explosions have been small and more frequent (Christiansen et al., 2007; Morgan et al., 2009) with negligible vegetation impacts, the depositional area of the larger and more infrequent hydrothermal explosions deserves consideration of a possible impact to nearby terrestrial ecosystems.

The objectives of this study are to use high-resolution pollen data to answer: (1) What was the vegetation impact of past volcanic and hydrothermal disturbances, such as rhyolitic lava flows, Cascades ashfall deposits, and large hydrothermal explosions, on the conifer forests of the NRM and GYE? (2) How did these disturbances impact the resilience and state of ecosystems in the NRM and GYE? This project is a component of the Hydrothermal Dynamics of Yellowstone Lake project (HD-YLAKE, Sohn et al., 2017), one the principal goals of which is to evaluate the effect of past hydrothermal events on terrestrial ecosystem dynamics.

Methods

Regional/site descriptions and sampling

The long-term influence of Pleistocene rhyolite flows on vegetation history is known from pollen records in the central GYE (Table 5.1). Hedrick Pond, Lily Lake, Fallback Lake, Divide Lake, Emerald Lake, and Mariposa Lake (Waddington and Wright, 1974; Whitlock, 1993) lie on non-rhyolitic substrate (Table 5.1) within mixed-conifer forests ranging from *Pinus-Pseudotsuga* parkland (Hedrick Pond, low-elevation) to *Pinus-Picea-Abies* forest (Mariposa Lake, high elevation). Cub Creek Pond lies on the contacts between rhyolite and non-rhyolite substrate (Prostka et al., 1975; Table 5.1) and is included with the non-rhyolite sites, consistent with a modern mixed-conifer forest (Waddington and Wright, 1974). Cygnet Lake, Yellowstone

Lake, and Goose Lake are located on or near rhyolite lava flows (Table 5.1) and surrounded by dense *P. contorta* forests. In addition to these sites, pollen data from exposed lake sediments dating to an earlier interglacial period (Baker and Richmond, 1978; Baker, 1986) describe central GYE vegetation prior to emplacement of rhyolite flows under a different climate regime at a site where *P. contorta* currently dominates.

Table 5.1: Rhyolite site descriptions

Site	Location	Elevation (m.a.s.l.)	Vegetation type	Dominant terrestrial geology	Source
Goose Lake	44.541°N 110.842°W	2510	*Pinus contorta* forest	Rhyolite	Waldrop and Pierce, 1975*; This study†
Yellowstone Lake (2C)	44.53927°N 110.38922°W	2360	Mosaic w/*P. contorta* forest	Rhyolite	Christiansen, 2001*; This study†
Yellowstone Lake (FD-2)	44.44265°N 110.39136°W	2360	Mosaic w/*P. contorta* forest	Rhyolite	Christiansen, 2001*; Theriot et al., 2006
Cygnet Lake	44.65°N 110.60°W	2530	*P. contorta* forest	Rhyolite	Christiansen, 1975*; Whitlock, 1993†
Hedrick Pond	43.75°N 110.60°W	2073	*P. contorta*/*Pseudotsuga* forest	Glacial till	Love, 2003*; Whitlock, 1993†
Lily Lake	43.77°N 110.32°W	2469	*Picea*/*Abies*/*Pinus* forest	Glacial till	Love and Christiansen, 1983*; Whitlock, 1993†
Cub Creek Pond	44.508 °N 110.247 °W	2512	*Picea*/*Abies*/*Pinus* forest	Rhyolite and andesitic volcaniclastics	Prostka et al., 1975*; Waddington and Wright, 1974†
Fallback Lake	43.97°N 110.43°W	2597	*Picea*/*Abies*/*Pinus* forest	Shale	Love, 1975*; Whitlock, 1993†
Divide Lake	43.93°N 110.23°W	2628	*Picea*/*Abies*/*Pinus* forest	Conglomerate and sandstone	Love and Christiansen, 1983*; Whitlock, 1993†
Emerald Lake	44.07°N 110.30°W	2634	*Picea*/*Abies*/*Pinus* forest	Andesitic volcaniclastics	Love, 1974*; Whitlock, 1993†
Mariposa Lake	44.15°N 110.23°W	2730	*Picea*/*Abies*/*Pinus* forest	Andesitic volcaniclastics	Smedes et al., 1989*; Whitlock, 1993†

*Source of dominant terrestrial geology
†Source of vegetation reconstruction

Impacts of the Mazama ashfall were examined at several sites (Table 5.2) chosen where (1) the Mazama ash was identified by microprobe analysis or local stratigraphic correlations, and (2) pollen was sampled immediately above and below the ash to determine conditions prior to and after the ashfall. These sites include Foy Lake (Power et al., 2011), Twin Lakes (Alt et al., 2018), Hoodoo Lake (Brunelle et al., 2005), and new records from Yellowstone Lake and Goose Lake. NRM sites include Foy and Twin Lakes, located within open, low-elevation *Pseudotsuga-Pinus-Larix* forest, and Hoodoo Lake within subalpine *Pinus-Abies-Picea-Pseudotsuga* forest. GYE sites include Yellowstone Lake, a large (352 km^2) lake within a mosaic of *P. contorta* forest, *Pinus-Abies-Picea* forest, and *Artemisia* meadows, and Goose Lake, a smaller lake (0.14 km^2), located in dense *P. contorta* forest. Since pollen source area increases with increasing lake surface area (Jacobson and Bradshaw, 1981), it is reasonable to infer that vegetation changes documented in the sediment archive at Yellowstone Lake represent ashfall impacts that occurred over a broad, regional area, while the other, smaller lakes may document more local impacts.

Table 5.2 Mazama site descriptions

Site	Location	Elevation (m.a.s.l.)	Antecedent vegetation type	Ash thickness (cm)	Source
Hoodoo Lake	46.320556°N 114.650278°W	1770	*Abies*/*Pinus*/*Pseudotsuga* forest	50	Brunelle et al., 2005*†
Foy Lake	48.17°N 114.35°W	1006	*Pseudotsuga*/*Larix* parkland	48	Power et al., 2011*†
Twin Lakes	47.241°N 113.911°W	1261	*Pseudotsuga*/*Larix* parkland	10	Alt et al., 2018*†
Goose Lake	44.541°N 110.842°W	2510	*P. contorta* forest	1	Morgan et al., 2019*; This study†
Yellowstone Lake (2C)	44.53927°N 110.38922°W	2360	*P. contorta* forest	0.5	Morgan et al., 2019*; This study†

*Source of ash attribution
†Source of vegetation reconstruction

Hydrothermal explosion deposits are preserved in the sediments of Yellowstone Lake (Tiller, 1995; Morgan et al., 2009; Table 5.3) and Cub Creek Pond (Whitlock, 1993; Lu et al., 2017; Table 5.3) a considerably smaller lake (0.36 km^2). As before, large lakes, such as Yellowstone Lake receive pollen from a large region, whereas very small Cub Creek Pond has a more local source area.

Table 5.3: Hydrothermal explosion site descriptions

Site	Location	Elevation (m.a.s.l.)	Antecedent vegetation type	Hydrothermal explosion intervals (thickness cm)	Source
Cub Creek Pond	44.508 °N 110.247 °W	2512	Tundra	434-465 (31)	Morgan et al., 2019*; Waddington and Wright, 1974†; Whitlock, 1993†
Yellowstone Lake (5A)	44.50782 °N 110.32685 °W	2360	*P. contorta* forest	531-538 (7), 805-937 (132)‡	Morgan et al., 2019*; Theriot et al., 2006†

*Source of lithological interpretation
†Source of vegetation reconstruction
‡Interval contains segment of non-instantaneous deposition (818-834 cm)

For this study, multiple sediment cores were collected from northern Yellowstone Lake with a Kullenberg sampler (Kelts et al., 1986) from the University of Minnesota, National Lacustrine Core Facility (LacCore) in September 2016 (YELL-YL16-2C-1K, herein 2C, 44.53927 °N, 110.38922 °W, water depth 61 m; and YELL-YL16-5A-1K, herein 5A, 44.50782 °N, 110.32685 °W, water depth 102 m; Figure 5.1). Cores also were collected from Cub Creek Pond (YNP4-CUB17, 44.50545 °N, 110.24685 °W, fen surface; Figure 5.1) and Goose Lake (YNP4-GOS18, 44.54135 °N, 110.84237 °W, 8.86 m water depth; Figure 5.1) with a Livingstone sampler (Wright et al., 1984) in August 2017 and June 2018, respectively.

Laboratory analyses

Lithology and geochemistry: New sediment cores from Yellowstone Lake, Goose Lake, and Cub Creek Pond were transported to the LacCore facility, University of Minnesota–Twin Cities, and kept under cool (4°C), dry conditions until opened, longitudinally split, photographed, and scanned at 0.5-cm resolution for geophysical and geochemical characteristics. Lithological descriptions were completed with visual examination of sediment and smear slide analysis. Identification of volcanic ashes was conducted through comparison of glass chemistry from single-grain electron microprobe analysis at the New Mexico Bureau of Geology and Mineral Resources (NMBGMR) Geochronology Lab (Morgan et al., 2019).

Chronology: Chronologies were developed for new sediment cores using tephrochronology, conducted at the New Mexico Bureau of Geology and Mineral Resources (NMBGMR) Geochronology Laboratory, and accelerator mass spectrometry (AMS) radiocarbon dating of terrestrial macrofossils, conducted at the National Ocean Sciences Accelerator Mass Spectrometry (NOSAMS) Laboratory. In Yellowstone Lake core 2C, the chronology was based on three terrestrial plant remains, the sediment-water interface, a 1700 CE fire episode inferred from charcoal data (Romme and Despain, 1989), and the Mazama ash (Egan et al., 2015; Appendix A). Pollen concentrates were dated as well but returned erroneously old ages and are excluded here. The age-depth model from Goose Lake was based on 15 charcoal samples and the Mazama ash (Appendix A). Age-depth models were constructed for each using the Bacon software package for R (Blaauw and Christen, 2011) and 7 and 10 yrs/cm as accumulation rate priors for each (Appendix A). Few sufficiently large, dateable materials were located near the sections of Yellowstone Lake core 5A and Cub Creek Pond cores containing hydrothermal explosion deposits; age-depth models produced for those sites were based on linear interpolation between a radiocarbon age, identified ashes, and the sediment-water interface (Supplementary Table 5.1; Appendix A).

Radiocarbon age determinations for previously published records were re-calibrated with IntCal13 and Bayesian age-depth models were reconstructed using the Bacon software (Blaauw and Christen, 2011) with accumulation rate priors approximated by earlier work (Waddington and Wright, 1974; Whitlock, 1993; Brunelle et al., 2005; Theriot et al., 2006; Power et al., 2011; Alt et al., 2018).

Pollen analysis: Pollen samples were taken at 0.5-cm intervals ~20 cm above and below hydrothermal explosion deposits and the Mazama ash, spanning a period approximately 200 years above and below each event. Additional pollen samples were obtained from the original cores at Hoodoo Lake and Twin Lakes to increase the sampling resolution around Mazama ash deposits. Pollen preparation followed traditional procedures (Bennett and Willis, 2001) and a known concentration of *Lycopodium* tracer was added to each sample to calculate pollen concentration (grains/cm^3) and influx (grains/cm^2/yr). A minimum of 300 pollen grains was identified at 400× magnification per sample to the lowest possible taxonomic level based on published keys (Moore et al., 1991; Kapp et al., 2000) and the modern pollen reference collection at Montana State University. *Pinus* pollen with intact distal membranes were separated into *Pinus* subgen. *Pinus* and *Pinus* subgen. *Strobus*. *Pinus* subg. *Pinus* is attributed to *P. contorta*-type, as *P. ponderosa* does not presently grow in the central GYE (Baker, 1976; Dorn, 2001), and *Pinus* subgen. *Strobus* is attributed to either *P. albicaulis* or *P. flexilis* and referred to as *P. albicaulis*-type. Degraded, crumpled, or otherwise unidentifiable pollen grains were classified as “Indeterminate”, and grains that could not be identified with available reference material were classified as “Unknown”. Normalized AP:NAP (arboreal pollen to non-arboreal pollen; AP-NAP/AP+NAP) was used to show the abundance of tree and shrub pollen relative to other terrestrial pollen types. Interpretation of AP:NAP ratios were supplemented with pollen influx data. Influx data are sensitive to variations in sedimentation rates and depositional environments (Hicks and Hyvärinen, 1999), but similar trends among sites were considered supporting evidence.

Results

Identification of Mazama ash and hydrothermal explosion deposits

Yellowstone Lake (2C) and Goose Lake cores contained layers of ash (Figure 5.2) assigned to the climactic Mount Mazama eruption through electron microprobe analysis. Ash was observed to be relatively clean through smear slide examination, suggesting chiefly primary deposition. The other Yellowstone Lake core (5A) also contained the Mazama ash (Morgan et al., 2019), but high-resolution pollen analysis was not conducted. Ash thickness at Yellowstone Lake (2C, 0.5 cm thick) and Goose Lake (1 cm thick) occupy the low endmember of Mazama ash thickness used in this study, with other sites reaching up to 50 cm (Table 5.2).

Hydrothermal explosion events were identified in Yellowstone Lake core 5A at 531-538 cm (7 cm thick) and 805-937 (132 cm thick) (Morgan et al., 2019). Yellowstone Lake hydrothermal deposits consisted of fining-upward lithic sediments from as coarse as pebble-sized sediments to clay and clayey sapropel (Morgan et al., 2019). The thicker deposit (805-937 cm) contains a unit rich in organic lake matter (818-834 cm), likely deposited non-instantaneously, which divides separate explosion-related sequences. For the remainder of this work, this deposit

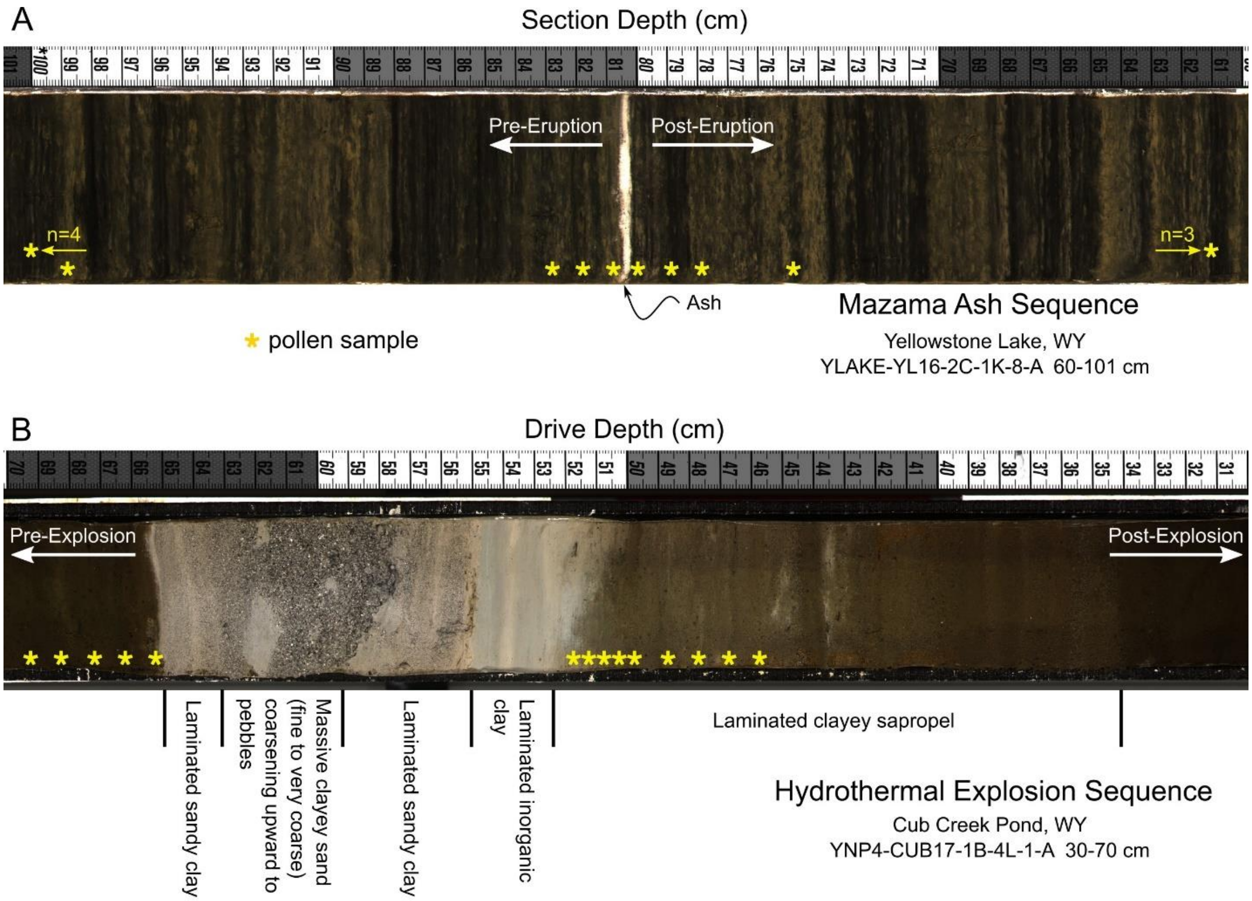

Figure 5.2: Example stratigraphic sequences including Mazama ash (A, Yellowstone Lake 2C) and a hydrothermal explosion deposit (B, Cub Creek Pond). Yellow asterisks indicate pollen sampling locations in these intervals. Deposit thicknesses varied greatly, ranging from 0.5 to 50 cm (Mazama ash) in studied sites and from 4 to 132 cm (hydrothermal explosion deposits).

is divided into two sequences, for which the vegetation response may be considered separately, 805-818 cm and 818-937 cm. For each sequence, pollen sampling was conducted within the explosion deposit where a component of organic lake sediments are first observed to derive a record of the vegetation impacts immediately chronologically following the explosion. The beginnings of the post-explosion pollen records are 534, 811, and 834 cm. The Yellowstone Lake core (2C) also contained a hydrothermal explosion deposit, but high-resolution pollen analysis there was not conducted.

The hydrothermal explosion deposit in Cub Creek Pond, occurring at 434-465 cm (31 cm thick), consisted of gray massive sandy clay, transitioning upward to a massive clayey sand (fine- to very coarse-grained) with lithic pebbles, into laminated sandy clays to silty clays, and then laminated clayey sapropel (Figure 5.2). As before, post-explosion pollen sampling began where sediments were initially organic-rich in the explosion deposit, 452 cm, to gain a sense of the vegetation impact immediately following the explosion.

Despite proximity to at least three large hydrothermal explosion craters in Lower Geyser Basin (Muffler et al., 1971; Morgan et al., 2009), Goose Lake sediment cores did not appear to contain any explosion deposits.

Pollen

Rhyolitic substrate sequences: Pollen records from non-rhyolitic substrates in the central GYE have been described elsewhere (Waddington and Wright 1974; Whitlock 1993). New records from lakes on rhyolitic substrates, including Goose Lake and Yellowstone Lake (2C), show high levels of *Pinus* pollen (55-77%), dominated by *P. contorta*-type with lower amounts of *P. albicaulis*-type (*P. albicaulis*-type to *P. contorta*-type ratio <0.16; Figure 5.3). These *Pinus* percentages match those of modern pollen samples within present-day *P. contorta* forest (~55-95%, Iglesias et al., 2018) and support previous findings of high levels of *Pinus* pollen in sediment cores from lakes on rhyolitic substrates (Whitlock, 1993; Figure 5.3).

Mazama ashfall sequences: Pre-Mazama intervals in Hoodoo Lake, Foy Lake, Twin Lakes, Goose Lake, and Yellowstone Lake (2C) consisted primarily of arboreal pollen types representative of early-Holocene forest in those regions (Brunelle et al., 2005; Power et al., 2011; Alt et al., 2018). Each site had high mean AP:NAP ratios in the 1500 years before the Mazama

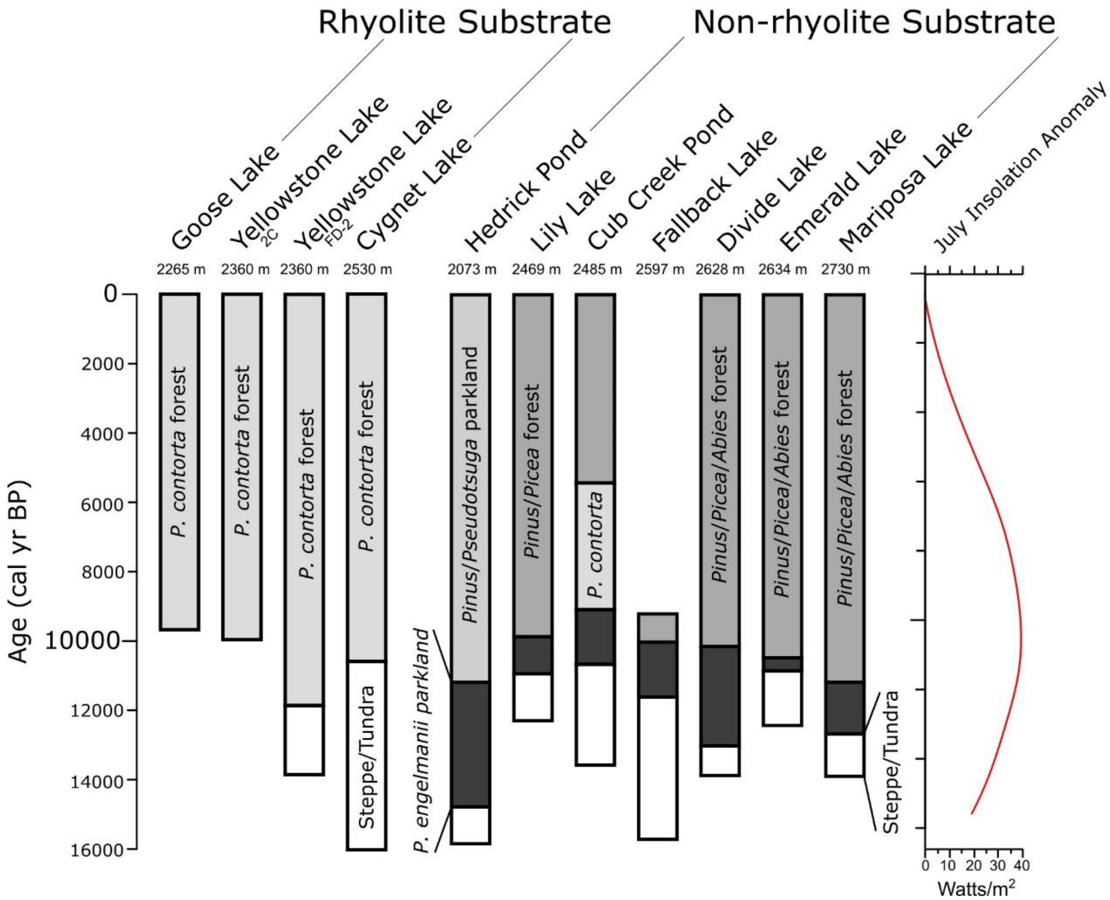

Figure 5.3: Simplified postglacial vegetation histories from central Greater Yellowstone Ecosystem sites on rhyolitic substrates and non-rhyolitic substrates. July insolation anomaly from Berger and others (1978). Sites located on non-rhyolitic substrates show greater postglacial change, responding to climate change (driven by the seasonal cycle of insolation) and postglacial plant migrations, while sites on rhyolitic substrates show less vegetation change.

eruption: 0.71 (Hoodoo Lake), 0.61 (Foy Lake), 0.43 (Twin Lake), 0.62 (Goose Lake), and 0.55 (Yellowstone Lake 2C) (Figure 5.4). AP:NAP ratios declined to precipitously lower values, -0.085 (Foy Lake), -0.27 (Twin Lake), -0.24 (Goose Lake), and 0.11 (Yellowstone Lake 2C), in strata immediately above the Mazama ash, marking the lowest AP:NAP Holocene values of each record (Figure 5.4). *Artemisia* was the dominant non-arboreal pollen type in this interval at each site, and its percentages increased following the ashfall event (Appendix B). This shift

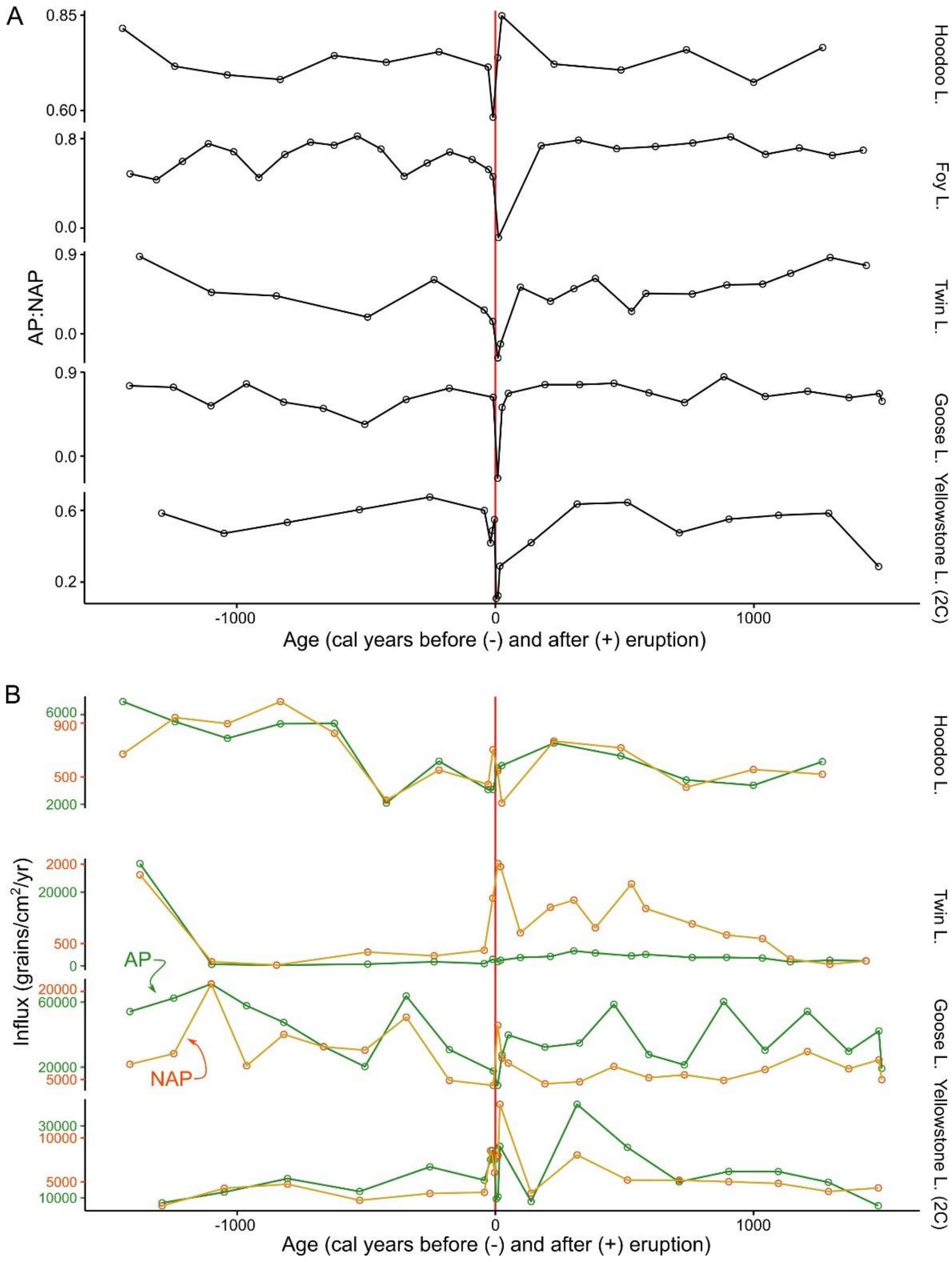

Figure 5.4: (A) AP:NAP (arboreal pollen:non-arboreal pollen) for the interval of 1500 cal years before and after the climactic Mazama eruption (red line). AP:NAP values declined at each site, except Hoodoo Lake, reaching the lowest values in each record immediately following the eruption. (B) Pollen influx of AP (green) vs. NAP (orange) plotted for the same interval, as available. All sites, except Hoodoo Lake, show a sharp decrease in AP:NAP, dominantly driven by increased NAP influx rather than decreased AP influx.

was primarily driven by increases in *Artemisia* abundance, as measured by pollen influx, while influx of *Pinus*, the dominant arboreal pollen producer at each site, remained relatively steady or declined slightly.

In central Yellowstone Plateau sites, *Artemisia* influx increased 47% (3935 to 6235 grains/cm^2/yr) at Yellowstone Lake and 614% (2367 to 14,536 grains/cm^2/yr) at Goose Lake, whereas *Pinus* values decreased by 41% (20,779 to 8494 grains cm^2/yr) and 59% (16,514 to 9741 grains/cm^2/yr), respectively. Twin Lakes in the NRM showed a similar trend as *Artemisia* influx increased by 260% (386 to 1005 grains/cm^2/yr) and *Pinus* values decreased by 13% (1011 to 879 grains/cm^2/yr). Influx data were not available for Foy Lake. All sites, except Hoodoo Lake, showed a decline in AP:NAP ratios that lasted for 1 or 2 cm (5 to 20 years) above the Mazama ash (Figure 5.4). Hoodoo Lake, in contrast, had a small decline (compared with other sites) in AP:NAP ratios (0.58) stratigraphically *preceding* the Mazama ash (Figure 5.4). AP:NAP values immediately following the Mazama ash were similar to the pre-Mazama mean (0.74). Mean AP:NAP values after the Mazama ash, up to 1500 cal years, were comparable to the pre-Mazama interval: 0.74 (Hoodoo Lake), 0.73 (Foy Lake), 0.55 (Twin Lake), 0.67 (Goose Lake), and 0.52 (Yellowstone Lake 2C) (Figure 5.4).

<u>Hydrothermal explosion sequences</u>: Pollen spectra from hydrothermal explosion intervals (Figure 5.5) in Yellowstone Lake core (5A) were dominated by *Pinus* (64.6-83.2%) mostly attributed to *P. contorta*-type (>40% of pollen total), with lower percentages of *P. albicaulis*-type (<10% of pollen total; Appendix C); *Artemisia* (<20%) and Amaranthaceae (<8%) also were present (Appendix C). AP:NAP ratios ranged from 0.34 to 0.73. Strata immediately following the two younger explosions in the Yellowstone Lake core (5A) did

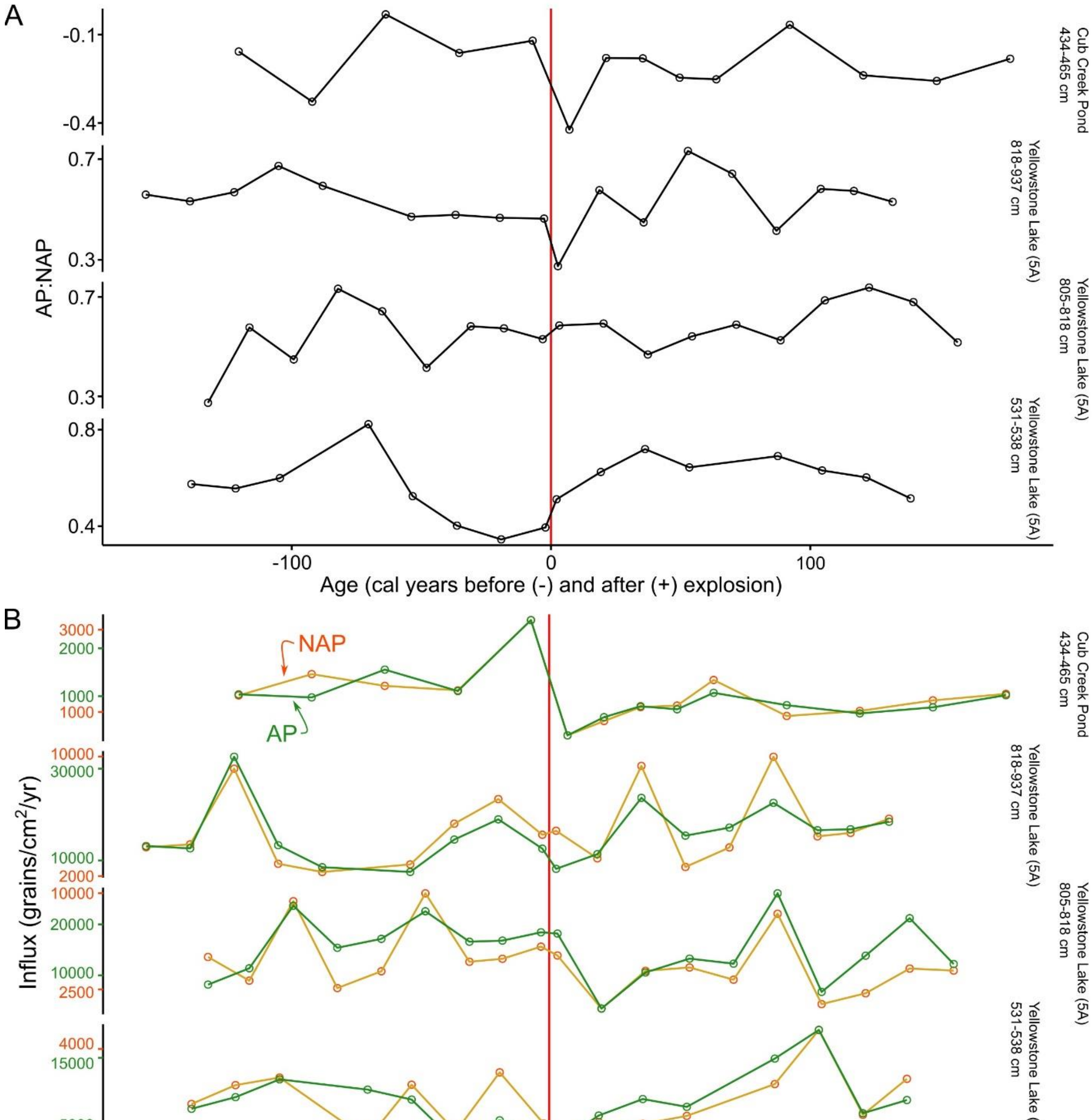

Figure 5.5: (A) AP:NAP (arboreal pollen:non-arboreal pollen) for several hydrothermal explosion deposits, occurring at given intervals, for the 150 cal years interval before and after the explosion (red line). (B) Pollen influx of AP (green) vs. NAP (orange) are plotted for the same interval. Explosion sequences at Cub Creek Pond (452-465 cm) and Yellowstone Lake (5A, 834-937 cm) show a show a sharp decline, dominantly driven by decreasing AP influx.

not show any sharp trends in AP:NAP values (Figure 5.5). A period of consistently lower AP:NAP values prior to youngest explosion (5A, 536.5-540.5 cm; Figure 5.5) instead suggest dry conditions in the centuries preceding this explosion at Yellowstone Lake, on the grounds that low AP:NAP ratios imply more open, xerophytic vegetation (Iglesias et al., 2018). Following the thickest explosion-related sequence in core 5A (818-937 cm), AP:NAP values sharply declined to the lowest value of the record, 0.27, and then returned to the pre-explosion range (Figure 5.5). The trend was driven by a 30% decline in *Pinus* pollen influx (460,290 to 326,388 grains/cm^2/yr) and a 25% increase in *Artemisia* influx (106,323 to 141,323 grains/cm^2/yr). After this briefly disturbed interval (impacted pollen spectra in <1 cm interval, representing less than a decade), the pollen assemblage returned to its pre-hydrothermal explosion state (Figure 5.5).

Pollen spectra from the pre-hydrothermal explosion interval in Cub Creek Pond were dominated by *Artemisia* (35.6-47.5%) with smaller components of *Pinus* (< 30%), *Betula* (<15%), and *Picea* (<5%; Appendix C). In the Cub Creek Pond core, sediments immediately following the hydrothermal explosion (434-465 cm) have AP:NAP values that declined to the lowest value of the record, -0.42, before returning to the pre-explosion range (Figure 5.5). Despite continued clay deposition into the lake, suggesting an unstable landscape, post-explosion AP:NAP values (-0.20) were similar to those before the event (-0.16; Figure 5.5).

Discussion

Impacts from Pleistocene rhyolite flows

GYE vegetation diversity has long been constrained by the infertile, well-drained substrates on rhyolite (Despain, 1990; Anderson and Romme, 1991). The Plateau Rhyolite of the central GYE (2200-2700 m.a.s.l.) is nearly exclusively dominated by *P. contorta* forests

(Despain, 1990), many of which are considered the climax condition for those sites (Despain, 1983). On andesitic and sedimentary substrates peripheral to the Yellowstone Caldera, mixed conifer forest of *Picea engelmannii*, *Abies lasiocarpa*, and *Pinus* (*P. contorta* at lower elevations and *P. albicaulis* at higher elevations) dominates between 2000-2800 m.a.s.l. (Arno, 1979). *P. contorta* dominance is attributed to sterile, well-drained soils derived from rhyolitic substrate, facilitated by stand-replacing fires that favor *P. contorta* regeneration (Pfister and Daubenmire, 1975). This forest has persisted since the postglacial migration of *P. contorta* into the GYE *ca.* 11,500 cal yr BP following a period of *Artemisia*-dominated tundra or steppe (Whitlock, 1993; Theriot et al., 2006; Figure 5.3). In contrast, on andesitic and sedimentary substrates in the GYE, plant communities shifted dynamically in response to postglacial climate change (Waddington and Wright, 1974; Whitlock, 1993). Following a late-glacial tundra period, these regions were colonized by *Picea* parkland in the late glacial to earliest Holocene (14,500 to 11,000 cal yr BP) and then *Pinus-Picea-Abies* (including *P. contorta)* forest (11,000 to 9500 cal yr BP; Iglesias et al., 2018). Trends in vegetation development at these sites are driven by postglacial plant migration and climate change, the latter driven chiefly by changing summer insolation (Whitlock, 1993; Theriot et al., 2006). Pollen data from Yellowstone Lake (FD-2, Theriot et al., 2006) and Cygnet Lake (Whitlock, 1993) suggest an early tundra or steppe period. However, infertile, well-drained rhyolitic substrate prevented establishment of *Picea* parkland, during late-glacial warming associated with rising summer insolation, and mixed conifer forest, during late-Holocene cooling and declining summer insolation as noted on non-rhyolitic sites, such as Cub Creek Pond (Figure 5.3).

A pollen and plant macrofossil record from exposed lake sediments at Grassy Lake Reservoir (Figure 5.1), stratigraphically dated to the last interglacial period (Baker and Richmond, 1978), locally *ca.* 70-130 ka (Licciardi and Pierce, 2018), contains abundant *Picea* (up to ~15%) and *Abies* (up to ~5%; Baker and Richmond, 1978), despite being situated deep within rhyolitic substrate (Figure 5.1). Abundant *Picea* and *Abies* macrofossils support local presence of these taxa (Baker, 1986). This vegetation reconstruction contrasts with the modern forest, which is dominated by *P. contorta* and modern pollen rain from the reservoir is dominated by *Pinus* (~81%) and minor components of *Picea* (~3%) and *Abies* (~2%; Whitlock 1993). The strong relationship between *P. contorta* dominance and rhyolite substrate at present suggests that forest grew on non-rhyolitic substrate. An area currently overlain by the Pitchstone Plateau rhyolite, emplaced at the end of the last interglacial *ca.* 75 ka (Stelten et al., 2015), located about 4 km north of Grassy Lake Reservoir (Christiansen et al., 1978) may have been the source region.

Impacts from distal Mazama ashfall

Impacts from the Mazama ashfall were recorded with remarkable similarity throughout the NRM and GYE, despite variable ash thickness. Mazama ash deposits at Foy Lake, Twin Lake, Goose Lake, and Yellowstone Lake are associated with a short-lived pulse in *Artemisia* productivity, and a smaller decline in *Pinus* forest cover. The assemblage returns to pre-eruption conditions within years to decades (Figure 5.4). A similar increase in *Artemisia* and decrease in *Pinus* following Mazama ash deposition was noted at Lost Trail Pass Bog (45.695 °N, 113.948 °W, 2147 m.a.s.l.; Mehringer et al., 1977a), Hager Pond (48.597 °N, 116.971 °W, 799 m.a.s.l.; Mack et al., 1978), and Teepee Pond (48.162 °N, 115.407 °W, 1275 m.a.s.l.; Mack et al., 1983) where tephra thickness was 7, ~10, and ~7 cm, respectively. The shared signal, and registration in a large lake like Yellowstone Lake, suggests a regional *Artemisia* expansion in response to the ashfall. At Hoodoo Lake, a decline in AP:NAP *preceded* the Mazama ash deposition and shows no discernible change immediately after the deposition of the ash. The decline in AP:NAP prior to the ashfall does not correlate with a significant fire episode or other disturbance at Hoodoo Lake (Brunelle et al., 2005) and may have been triggered by a short-term climate event such as decadal drought. The atypical record at Hoodoo Lake following Mazama ashfall suggests negligible impacts from the eruption at sites not situated near steppe, as compared to the stronger response in low-elevation sites near steppe (Foy Lake and Twin Lakes) and dry forest (Goose Lake and 2C).

A brief increase occurred in non-arboreal pollen influx, while arboreal pollen influx decreased to a lesser degree or remained relatively constant (Figure 5.4). Apparently, the primary impact of an ash eruption was on steppe communities, consistent with modern observations that suggest limited tree mortality at ashfall thicknesses of <1 m (Dale et al., 2005; Payne and Egan, 2019). Although the impact of the Mazama eruption can be seen at all sites except Hoodoo Lake, the reason for the expansion of shrubs is not readily evident. Mazama ash is thought to be infertile, depleted in nitrogen, phosphorous, and sulfur (Geist and Cochran, 1991; McDaniel et al., 2005), so a fertilization effect seems unlikely. We favor a hypothesis, first proposed by Mehringer et al. (1977b), suggesting that the increase represented a mulching effect that stimulates increased growth of *Artemisia* locally, or in adjacent steppe regions. Soils containing clay-sized Mazama ash retain more moisture (up to 100% increase, McDaniel et al., 2005), which is favorable to moisture-limited steppe vegetation, particularly *Artemisia*. Taller sagebrush has long been associated with moist, fertile soils, the so-called “Stegner rule”, by which suitable farmland was identified by Mormon settlers (Stegner, 1942). Although it has been observed that coarse-grained ash creates well-drained substrates that increase soil aridity (which does not necessarily impede *Artemisia* growth; Black and Mack, 1986), ash deposits in the cores studied were in the smaller, silt-size fraction, supporting an increase in soil moisture.

The vegetation changes that followed the climactic Mazama eruption have been attributed in some studies to the additive or coincident role of climate change. Indeed, the timing of the climactic Mazama eruption in the mid-Holocene coincides with the transition to generally cooler, wetter conditions (compared with the early Holocene, but warmer and drier than the present, Diffenbaugh et al., 2006) in the northwestern United States (Bartlein et al., 1998). Egan et al. (2016), for example studied a site in the Washington Cascades where no regional impact of Mazama ashfall was found, but vegetation was concurrently shifting due to increasingly cool and wet climate conditions. In contrast, deposition of thick, proximal deposits of Mazama pumice in central Oregon, which support only *P. contorta* forest today, occur in a bioclimatic zone favorable for *P. ponderosa.* Roach (1952) and Franklin and Dyrness (1973), suggest a clear, direct impact of the volcanic eruption on forest composition, similar to that of rhyolitic substrates in the GYE.

It is also possible that vegetation shifts underway as a result of gradual climate change were catalyzed as a result of ashfall-driven vegetation mortality (Ogden et al., 2005). Although our distal sites in the NRM and GYE did not experience lasting vegetation change catalyzed by Mazama ashfall, a pollen record from northern Idaho, Dismal Lake (47.117 °N, 115.633 °W, 1630 m.a.s.l.) with 141 cm of Mazama ash (in 2 deposits separated by sapropel, likely involving significant reworking) featured an abrupt transition from *Abies* and *Pseudotsuga* dominance prior to ashfall to an assemblage of *P. contorta* concurrent with ash deposition (Herring, 2014). The transition was attributed to the onset of cooler, wetter conditions favoring *Pinus* (and later *Picea*) over *Abies* and *Pseudotsuga*, with ash-caused tree mortality as a catalyst (Herring, 2014).

<u>Impacts from hydrothermal explosions</u>

The vegetation impact from past hydrothermal explosions varied with the size of the event and thickness of the breccia deposit. The explosion deposit in Cub Creek Pond (434-465 cm) is 30 cm above a tephra previously identified as the Glacier Peak ash (B or G, Waddington and Wright, 1974; Whitlock, 1993; 13,710 to 13,410 cal yr BP, 2σ range, Kuehn et al., 2009) and was emplaced during a tundra period dominated by *Artemisia*, Poaceae, *Betula*, and minor *Pinus* and *Picea* (Waddington and Wright, 1974; Whitlock, 1993). The recently deglaciated landscape was characterized by unstable slopes and little soil development (Lu et al., 2017). After the explosion, some tree mortality occurred, indicated by a decline in AP:NAP values and arboreal pollen influx decreasing more than non-arboreal pollen influx (Figure 5.5). The younger hydrothermal explosions recorded in Yellowstone Lake occurred during a period of *P. contorta* forest (Theriot et al., 2006). Following the thickest hydrothermal explosion-related sequence identified in core 5A (818-937 cm), similar tree mortality occurred and *Artemisia* modestly increased, indicated by a decline in AP:NAP values with a decline in arboreal pollen influx and a modest increase in *Artemisia* influx. A decline in AP:NAP above the thickest explosion deposit in the Yellowstone Lake core (5A) was observed only in the sample immediately above the deposit, suggesting a short-lived impact (years) but impacting a large area. No vegetation shift was observed after the smaller explosions in Yellowstone Lake (Figure 5.5).

The preferential impacts to conifers following hydrothermal explosions in the Yellowstone Caldera are inconsistent with vegetation studies following ashfall impacts, that suggest low-lying plants experienced the highest mortality (Antos and Zobel, 1986; Dale et al., 2005; Payne and Egan, 2019). In our study, conifers were most impacted, reminiscent of the eruption of lapilli (volcaniclastic ejecta, 2 to 64 mm clast diameter) at Mt. Taranaki (1655 CE) in New Zealand forests, where canopy and emergent taxa experienced the highest rates of mortality as foliage was inferred to have been stripped from trees (Efford et al., 2014). This response may have enabled surviving understory and light-dependent species to thrive in the opened canopy (Efford et al., 2014). In this scenario, herbs and shrubs increased in abundance due to partial destruction of the canopy.

Factors influencing vegetation resilience

Ecological and paleoecological trends are viewed increasingly through the lens of resilience, defined as a property of a system to be disturbed and maintain characteristic population and state variable relationships (Holling, 1973). In this framework, ecosystems are conceptualized as existing within one of multiple potential stable states, defined by abiotic factors, such as climate or soil conditions. A change in disturbance regime often serves as the trigger for a state shift to new ecosystem conditions (Beisner et al., 2003). This paradigm can be visualized using a ball-and-cup diagram (Figure 5.6), wherein the ball (an ecosystem) lies within a cup, which signifies the current range of environmental space (Beisner et al., 2003; Johnstone et al., 2016). A shift in the frequency, or severity of a disturbance regime has the capacity to push the ball (ecosystem) across a threshold into another cup (ecosystem condition). Depending on the dimensions of the threshold and the new cup, the ball will either be resilient to the imposed

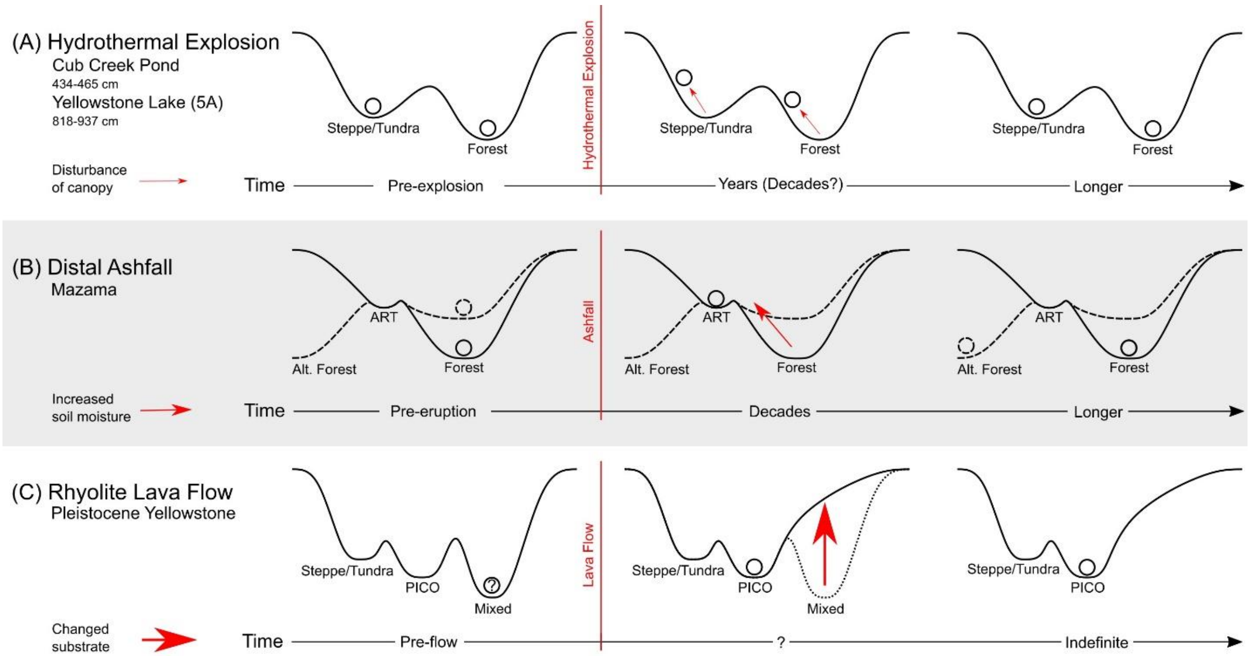

Figure 5.6: Ball-and-cup diagram of vegetation community resilience to three types of hydrothermal/volcanic disturbances in the Northern Rocky Mountains and Greater Yellowstone Ecosystem. (A) Forested and non-forested steppe/tundra subject to hydrothermal explosions in the central Greater Yellowstone Ecosystem. Responding to the disturbance, the state of the ecosystem changes, but the size of the disturbance (arrow) is not great enough to force the ecosystem into a new stable state (cup). (B) The state change created by the ashfall forced the ecosystem into a short-lived state where *Artemisia* proliferated for years to decades, before returning to the original state (cup). Dashed lines indicate situations, such as at Dismal Lake (Herring 2014), where distal ashfalls may have catalyzed a transition to a new stable state, which was already favored by changing climate conditions (Herring 2014). (C) Sites on rhyolite substrate today may have hosted mixed conifer forests in previous interglacial intervals.

condition and maintain a dynamic equilibrium in the original cup, or it will move to another cup, creating an environmental change. Environmental changes can take two forms in this model: (1) a state shift, in which some factor, usually an ecological disturbance, pushes the ball and forces it to a new condition; or (2) a parameter shift in which underlying environmental conditions change the shape and distribution of the cups (Beisner et al., 2003).

In this analogy, volcanic and hydrothermal disturbances function as either a state shift or a parameter shift in the environment. For paleoecologists and ecologists working in settings where volcanic and hydrothermal disturbances have occurred in the past, it is relevant to consider whether these disturbances acted as a disturbance, not dissimilar to fire or insect outbreaks, that instigated successional processes or fundamentally changed ecosystem parameters. Small-magnitude disturbances foment short-term state shifts but pose little threat to the long-term stability of an ecosystem, while large-magnitude parameter changes can permanently modify ecosystem states. Emplacement of large-volume rhyolitic volcanic rocks had the most persistent impact on ecosystems in the region. Pre-eruption ecosystems in central GYE were destroyed by massive rhyolitic lava flows and the change in substrate led to a unidirectional change in vegetation. Hypothetically, this parameter shift will be long lasting, persisting until the emplacement of a new, more fertile substrate.

Distal ashfall from the climactic Mount Mazama eruption had a shorter impact in the NRM and GYE in settings where the depositional thickness was thin (<1 m). The shift was likely driven by soil mulching (Mehringer et al., 1977b; Black and Mack, 1986). In terms of the cup-and-ball analogy, the ashfall pushed the ecosystem to a new *Artemisia*-rich state for a short period but the previous ecosystem space was re-inhabited within decades. A permanent, catalyzed state change occurred at Dismal Lake (Herring, 2014), where ashfall was exceptionally thick (>1 m, discounting probably overthickening). The pre-eruption ecosystem can be conceptualized as occupying a cup that became gradually less stable as a result of changing climate conditions (cooler and wetter), and thus highly vulnerable to disturbance. The thick ashfall provided a trigger and state change that were reinforced by long-term climate change.

Post-Pinedale hydrothermal explosions have taken place in multiple antecedent vegetation regimes on the Yellowstone Plateau. Large events altered the ecosystem briefly by killing trees, as evidenced by the decline of conifer pollen. The prevailing vegetation was reestablished soon after, suggesting no state change and that the GYE ecosystems are fundamentally resilient to this type of disturbance. Despite the large size and frequency of postglacial hydrothermal explosions in this area, vegetation communities were able to rapidly return to pre-explosion states.

Conclusions

Hydrothermal explosions, distal ashfalls, and rhyolite lava flows in the NRM and GYE have impacted past vegetation in distinct ways: (1) Rhyolite flows from Pleistocene volcanism in the central GYE shifted vegetation from mixed conifer to *P. contorta* forests. The lasting impacts of this disturbance are evident since the emplacement of the rhyolite flows. (2) Ashfall from the climactic Mount Mazama eruption had variable impacts in the NRM and GYE depending on geography and depth of burial. At low elevations and in dry forests, even relatively thin ash deposits facilitated the spread of *Artemisia*, while a site far-removed from *Artemisia* steppe showed little impact from the eruption. The impact was short lived, where evident, with a return to pre-ashfall conditions within years to decades. (3) Hydrothermal explosions preferentially impacted arboreal taxa in the central GYE, but the impacts are short lived and localized.

Post-disturbance vegetation response in each of the three types of disturbances studied (rhyolite lava flows, Mazama ashfall, and hydrothermal explosions) was largely determined by the nature of the antecedent vegetation and its resilience to disturbance as well as the magnitude of the volcanic/ash/hydrothermal event and thickness of its deposit. Rhyolite flows create significant changes in vegetation, parameter shifts in ecosystem space, whereas distal ashfalls and local hydrothermal explosions are less impactful disturbance events that only force a short-lived shift in ecosystem state. This range of ecosystem responses to volcanic and hydrothermal disturbances is useful when considering the potential ecosystem impacts of future events and conceptualizing the ecosystem dynamics of the past.

Acknowledgements

This work was supported by NSF Grant No. 1515353 to C. Whitlock and conducted under Yellowstone National Park Research Permits YELL-SCI-0009 and YELL-SCI-5054. M.J. Power and A.D. Brunelle provided data and new samples from Foy Lake and Hoodoo Lake, respectively. We thank M. Baker, S.R. Brown, A. Carlson, D.J. Conley, S. Fritz, R.E. Gresswell, V. Iglesias, C. Linder, W.P. Nanavati, J. Mulder-Rosi, R. O'Grady, W.C. Shanks III, M. Shapley, R. Sohn, M. Weingart, and N. Zeibig-Kichas for their help with field work. Core analysis in the LacCore lab was facilitated by S. Brady, A. Stone, and M. Shapley. Any use of trade, firm, or product names is for descriptive purposes only and does not imply endorsement by the U.S. Government.

CHAPTER SIX

CONCLUSIONS, IMPLICATIONS, AND FUTURE DIRECTIONS

Key findings

The overarching questions addressed in this dissertation were: How does past hydrothermal activity influence the radiocarbon content of lake sediments and the development of a chronology for documenting environmental change (Chapter 2)? How did vegetation and fire respond to short-term hydrothermal explosions and long-term climate change in the Yellowstone Lake region (Chapter 3)? What was influence of hydrothermal activity on local vegetation history, in comparison to the influences of broad-scale climate change (Chapter 4)? What was the relative influence of volcanism, ashfall, and hydrothermal activity in shaping the Quaternary vegetation history of Yellowstone National Park and the western U.S. (Chapter 5)? Several conclusions can be drawn from the results described in these chapters.

Chapter 2

Accelerator mass spectrometry radiocarbon ages from pollen concentrates in a sediment core from Yellowstone Lake were found to be systematically older than ages from terrestrial plant remains, the Mazama ash, and the age of the sediment-water interface. First, an age-depth model produced from chemically concentrated pollen was up to 4300 cal years older than a model established by terrestrial plant remains, the latter of which produced a model consistent with the age of the Mazama ash. Second, picked pollen concentrates were erroneously old compared with the age of the sediment-water interface or the Mazama ash by 1900 to 4300 cal years. Finally, pollen from living *Pinus contorta* near Yellowstone Lake produced virtually modern ages. The most likely sources of dead carbon remaining were determined to be reworked pollen from some unknown source or incorporation of hydrothermally degassed CO_2 in the water column or surficial sediments.

<u>Chapter 3</u>

Multi-proxy study of a 9880-yr-old sediment core from Yellowstone Lake was conducted to determine the influence of past climate change and, potentially, hydrothermal activity on Holocene-scale terrestrial ecosystem development and hydroclimate. The vegetation history was reconstructed from pollen data, past fire activity from macroscopic charcoal data, and the hydroclimatic history from the oxygen isotope content of diatom frustules. Summer insolation was enhanced during the early Holocene portion of the record (9880 to 6300 cal yr BP), leading to warmer and drier summers than present in central Yellowstone. This pattern occurs throughout summer-dry areas of the Yellowstone Lake watershed. Vegetation at that time was dominated by *Pinus contorta* (less forest cover or extent than today), and fire episodes were smaller and less frequent than today. The suggestion of a less-dense *P. contorta* forest with lower overall fire activity is consistent with reconstructions from small lake sites in the Yellowstone vicinity. From the middle Holocene to the present day (the last 6300 cal yr), summer insolation declined, leading to incrementally cooler and wetter conditions to the present. *P. contorta* continued to dominate vegetation and became increasingly abundant to the present, with larger, more frequent fire episodes than before. Increasing forest density with more overall burning is recorded at other *P. contorta* sites as well, suggesting a regional response to cooler, wetter summers. Incremental change since 9880 cal yr BP is documented in $\delta^{18}O_{diatom}$ measured in the Yellowstone Lake core, reflecting the slow shifts in lake evaporation, in close concert with the climate trends. The core analyzed contained a hydrothermal explosion deposit, but there was no evidence of a lasting vegetation response to any of this event.

Chapter 4

The development of a hydrothermal landscape was investigated through the multi-proxy investigation of a 10,300-yr-long sediment core from Goose Lake in Lower Geyser Basin. From 10,300 to 3800 cal yr BP, hydrothermal fluids discharged directly into Goose Lake, evidenced by the deposition of arsenic-rich sediment, antimony-rich fluorite mud, and relatively heavy $\delta^{13}C_{sediment}$ values. Diatoms and coccal algae communities consisted of taxa adapted to extreme, warm conditions. In contrast, the terrestrial ecosystem had little discernable response to local hydrothermal activity. Pollen data indicate the vegetation was composed of *Pinus contorta* forest with abundant fire activity at this time, which became more closed or more extensive as summers became cooler and effectively wetter. The vegetation reconstruction matches that of another, non-hydrothermal site in central Yellowstone today, but no significant hydrothermal activity occurs.

At 3800 cal yr BP, hydrothermal activity at Goose Lake abruptly ceased, evidenced by the absence of arsenic-enriched sediment and lighter $\delta^{13}C_{sediment}$ values. Diatoms and coccal algae responded to this change by shifting towards taxa more typical of oligotrophic lakes without hydrothermal influence. Contemporaneously, *P. contorta* forest became more open or less extensive with greatly diminished fire activity. This vegetation reconstruction departs from that of another site in *P. contorta* forest, Cygnet Lake, that shows increased forest closure to the present as summers continued to become cooler and effectively wetter than before. Pollen evidence of an opening forest coincides with a cessation of hydrothermal activity ceased into

Goose Lake. This shift is interpreted as a basin-wide reorganization of the LGB hydrothermal system *ca.* 3800 cal yr BP.

Chapter 5

In this chapter, the vegetation response to an array of volcanic and hydrothermal disturbances are synthesized from the Northern Rocky Mountains and Greater Yellowstone Ecosystem. The impact of Pleistocene rhyolite lava flows in the central part of the Greater Yellowstone Ecosystem was examined through the comparison of existing research from lake sediment cores on rhyolitic and non-rhyolitic substrate. Vegetation response to the climactic, 7.6 ka eruption of Mount Mazama was studied through the use of existing high-resolution pollen records bracketing the ash deposit, supplemented with new records from Yellowstone. Finally, the impact of local hydrothermal explosions was considered through the study of new high-resolution pollen sections bracketing four explosion deposits in Yellowstone. It was found that vegetation resilience variated greatly by the type of disturbance. Pleistocene rhyolite flows created nutrient-poor, well-drained soils throughout much of the central Greater Yellowstone Ecosystem, causing that region to support only low-diversity grassland in late-glacial time and *Pinus contorta* forest in interglacial periods. The Mazama ash apparently caused a short-lived expansion of *Artemisia* at sites through much of the Northern Rocky Mountains and Greater Yellowstone Ecosystem, possibly driven by a mulching effect in ash deposition. Local hydrothermal explosions had the most transient impacts, causing conifer mortality, followed by forest recovery within years.

Implications

These findings emphasize two important aspects of the development of vegetation on the Yellowstone Plateau: (1) Holocene climate change, chiefly driven by slow changes in the seasonal cycle of insolation, has been the dominant driver of the vegetation and fire history on the Yellowstone Plateau. (2) The ecological impacts of hydrothermal activity are locally important, where hydrothermal activity is pervasive, as in Lower Geyser Basin, and where recently affected by hydrothermal explosions, albeit briefly, as in the Yellowstone Lake vicinity.

Regional vegetation response to climate

Patterns of vegetation and fire regime history in the Yellowstone Plateau ecoregion point towards insolation-driven climate change being the primary forcing of regional terrestrial ecological change on millennial time scales. The *Pinus* pollen percentage data from Yellowstone Lake, a regional record, suggest a Holocene-length trend towards more closed or more extensive *P. contorta* forest to the present (Chapter 3, Figure 3.4). Charcoal data suggest a matching trend towards increasingly large fire episodes to the present (Chapter 3, Figure 3.4). Pollen data from Cygnet Lake, with modern *P. contorta* forests on rhyolitic soils, similarly suggest increasingly closed or more extensive *P. contorta* forest to the present (Whitlock, 1993). Cub Creek Pond and Buckbean Fen, with more diverse forests situated on andesitic soils, had initially more closed or extensive *P. contorta* forests to the early to middle Holocene and then establishment of mixed conifer forests or parklands with *Abies lasiocarpa* and *Picea engelmannii* (Waddington and Wright, 1974; Baker, 1976). These steady trends towards more closed or extensive *P. contorta* forest with *A. lasiocarpa* and *P. engelmannii* in the Holocene bears striking similarity to the curve of diminishing summer insolation from the early Holocene to present in the Northern

Hemisphere (Laskar et al., 2004). Decreasing summer insolation would create increasingly cool summers that were effectively wetter, due to enhanced moisture as the northeastern Pacific subtropical high weakened and conditions became effectively wetter, in this “summer-dry” climate regime (Whitlock and Bartlein, 1993; Bartlein et al., 1998). A trend towards increased evaporation is inferred from the $\delta^{18}O_{diatom}$ record from Yellowstone Lake (Chapter 3, Figure 3.4), but increasing forest closure or extent is more consistent with cooler, wetter conditions. In this model, we hypothesize that *P. contorta* forests became incrementally more closed or extensive through the Holocene as cooler, effectively wetter conditions outweighed the effects of summer aridity. *A. lasiocarpa* and *P. engelmannii* became established where soil conditions permitted. Concurrently, fire activity increased due to increased fuel biomass as *P. contorta* became more abundant.

At no site, except for Goose Lake after 3800 cal yr BP, was the Holocene-scale vegetation history affected by hydrothermal activity in an enduring way. At Yellowstone Lake (Chapter 3), the deposition of hydrothermal explosion ejecta had no long-term influence on the *Pinus contorta* forest, and pollen and charcoal data from a site that is not located near extensive hydrothermal areas do not show these changes.

Local vegetation response to hydrothermal influences

Although a relatively minor component of Yellowstone by area—about 0.5% of the area of Yellowstone consists of active hydrothermal areas (Vaughan et al., 2014)—hydrothermal processes have a dramatic influence on the landscape, where locally present. The records discussed in this dissertation, Yellowstone Lake (Chapters 3, 5), Goose Lake (Chapter 4), and Cub Creek Pond (Chapter 5) are situated near active subaerial hydrothermal areas (Vaughan et al., 2014) and Yellowstone Lake contains an extensive subaqueous hydrothermal field (Morgan et al., 2007). Each record provides evidence of at least short-term vegetation impacts from past hydrothermal processes. The Goose Lake core notably contains sediments enriched in arsenic with heavy $\delta^{13}C_{sediment}$ values that suggest hydrothermal fluids discharged directly into the lake prior to 3800 cal yr BP (Chapter 4, Figure 4.2). The cessation of hydrothermal inputs at Goose Lake at 3800 cal yr BP was synchronous with the landscape becoming more open, which is attributed to the creation of the modern broad hydrothermal flat. High-resolution pollen data bracketing a late-glacial hydrothermal explosion deposit at Cub Creek Pond and one of three hydrothermal deposits in Yellowstone Lake show a decline in conifer cover (Chapter 5, Figure 5.5). This decline is attributed to conifer mortality caused by the hydrothermal explosions, but vegetation returned to pre-explosion conditions within years.

Directions for future research

Use of pollen concentrates for radiocarbon dating remains desirable, where suitable terrestrial plant macrofossils are unavailable. Although previous work has identified sources of dating error including incomplete separation of non-pollen material (Regnéll, 1992; Richardson and Hall, 1994) or incorporation of reworked pollen grains (Mensing and Southon, 1999; Zimmerman et al., 2019), these explanations were inadequate to explain erroneously old ages from pollen concentrates obtained from Yellowstone Lake (Chapter 2). This difficulty will continue to limit our ability to provide precise age control for paleoenvironmental and geological events in Yellowstone Lake. Future work should focus on identifying the source of old carbon, through an analysis of the carbon source in pollen from source to sink.

Analyses of lake sediments from hydrothermal basins complement studies of past hydrothermal activity based on radiometric dating of sinter deposits by providing information on landscape-scale processes and ecological responses (Chapter 4). Several lakes in Yellowstone National Park exist near hydrothermal features and allow for further study of the history of hydrothermal events and their impact on terrestrial and aquatic ecology, including Nuphar Lake (Norris Geyser Basin), South Twin Lake (Roaring Mountain Area), Feather Lake (Lower Geyser Basin), and Fern Lake (Sour Creek Thermal Area). Additional records examining the linkages between past vegetation and hydrothermal disturbances would test our hypothesis about the local and short-lived influence on terrestrial and aquatic ecosystems.

New records of hydrothermal history in Yellowstone are also needed to further elucidate the cause of major shifts in hydrothermal activity. At Goose Lake (Chapter 4), late Holocene reorganization of hydrothermal activity may have been triggered by past earthquake activity (Marler and White, 1975; Pitt and Hutchinson, 1982) or a periods of ground deformation (Vaughan et al., 2020), but this bears further study. In addition, the sensitivity of hydrothermal features to climate-driven changes in water supply is increasingly recognized (Hurwitz et al, 2020), and one might hypothesize that Yellowstone hydrothermal activity could have been suppressed during arid periods in the past, such as in the early Holocene. Analysis of new lake sediment cores may better correlate evidence of climate change (particularly periods of aridity) with past hydrothermal activity or presence of hydrothermal explosion deposits.

This dissertation fits within a larger body of research devoted to examining the influence of geology on long-term vegetation dynamics. Substrate is an important control on many ecosystems, strongly limiting floral diversity when substrates are nutrient poor, toxic, or problematically drained (Brubaker, 1975; Whitlock, 1993; Briles et al., 2011). In volcanic settings, not only are substrate constraints often present (Roach, 1952), but volcanic and hydrothermal processes often function as triggers of ecological change. In the western United States, studies have long considered the impacts of the climactic Mount Mazama eruption on vegetation, chiefly focusing on the effects of distal ashfall (Hansen, 1942a, 1942b; Mehringer et al., 1977b; Long et al., 2011, 2014; Egan et al., 2016). Similar investigations have been conducted to study the ecological response of large, explosive eruptions elsewhere, including in New Zealand (McGlone et al., 1988; Lees and Neall, 1993; Ogden et al., 2005), Mexico (del Socorro Lozano-García and Xelhuantzi-López, 1997), Alaska (Heusser, 1990), and Germany (Baales et al., 2002). Our contribution is to show that, in Yellowstone National Park, past volcanic and hydrothermal disturbances resulted in short-lived and localized perturbations (Chapter 5) in climate-driven terrestrial and limnological dynamics.

A better epistemological link between volcanic or hydrothermal disturbance and the paleoecological record could be provided by studying lacustrine records in volcanic settings where pre- and post-eruption ecology is well documented, such as at Mount St. Helens. In addition, large volcanic eruptions in the Cenozoic provide an opportunity to study the ecological impact in ancient ecosystems, as registered by proxy data in ancient lake beds or marine records.

REFERENCES CITED

REFERENCES CITED

Alt, M., McWethy, D.B., Everett, R., and Whitlock, C., 2018, Millennial scale climate-fire-vegetation interactions in a mid-elevation mixed coniferous forest, Mission Range, northwestern Montana, USA: Quaternary Research, v. 90, p. 66–82, doi:10.1017/qua.2018.25.

Anderson, L., 2011, Holocene record of precipitation seasonality from lake calcite $\delta^{18}O$ in the central Rocky Mountains, United States: Geology, v. 39, p. 211–214, doi:10.1130/G31575.1.

Anderson, L., Berkelhammer, M., Barron, J.A., Steinman, B.A., Finney, B.P., and Abbott, M.B., 2016, Lake oxygen isotopes as recorders of North American Rocky Mountain hydroclimate: Holocene patterns and variability at multi-decadal to millennial time scales: Global and Planetary Change, v. 137, p. 131–148, doi:10.1016/j.gloplacha.2015.12.021.

Anderson, J.E., and Romme, Wi.H., 1991, Initial Floristics in Lodgepole Pine (*Pinus contorta*) Forests Following the 1988 Yellowstone Fires: International Journal of Wildland Fire, v. 1, p. 119, doi:10.1071/WF9910119.

Antos, J.A., and Zobel, D.B., 1985, Plant form, developmental plasticity, and survival following burial by volcanic tephra: Canadian Journal of Botany, v. 63, p. 2083–2090, doi:10.1139/b85-293.

Antos, J.A., and Zobel, D.B., 1986, Recovery of Forest Understories Buried by Tephra from Mount St. Helens: Vegetatio, v. 64, p. 103–111.

Arguez, A., Durre, I., Applequist, S., Squires, M., Vose, R., Yin, X., and Bilotta, R., 2010, NOAA's U.S. Climate Normals (1981-2010): NOAA National Centers for Environmental Information, doi:10.7289/V5PN93JP.

Arno, S.F., 1979, Forest Regions of Montana: USDA Forest Service Research Paper INT-218, 39 p.

Arnold, P.G., and Sharpe, F.P., 1967, Summary report of lake and stream investigations for 1966: U.S. Fish and Wildlife Service.

Baales, M., Jöris, O., Street, M., Bittmann, F., Weninger, B., and Wiethold, J., 2002, Impact of the Late Glacial Eruption of the Laacher See Volcano, Central Rhineland, Germany: Quaternary Research, v. 58, p. 273–288, doi:10.1006/qres.2002.2379.

Bahls, L., 2005, Northwest diatoms: a photographic catalogue of species in the Montana Diatom Collection, with ecological optima, associates, and distribution records for the nine northwestern Unived States, *in* Northwest diatoms, Helena, MT, The Montana Diatom Collection, v. 2.

Bahls, L.L., 2012, Seven new species in Navicula sensu stricto from the Northern Great Plains and Northern Rocky Mountains: Nova Hedwigia, Beiheft, v. 141, p. 19–38.

Baker, R.G., 1976, Late Quaternary Vegetation History of the Yellowstone Lake Basin, Wyoming: U.S. Geological Survey Professional Paper 729-E, 78 p.

Baker, R.G., 1986, Sangamonian(?) and Wisconsinan paleoenvironments in Yellowstone National Park: GSA Bulletin, v. 97, p. 717–736, doi:10.1130/0016-7606(1986)97<717:SAWPIY>2.0.CO;2.

Baker, R.G., and Richmond, G.M., 1978, Geology, Palynology, and Climatic Significance of Two Pre-Pinedale Lake Sediment Sequences in and Near Yellowstone National Park: Quaternary Research, v. 10, p. 226–240, doi:10.1016/0033-5894(78)90103-5.

Balistrieri, L., Shanks, W., Cuhel, R., Aguilar, C., and Klump, J., 2007, The Influence of Sublacustrine Hydrothermal Vent Fluids on the Geochemistry of Yellowstone Lake, *in* Morgan, L.A. ed., Integrated Geoscience Studies in the Greater Yellowstone Area--Volcanic, Tectonic, and Hydrothermal Processes in the Yellowstone Geoecosystem, Reston, VA, U.S. Geological Survey, Professional Paper 1717, p. 169–200.

Ball, J.W., McCleskey, R.B., Nordstrom, D.K., and Holloway, J.M., 2006, Water-Chemistry Data for Selected Springs, Geysers, and Streams in Yellowstone National Park, Wyoming, 2003–2005: U.S. Dept. of the Interior, Geological Survey, Open-File Report 2006–1339, 146 p.

Bargar, K.E., and Beeson, M.H., 1981, Hydrothermal alteration in research drill hole Y-2, Lower Geyser Basin, Yellowstone National Park, Wyoming: American Mineralogist, v. 66, p. 473–490.

Bargar, K.E., and Beeson, M.H., 1985, Hydrothermal Alteration in Research Drill Hole Y-3, Lower Geyser Basin, Yellowstone National Park, Wyoming: U.S. Geological Survey Professional Paper 1054–C, 26 p.

Bargar, K.E., Beeson, M.H., Fournier, R.O., and Muffler, L.J.P., 1973, Present-day deposition of lepidolite from thermal waters in Yellowstone National Park: American Mineralogist, v. 58, p. 901–904.

Bartlein, P.J., Anderson, K.H., Anderson, P.M., Edwards, M.E., Mock, C.J., Thompson, R.S., Webb, R.S., Iii, T.W., and Whitlock, C., 1998, Paleoclimate simulations for North America over the past 21,000 years: Features of the simulated climate and comparisons with paleoenvironmental data: Quaternary Science Reviews, v. 17, p. 47.

Bartlein, P.J., Whitlock, C., and Shafer, S.L., 1997, Future Climate in the Yellowstone National Park Region and Its Potential Impact on Vegetation: Conservation Biology, v. 11, p. 782–792.

Bassett, I.J., Crompton, C.W., and Parmelee, J.A., 1978, An atlas of airborne pollen grains and common fungus spores of Canada: Canada Department of Agriculture Monograph.

Battarbee, R.W., Jones, V.J., Flower, R.J., and Cameron, N.G., 2001, Diatoms, *in* Tracking Environmental Change Using Lake Sediments, Dordrecht, The Netherlands, Springer, v. 3, p. 155–202, https://doi.org/10.1007/0-306-47668-1_8.

Bauer, C., 1962, Yellowstone, its underground world: Albuquerque, NM, University of New Mexico Press, 122 p.

Baydoun, R., El Samad, O., Nsouli, B., and Younes, G., 2015, Measurement of ^{14}C Content in Leaves near a Cement Factory in Mount Lebanon: Radiocarbon, v. 57, p. 153–159, doi:10.2458/azu_rc.57.18108.

Beisner, B., Haydon, D., and Cuddington, K., 2003, Alternative stable states in ecology: Frontiers in Ecology and the Environment, v. 1, p. 376–382, doi:10.1890/1540-9295(2003)001[0376:ASSIE]2.0.CO;2.

Bennett, K.D., and Willis, K.J., 2001, Pollen, *in* Tracking Environmental Change Using Lake Sediments, Dordrecht, The Netherlands, Kluwer Academic Publishers, v. 3: Terrestrial, Algal, and Siliceous indicators, p. 1–28.

Blaauw, M., and Christen, J.A., 2011, Flexible paleoclimate age-depth models using an autoregressive gamma process: Bayesian Analysis, v. 6, p. 457–474, doi:10.1214/11-BA618.

Blaauw, M., Christen, J.A., Bennett, K.D., and Reimer, P.J., 2018, Double the dates and go for Bayes — Impacts of model choice, dating density and quality on chronologies: Quaternary Science Reviews, v. 188, p. 58–66, doi:10.1016/j.quascirev.2018.03.032.

Black, R.A., and Mack, R.N., 1986, Mount St. Helens Ash: Recreating Its Effects on the Steppe Environment and Ecophysiology: Ecology, v. 67, p. 1289–1302, doi:10.2307/1938685.

Brant, L.A., 1980, A palynological investigation of postglacial sediments at two locations along the continental divide near Helena, Montana [Dissertation]: Pennsylvania State University, 162 p.

Briles, C.E., Whitlock, C., Skinner, C.N., and Mohr, J., 2011, Holocene forest development and maintenance on different substrates in the Klamath Mountains, northern California, USA: Ecology, v. 92, p. 590–601, doi:10.1890/09-1772.1.

Brooks, J., and Shaw, G., 1978, Sporopollenin: A review of its chemistry, palaeochemistry and geochemistry: Grana, v. 17, p. 91–97, doi:10.1080/00173137809428858.

Brown, S., 2019, Diatom-inferred records of paleolimnological variability and continental hydrothermal activity in Yellowstone National Park, USA [Dissertation]: University of Nebraska, 113 p.

Brown, T.A., Nelson, D.E., Mathews, R.W., Vogel, J.S., and Southon, J.R., 1989, Radiocarbon Dating of Pollen by Accelerator Mass Spectrometry: Quaternary Research, v. 32, p. 205–212, doi:10.1016/0033-5894(89)90076-8.

Browne, P.R.L., and Lawless, J.V., 2001, Characteristics of hydrothermal eruptions, with examples from New Zealand and elsewhere: Earth-Science Reviews, v. 52, p. 299–331, doi:10.1016/S0012-8252(00)00030-1.

Brubaker, L.B., 1975, Postglacial Forest Patterns Associated with Till and Outwash in Northcentral Upper Michigan: Quaternary Research, v. 5, p. 499–527, doi:10.1016/0033-5894(75)90013-7.

Brunelle, A., Whitlock, C., Bartlein, P., and Kipfmueller, K., 2005, Holocene fire and vegetation along environmental gradients in the Northern Rocky Mountains: Quaternary Science Reviews, v. 24, p. 2281–2300, doi:10.1016/j.quascirev.2004.11.010.

Bryan, T., 1995, The Geysers of Yellowstone: Niwot, CO, The University Press of Colorado, 463 p.

Bryson, R.A., and Hare, F.K., 1974, The climates of North America, *in* Climates of North America, World Survey of Climatology, Elsevier, v. 11, p. 1–47.

Buckland, H.M., Cashman, K.V., Engwell, S.L., and Rust, A.C., 2020, Sources of uncertainty in the Mazama isopachs and the implications for interpreting distal tephra deposits from large magnitude eruptions: Bulletin of Volcanology, v. 82, p. 23, doi:10.1007/s00445-020-1362-1.

Chaneton, E.J., Mazía, N., Garibaldi, L.A., Chaij, J., and Kitzberger, T., 2014, Impact of volcanic ash deposition on foliar productivity and insect herbivory in northern Patagonia deciduous forests: Ecología Austral, p. 13.

Channing, A., and Edwards, D., 2003, Experimental taphonomy: silicification of plants in Yellowstone hot-spring environments: Transactions of the Royal Society of Edinburgh: Earth Sciences, v. 94, p. 503–521.

Chapman, S.S., Bryce, S.A., Omernik, J.M., Despain, D.G., ZumBerge, J., and Conrad, M., 2004, Ecoregions of Wyoming (color poster with map, descriptive text, summary tables, and photographs): U.S. Geological Survey Level IV Ecoregions Map (1:1,400,000).

Christen, J.A., and Perez E, S., 2009, A New Robust Statistical Model for Radiocarbon Data: Radiocarbon, v. 51, p. 1047–1059, doi:10.1017/S003382220003410X.

Christiansen, R.L., 1975, Geologic map of the Norris Junction Quadrangle, Yellowstone National Park, Wyoming: U.S. Geological Survey Geologic Quadrangle Map GQ-1193 (1:62,500).

Christiansen, R.L., 2001, The Quaternary and Pliocene Yellowstone Plateau volcanic field of Wyoming, Idaho, and Montana: U.S. Geological Survey Professional Paper-729-G.

Christiansen, R.L., Blank, H.R.Jr., Love, J.D., and Reed, J.C.Jr., 1978, Geologic map of the Grassy Lake Reservoir Quadrangle, Yellowstone National Park and vicinity, Wyoming: U.S. Geological Survey Geologic Quadrangle Map GQ-1459 (1:52,500).

Christiansen, R.L., Lowenstern, J.B., Smith, R.B., Heasler, H., Morgan, L.A., Mastin, L.G., Muffler, L.J.P., and Robinson, J.E., 2007, Preliminary Assessment of Volcanic and Hydrothermal Hazards in Yellowstone National Park and Vicinity: U.S. Geological Survey Open-file Report 2007–1071, 98 p.

Ciniglia, C., Cennamo, P., De Stefano, M., Pinto, G., Caputo, P., and Pollio, A., 2007, *Pinnularia obscura* Krasske (Bacillariophyceae, Bacillariophyta) from acidic environments: characterization and comparison with other acid-tolerant *Pinnularia* species: Fundamental and Applied Limnology, v. 170, p. 29–47, doi:10.1127/1863-9135/2007/0170-0029.

Clarkson, B.R., and Clarkson, B.D., 1983, Mt Tarawera: 2. Rates of Change in the Vegetation and Flora of the High Domes: New Zealand Journal of Ecology, v. 6, p. 107–119.

Clayton, R.N., and Mayeda, T.K., 1963, The use of bromine pentafluoride in the extraction of oxygen from oxides and silicates for isotopic analysis: Geochimica et Cosmochimica Acta, v. 27, p. 43–52.

Clifton, C.G., Walters, C.C., and Simoneit, B.R.T., 1990, Hydrothermal petroleums from Yellowstone National Park, Wyoming, U.S.A.: Applied Geochemistry, v. 5, p. 169–191, doi:10.1016/0883-2927(90)90047-9.

Cook, A.C., Hainsworth, L.J., Sorey, M.L., Evans, W.C., and Southon, J.R., 2001, Radiocarbon studies of plant leaves and tree rings from Mammoth Mountain, CA: a long-term record of magmatic CO_2 release: Chemical Geology, v. 177, p. 117–131, doi:10.1016/S0009-2541(00)00386-7.

Craig, H., 1963, The isotopic geochemistry of water and carbon in geothermal areas, *in* Proceedings of the Conference on Nuclear Geology in Geothermal Areas, Spoleto, ITL, p. 17–53.

Dale, V.H., Swanson, F.J., and Crisafulli, C.M. (Eds.), 2005, Ecological responses to the 1980 eruption of Mount St. Helens: New York, NY, Springer, 342 p.

De Vries, Hl., and Barendsen, G.W., 1954, Measurements of Age by the Carbon-14 Technique: Nature, v. 174, p. 1138–1141, doi:10.1038/1741138a0.

Despain, D.G., 1983, Nonpyrogenous Climax Lodgepole Pine Communities in Yellowstone National Park: Ecology, v. 64, p. 231–234, doi:10.2307/1937070.

Despain, D.G., 1987, The two climates of Yellowstone National Park: Proceedings of the Montana Academy of Science, v. 47, p. 11–20.

Despain, D.G., 1990, Yellowstone Vegetation: Consequences of Environment and History in a Natural Setting: Boulder, CO, Robert Rinehart Publishers, 239 p.

Diffenbaugh, N.S., Ashfaq, M., Shuman, B., Williams, J.W., and Bartlein, P.J., 2006, Summer aridity in the United States: Response to mid-Holocene changes in insolation and sea surface temperature: Geophysical Research Letters, v. 33, p. L22712, doi:10.1029/2006GL028012.

Doher, L.I., 1980, Palynomorph preparation procedures currently used in the paleontology and stratigraphy laboratories, U.S. Geological Survey: U.S. Dept. of the Interior, Geological Survey, Circular USGS Numbered Series 830, http://pubs.er.usgs.gov/publication/cir830 (accessed September 2018).

Dorf, E., 1964, The Petrified Forests of Yellowstone Park: Scientific American, v. 210, p. 106–114, doi:10.1038/scientificamerican0464-106.

Dorn, R.D., 2001, Vascular Plants of Wyoming: Cheyenne, WY, Mountain West Publishing.

Efford, J., Clarkson, B., and Bylsma, R., 2014, Persistent effects of a tephra eruption (AD 1655) on treeline composition and structure, Mt Taranaki, New Zealand: New Zealand Journal of Botany, v. 52, p. 245–261, doi:10.1080/0028825X.2014.886599.

Egan, J., Fletcher, W.J., Allott, T.E.H., Lane, C.S., Blackford, J.J., and Clark, D.H., 2016, The impact and significance of tephra deposition on a Holocene forest environment in the North Cascades, Washington, USA: Quaternary Science Reviews, v. 137, p. 135–155, doi:10.1016/j.quascirev.2016.02.013.

Egan, J., Staff, R., and Blackford, J., 2015, A high-precision age estimate of the Holocene Plinian eruption of Mount Mazama, Oregon, USA: The Holocene, v. 25, p. 1054–1067, doi:10.1177/0959683615576230.

Engstrom, D.R., Whitlock, C., Fritz, S.C., and Wright, H.E., 1991, Recent environmental changes inferred from the sediments of small lakes in Yellowstone's northern range: Journal of Paleolimnology, v. 5, p. 139–174, doi:10.1007/BF00176875.

Evans, W.C., Bergfeld, D., McGeehin, J.P., King, J.C., and Heasler, H., 2010, Tree-ring ^{14}C links seismic swarm to CO2 spike at Yellowstone, USA: Geology, v. 38, p. 1075–1078, doi:10.1130/G31345.1.

Fall, P.L., 1992, Spatial patterns of atmospheric pollen dispersal in the Colorado Rocky Mountains, USA: Review of Palaeobotany and Palynology, v. 74, p. 293–313, doi:10.1016/0034-6667(92)90013-7.

Firmage, D.S., 2019, Late Holocene climate, fire, and vegetation history of the northern range, Yellowstone National Park [Thesis]: Montana State University, 106 p.

Fletcher, W.J., Zielhofer, C., Mischke, S., Bryant, C., Xu, X., and Fink, D., 2017, AMS radiocarbon dating of pollen concentrates in a karstic lake system: Quaternary Geochronology, v. 39, p. 112–123, doi:10.1016/j.quageo.2017.02.006.

Franklin, J.F., and Dyrness, C.T., 1973, Natural vegetation of Oregon and Washington: USDA Forest Service General Technical Report PNW-8, 185 p.

Friedman, I., 1970, Some investigations of the deposition of travertine from Hot Springs - I. The isotopic chemistry of a travertine-depositing spring: Geochimica et Cosmochimica Acta, v. 34, p. 1303–1315.

Fritz, W.J., 1980, Reinterpretation of the depositional environment of the Yellowstone “fossil forests”: Geology, v. 8, p. 308–313.

Geist, J.M., and Cochran, P.H., 1991, Influences of Volcanic Ash and Pumice Deposition on Productivity of Western Interior Forest Soils: Intermountain Forest and Range Experiment Station, Forest Service, U.S. Department of Agriculture General Technical Report INT 280, 82–89 p.

Gennett, J.A., and Baker, R.G., 1986, A late quaternary pollen sequence from Blacktail Pond, Yellowstone National Park, Wyoming, U.S.A.: Palynology, v. 10, p. 61–71, doi:10.1080/01916122.1986.9989303.

Grimm, E.C., 1987, CONISS: a FORTRAN 77 program for stratigraphically constrained cluster analysis by the method of incremental sum of squares: Computers & Geosciences, v. 13, p. 13–35, doi:10.1016/0098-3004(87)90022-7.

Hansen, H.P., 1942a, Post-Mount Mazama Forest Succession on the East Slope of the Central Cascades of Oregon: American Midland Naturalist, v. 27, p. 523, doi:10.2307/2421018.

Hansen, H.P., 1942b, The Influence of Volcanic Eruptions Upon Post-Pleistocene Forest Succession in Central Oregon: American Journal of Botany, v. 29, p. 214, doi:10.2307/2437672.

Hedberg, O., 1946, Pollen morphology in the genus *Polygonum* L. s. lat. and its taxonomical significance: Svensk Botanisk Tidskrift, v. 40, p. 371–404.

Herring, E.M., 2014, Late Quaternary and Holocene Paleoecology of Interior Mesic Forests of Northern Idaho [Dissertation]: University of Oregon, 112 p.

Heusser, C.J., 1990, Late Quaternary vegetation of the Aleutian Islands, southwestern Alaska: Canadian Journal of Botany, v. 68, p. 1320–1326, doi:10.1139/b90-168.

Hicks, S., and Hyvärinen, H., 1999, Pollen influx values measured in different sedimentary environments and their palaeoecological implications: Grana, v. 38, p. 228–242, doi:10.1080/001731300750044618.

Higuera, P.E., Brubaker, L.B., Anderson, P.M., Hu, F.S., and Brown, T.A., 2009, Vegetation mediated the impacts of postglacial climate change on fire regimes in the south-central Brooks Range, Alaska: Ecological Monographs, v. 79, p. 201–219, doi:10.1890/07-2019.1.

Higuera, P.E., Gavin, D.G., Bartlein, P.J., and Hallett, D.J., 2011, Peak detection in sediment–charcoal records: impacts of alternative data analysis methods on fire-history interpretations: International Journal of Wildland Fire, v. 19, p. 996–1014, doi:10.1071/WF09134.

Higuera, P.E., Whitlock, C., and Gage, J.A., 2010, Linking tree-ring and sediment-charcoal records to reconstruct fire occurrence and area burned in subalpine forests of Yellowstone National Park, USA: The Holocene, v. 21, p. 327–341, doi:10.1177/0959683610374882.

Holling, C.S., 1973, Resilience and Stability of Ecological Systems: Annual Review of Ecology and Systematics, v. 4, p. 1–23, doi:10.1146/annurev.es.04.110173.000245.

Howarth, J.D., Fitzsimons, S.J., Jacobsen, G.E., Vandergoes, M.J., and Norris, R.J., 2013, Identifying a reliable target fraction for radiocarbon dating sedimentary records from lakes: Quaternary Geochronology, v. 17, p. 68–80, doi:10.1016/j.quageo.2013.02.001.

Hua, Q., Barbetti, M., and Rakowski, A.Z., 2013, Atmospheric Radiocarbon for the Period 1950–2010: Radiocarbon, v. 55, p. 2059–2072, doi:10.2458/azu_js_rc.v55i2.16177.

Huerta, M.A., Whitlock, C., and Yale, J., 2009, Holocene vegetation–fire–climate linkages in northern Yellowstone National Park, USA: Palaeogeography, Palaeoclimatology, Palaeoecology, v. 271, p. 170–181, doi:10.1016/j.palaeo.2008.10.015.

Hurwitz, S., and Lowenstern, J.B., 2014, Dynamics of the Yellowstone hydrothermal system: Reviews of Geophysics, v. 52, p. 375–411, doi:10.1002/2014RG000452.

Iglesias, V., Krause, T.R., and Whitlock, C., 2015, Complex Response of White Pines to Past Environmental Variability Increases Understanding of Future Vulnerability: PLoS ONE, v. 10, p. 1–12, doi:10.1371/journal.pone.0124439.

Iglesias, V., and Whitlock, C., 2020, If the trees burn, is the forest lost? Past dynamics in temperate forests help inform management strategies: Philosophical Transactions of the Royal Society B: Biological Sciences, v. 375, p. 20190115, doi:10.1098/rstb.2019.0115.

Iglesias, V., Whitlock, C., Krause, T.R., and Baker, R.G., 2018, Past vegetation dynamics in the Yellowstone region highlight the vulnerability of mountain systems to climate change: Journal of Biogeography, v. 45, p. 1768–1780, doi:10.1111/jbi.13364.

Interlandi, S.J., Kilham, S.S., and Theriot, E.C., 2003, Diatom—chemistry relationships in Yellowstone Lake (Wyoming) sediments: Implications for climatic and aquatic processes research: Limnology and Oceanography, v. 48, p. 79–92, doi:10.4319/lo.2003.48.1.0079.

Jacobson, G.L., and Bradshaw, R.H.W., 1981, The Selection of Sites for Paleovegetational Studies: Quaternary Research, v. 16, p. 80–96, doi:10.1016/0033-5894(81)90129-0.

Jankovská, V., and Komárek, J., 2000, Indicative value of Pediastrum and other coccal green algae in palaeoecology: Folia Geobotanica, v. 35, p. 59–82, doi:10.1007/BF02803087.

Jensen, B., and Beaudoin, A.B., 2016, Geochemical characterization of tephra deposits at archeological and paleoenvironmental sites across south-central Alberta and Saskatchewan: Archeological Survey of Alberta Occasional Paper 36, 154–160 p.

Johnson, S.Y., Stephenson, W.J., Morgan, L.A., Shanks, W.C., and Pierce, K.L., 2003, Hydrothermal and tectonic activity in northern Yellowstone Lake, Wyoming: Geological Society of America Bulletin, v. 115, p. 954–971, doi:10.1130/B25111.1.

Johnstone, J.F. et al., 2016, Changing disturbance regimes, ecological memory, and forest resilience: Frontiers in Ecology and the Environment, v. 14, p. 369–378, doi:10.1002/fee.1311.

Jones, M.D., 2004, High-resolution records of climate change from lacustrine stable isotopes through the last two millennia in Western Turkey: University of Plymouth, 288 p.

Kapp, R.O., Davis, O.K., and King, J.E., 2000, Ronald O. Kapp's Pollen and Spores: College Station, TX, American Association of Stratigraphic Palynologists, 279 p.

Kelts, K., Briegel, U., Ghilardi, K., and Hsu, K., 1986, The limnogeology-ETH coring system: Swiss Journal of Hydrology, v. 48, p. 104–115, doi:10.1007/BF02544119.

Kittleman, L.R., 1973, Mineralogy, Correlation, and Grain-Size Distributions of Mazama Tephra and Other Postglacial Pyroclastic Layers, Pacific Northwest: Geological Society of America Bulletin, v. 84, p. 2957–2980.

Krammer, K., 2000, The genus *Pinnularia*, *in* Lange-Bertalot, H. ed., Diatoms of Europe : Diatoms of the European Inland Waters and Comparable Habitats, Ruggell, Gantner Verlag, v. 1, p. 703.

Krammer, K., 1997, *in* Die cymbellioden Diatomeen. Eine Monographie der weltweit bekannten Taza. Teil 1. Allgemeines und Encyonema Bibliiotheca Diatomologica, v. 36, p. 1–382.

Krause, T.R., Lu, Y., Whitlock, C., Fritz, S.C., and Pierce, K.L., 2015, Patterns of terrestrial and limnologic development in the northern Greater Yellowstone Ecosystem (USA) during the late-glacial/early-Holocene transition: Palaeogeography, Palaeoclimatology, Palaeoecology, v. 422, p. 46–56, doi:10.1016/j.palaeo.2014.12.018.

Krause, T.R., and Whitlock, C., 2013, Climate and vegetation change during the late-glacial/early-Holocene transition inferred from multiple proxy records from Blacktail Pond, Yellowstone National Park, USA: Quaternary Research, v. 79, p. 391–402, doi:10.1016/j.yqres.2013.01.005.

Kuehn, S.C., Froese, D.G., Carrara, P.E., Foit, F.F., Pearce, N.J.G., and Rotheisler, P., 2009, Major- and trace-element characterization, expanded distribution, and a new chronology for the latest Pleistocene Glacier Peak tephras in western North America: Quaternary Research, v. 71, p. 201–216, doi:10.1016/j.yqres.2008.11.003.

Laskar, J., Robutel, P., Joutel, F., Gastineau, M., Correia, A.C.M., and Levrard, B., 2004, A long-term numerical solution for the insolation quantities of the Earth: Astronomy & Astrophysics, v. 428, p. 261–285, doi:10.1051/0004-6361:20041335.

Lawrence, R.L., and Ripple, W.J., 2000, Fifteen Years of Revegetation of Mount St. Helens: A Landscape-Scale Analysis: Ecology, v. 81, p. 2742–2752, doi:10.1890/0012-9658(2000)081[2742:FYOROM]2.0.CO;2.

Lees, C.M., and Neall, V.E., 1993, Vegetation response to volcanic eruptions on Egmont Volcano, New Zealand, during the last 1500 years: Journal of the Royal Society of New Zealand, v. 23, p. 91–127, doi:10.1080/03036758.1993.10721220.

Leng, M.J., and Barker, P.A., 2006, A review of the oxygen isotope composition of lacustrine diatom silica for palaeoclimate reconstruction: Earth-Science Reviews, v. 75, p. 5–27.

Leng, M.J., and Sloane, H.J., 2008, Combined oxygen and silicon isotope analysis of biogenic silica: Journal of Quaternary Science: Published for the Quaternary Research Association, v. 23, p. 313–319.

Lesica, P., 2012, Manual of Montana Vascular Plants: Fort Worth, Botanical Research Institute of Texas Press, 779 p.

Lewicki, J.L., and Hilley, G.E., 2014, Multi-scale observations of the variability of magmatic CO2 emissions, Mammoth Mountain, CA, USA: Journal of Volcanology and Geothermal Research, v. 284, p. 1–15, doi:10.1016/j.jvolgeores.2014.07.011.

Licciardi, J.M., and Pierce, K.L., 2008, Cosmogenic exposure-age chronologies of Pinedale and Bull Lake glaciations in greater Yellowstone and the Teton Range, USA: Quaternary Science Reviews, v. 27, p. 814–831, doi:10.1016/j.quascirev.2007.12.005.

Licciardi, J.M., and Pierce, K.L., 2018, History and dynamics of the Greater Yellowstone Glacial System during the last two glaciations: Quaternary Science Reviews, v. 200, p. 1–33, doi:10.1016/j.quascirev.2018.08.027.

Long, A., Davis, O.K., and Lanois, J.D., 1992, Separation and ^{14}C Dating of Pure Pollen from Lake Sediments: Nanofossil AMS Dating: Radiocarbon, v. 34, p. 557–560, doi:10.1017/S0033822200051110.

Long, C.J., Power, M.J., and Bartlein, P.J., 2011, The effects of fire and tephra deposition on forest vegetation in the Central Cascades, Oregon: Quaternary Research, v. 75, p. 151–158, doi:10.1016/j.yqres.2010.08.010.

Long, C.J., Power, M.J., Minckley, T.A., and Hass, A.L., 2014, The impact of Mt. Mazama tephra deposition on forest vegetation in the Central Cascades, Oregon, USA: The Holocene, v. 24, p. 503–511, doi:10.1177/0959683613520258.

Love, J.D., 2003, Geologic map of the Moran Quadrangle, Teton County, Wyoming: Wyoming State Geological Survey J. David Love Map Series LMS 11 (1:24,000).

Love, J.D., 1974, Geologic map of the south half of the Mount Hancock quadrangle, Teton County, Wyoming: U.S. Geological Survey Open-File Report OF-74-127 (1:24,000).

Love, J.D., 1975, Geologic map of Whetstone Mountain quadrangle, Teton County, WYoming: U.S. Geological Survey Open-File Report OF-75-138 (1:24,000).

Love, J.D., and Christiansen, A.C., 1983, Preliminary geologic map of Wyoming: U.S. Geological Survey Open-File Report OF-83-802 (1:500,000).

Love, J.D., and Good, J.M., 1970, Hydrocarbons in Thermal Areas, Northwestern Wyoming: U.S. Geological Survey Professional Paper 644-B, 36 p.

Love, J., Good, J., and Browne, D., 2007, Reconnaissance Study of Pleistocene Lake and Fluvial Deposits In and Near Ancestral Yellowstone Lake, Wyoming, *in* Morgan, L.A. ed., Integrated Geoscience Studies in the Greater Yellowstone Area--Volcanic, Tectonic, and Hydrothermal Processes in the Yellowstone Geoecosystem, Reston, VA, U.S. Geological Survey, Professional Paper 1717, p. 53–90.

Lowenstern, J.B., Christiansen, R.L., Smith, R.B., Morgan, L.A., and Heasler, H., 2005, Steam Explosions, Earthquakes, and Volcanic Eruptions--What's in Yellowstone's Future? U.S. Geological Survey Fact Sheet Fact Sheet 2005–3024, 6 p.

Lowenstern, J.B., Heasler, H., and Smith, R.B., 2003, Hydrothermal disturbances at the Norris Geyser Basin, Yellowstone National Park (USA) in 2003, *in* p. #V31B-05.

Lowenstern, J.B., Hurwitz, S., and McGeehin, J.P., 2016, Radiocarbon dating of silica sinter deposits in shallow drill cores from the Upper Geyser Basin, Yellowstone National Park: Journal of Volcanology and Geothermal Research, v. 310, p. 132–136, doi:10.1016/j.jvolgeores.2015.12.005.

Lu, Y., Fritz, S.C., Stone, J.R., Krause, T.R., Whitlock, C., Brown, E.T., and Benes, J.V., 2017, Trends in catchment processes and lake evolution during the late-glacial and early- to mid-Holocene inferred from high-resolution XRF data in the Yellowstone region: Journal of Paleolimnology, v. 58, p. 551–569, doi:10.1007/s10933-017-9991-x.

Lynn, S.G., Kilham, S.S., Kreeger, D.A., and Interlandi, S.J., 2000, Effect of Nutrient Availability on the Biochemical and Elemental Stoichiometry in the Freshwater Diatom Stephanodiscus minutulus (bacillariophyceae): Journal of Phycology, v. 36, p. 510–522, doi:10.1046/j.1529-8817.2000.98251.x.

Mack, R.N., Rutter, N.W., Bryant, V.M., and Valastro, S., 1978, Reexamination of Postglacial Vegetation History in Northern Idaho: Hager Pond, Bonner Co.: Quaternary Research, v. 10, p. 241–255, doi:10.1016/0033-5894(78)90104-7.

Mack, R.N., Rutter, N.W., and Valastro, S., 1983, Holocene Vegetational History of the Kootenai River Valley, Montana: Quaternary Research, v. 20, p. 177–193, doi:10.1016/0033-5894(83)90076-5.

Marler, G.D., 1956, How old is Old Faithful Geyser? American Journal of Science, v. 254, p. 615–622.

Marler, G.D., and White, D.E., 1975, Seismic Geyser and Its Bearing on the Origin and Evolution of Geysers and Hot Springs of Yellowstone National Park: Geological Society of America Bulletin, v. 86, p. 749–759.

Martin, R.S., Watt, S.F.L., Pyle, D.M., Mather, T.A., Matthews, N.E., Georg, R.B., Day, J.A., Fairhead, T., Witt, M.L.I., and Quayle, B.M., 2009, Environmental effects of ashfall in Argentina from the 2008 Chaitén volcanic eruption: Journal of Volcanology and Geothermal Research, v. 184, p. 462–472, doi:10.1016/j.jvolgeores.2009.04.010.

Matthews, N.E., Vazquez, J.A., and Calvert, A.T., 2015, Age of the Lava Creek supereruption and magma chamber assembly at Yellowstone based on $^{40}Ar/^{39}Ar$ and U-Pb dating of sanidine and zircon crystals: Geochemistry, Geophysics, Geosystems, v. 16, p. 2508–2528, doi:10.1002/2015GC005881.

Matz, S.E., 1987, The effects of the Mazama tephra-falls: A geoarchaeological approach [Thesis]: Oregon State University, 235 p.

McCleskey, R.B., Ball, J.W., Nordstrom, D.K., and Taylor, H.E., 2005, Water-Chemistry Data for Selected Hot Springs, Geysers, and Streams in Yellowstone National Park, Wyoming, 2001-2002: U.S. Geological Survey Open-File Report 2004–1316, 102 p.

McDaniel, P.A., Wilson, M.A., Burt, R., Lammers, D., Thorson, T.D., McGrath, C.L., and Peterson, N., 2005, Andic soils of the inland Pacific Northwest, USA: Properties and ecological significance: Soil Science, v. 170, p. 300–311.

McGlone, M.S., Neall, V.E., and Clarkson, B.D., 1988, The effect of recent volcanic events and climatic changes on the vegetation of Mt. Egmont (Mt. Taranaki), New Zealand: New Zealand Journal of Botany, v. 26, p. 123–144, doi:10.1080/0028825X.1988.10410105.

McNichol, A.P., Osborne, E.A., Gagnon, A.R., Fry, B., and Jones, G.A., 1994, TIC, TOC, DIC, DOC, PIC, POC — unique aspects in the preparation of oceanographic samples for ^{14}C-AMS: Nuclear Instruments and Methods in Physics Research Section B: Beam Interactions with Materials and Atoms, v. 92, p. 162–165, doi:10.1016/0168-583X(94)95998-6.

Meeinkuirt, W., Sirinawin, W., Angsupanich, S., and Polpunthin, P., 2008, Changes in relative abundance of phytoplankton in arsenic contaminated waters at the Ron Phibun district of Nakhon Si Thammarat province, Thailand: International Journal on Algae, v. 10, p. 141–162, doi:10.1615/InterJAlgae.v10.i2.40.

Mehringer, P.J., Arno, S.F., and Petersen, K.L., 1977a, Postglacial History of Lost Trail Pass Bog, Bitterroot Mountains, Montana: Arctic and Alpine Research, v. 9, p. 345, doi:10.2307/1550528.

Mehringer, P.J., Blinman, E., and Petersen, K.L., 1977b, Pollen Influx and Volcanic Ash: Science, New Series, v. 198, p. 257–261.

Menounos, B., Osborn, G., Clague, J.J., and Luckman, B.H., 2009, Latest Pleistocene and Holocene glacier fluctuations in western Canada: Quaternary Science Reviews, v. 28, p. 2049–2074, doi:10.1016/j.quascirev.2008.10.018.

Mensing, S.A., and Southon, J.R., 1999, A Simple Method to Separate Pollen for AMS Radiocarbon Dating and its Application to Lacustrine and Marine Sediments: Radiocarbon, v. 41, p. 1–8, doi:10.1017/S0033822200019287.

Miller, L., and Cooper, C., 1969, Analysis of environmental vegetative gradients in Yellowstone National Park from remote multispectral sensing, *in* Johnson, P. ed., Remote Sensing in Ecology, Athens, GA, University of Georgia Press, p. 108–131.

Millspaugh, S.H., and Whitlock, C., 1995, A 750-year fire history based on lake sediment records in central Yellowstone National Park, USA: The Holocene, v. 5, p. 283–292, doi:10.1177/095968369500500303.

Millspaugh, S.H., Whitlock, C., and Bartlein, P.J., 2004, Postglacial Fire, Vegetation, Climate History of the Yellowstone-Lamar and Central Plateau Provinces, Yellowstone National Park, *in* Wallace, L.L. ed., After the Fires: The Ecology of Change in Yellowstone National Park, New Haven, CT, Yale University Press, p. 10–28.

Millspaugh, S.H., Whitlock, C., and Bartlein, P.J., 2000, Variations in fire frequency and climate over the past 17 000 yr in central Yellowstone National Park: Geology, v. 28, p. 211–214, doi:10.1130/0091-7613(2000)28<211:VIFFAC>2.0.CO;2.

Mock, C.J., 1996, Climatic Controls and Spatial Variations of Precipitation in the Western United States: Journal of Climate, v. 9, p. 1111–1125, doi:10.1175/1520-0442(1996)009<1111:CCASVO>2.0.CO;2.

Moore, P.D., Webb, J.A., and Collinson, M.E., 1991, Pollen Analysis: Oxford, UK, Blackwell Scientific Publications, 166 p.

del Moral, R., and Grishin, S.Yu., 1999, Volcanic Disturbances and Ecosystem Recovery, *in* Ecosystems of Disturbed Ground, New York, NY, Elsevier, p. 137–160.

Morgan, L.A. et al., 2003, Exploration and discovery in Yellowstone Lake: results from high-resolution sonar imaging, seismic reflection profiling, and submersible studies: Journal of Volcanology and Geothermal Research, v. 122, p. 221–242, doi:10.1016/S0377-0273(02)00503-6.

Morgan, L.A. et al., 2007, The Floor of Yellowstone Lake is Anything but Quiet—New Discoveries from High-Resolution Sonar Imaging, Seismic- Reflection Profiling, and Submersible Studies, *in* Morgan, L.A. ed., Integrated Geoscience Studies in the Greater Yellowstone Area--Volcanic, Tectonic, and Hydrothermal Processes, Reston, VA, U.S. Geological Survey, Professional Paper 1717, p. 91–126.

Morgan, P., Blackwell, D.D., Spafford, R.E., and Smith, R.B., 1977, Heat flow measurements in Yellowstone Lake and thermal structure of the Yellowstone Caldera: Journal of Geophysical Research, v. 82, p. 3719–3732.

Morgan, L.A., Shanks, W.C., Iverson, N.A., Schiller, C.M., Brown, S.R., Whitlock, C., Fritz, S.C., Cartier, R., and Zahajská, P., 2019, The Dynamic Floor of Yellowstone Lake: A Geologic Record Over the Past 14 ka of Hydrothermal Explosions, Doming, and Faulting, *in* American Geophysical Union, Fall Meeting 2019, v. abstract #V24B-07.

Morgan, L.A., Shanks, W.C., and Pierce, K.L., 2009, Hydrothermal Processes Above the Yellowstone Magma Chamber: Large Hydrothermal Systems and Large Hydrothermal Explosions: Geological Society of America Special Paper 459, 95 p.

Morley, D.W., Leng, M.J., Mackay, A.W., Sloane, H.J., Rioual, P., and Battarbee, R.W., 2004, Cleaning of lake sediment samples for diatom oxygen isotope analysis: Journal of Paleolimnology, v. 31, p. 391–401, doi:10.1023/B:JOPL.0000021854.70714.6b.

Morrison, J., Brockwell, T., Merren, T., Fourel, F., and Phillips, A.M., 2001, On-line high-precision stable hydrogen isotopic analyses on nanoliter water samples: Analytical Chemistry, v. 73, p. 3570–3575.

Muffler, L.J.P., White, D.E., and Truesdell, A.H., 1971, Hydrothermal Explosion Craters in Yellowstone National Park: Geological Society of America Bulletin, v. 82, p. 723–740, doi:10.1130/0016-7606(1971)82[723:HECIYN]2.0.CO;2.

Muffler, L.J.P., White, D.E., Truesdell, A.H., and Fournier, R.O., 1982, Geologic map of Lower Geyser Basin, Yellowstone National Park, Wyoming: U.S. Geological Survey Miscellaneous Geologic Investigations I-1373 (1:24,000).

Mullineaux, D.R., 1974, Pumice and other pyroclastic deposits in Mount Rainier National Park, Washington: U.S. Geological Survey Geological Survey Bulletin 1326, 92 p.

Nanavati, W.P., Whitlock, C., Iglesias, V., and de Porras, M.E., 2019, Postglacial vegetation, fire, and climate history along the eastern Andes, Argentina and Chile (lat. 41–55°S): Quaternary Science Reviews, v. 207, p. 145–160, doi:10.1016/j.quascirev.2019.01.014.

Neulieb, T., Levac, E., Southon, J., Lewis, M., Pendea, I.F., and Chmura, G.L., 2013, Potential Pitfalls of Pollen Dating: Radiocarbon, v. 55, p. 1142–1155.

Newnham, R.M., Vandergoes, M.J., Garnett, M.H., Lowe, D.J., Prior, C., and Almond, P.C., 2007, Test of AMS 14C dating of pollen concentrates using tephrochronology: Journal of Quaternary Science, v. 22, p. 37–51, doi:10.1002/jqs.1016.

Ogden, J., Fordham, R.A., Horrocks, M., Pilkington, S., and Serra, R.G., 2005, Long-Term Dynamics of the Long-Lived Conifer Libocedrus bidwillii after a Volcanic Eruption 2000 Years Ago: Journal of Vegetation Science, v. 16, p. 321–330.

Onalo, J.I., Matias-Peralta, H.M., and Sunar, N.M., 2014, Growth of Freshwater Microalga, Botryococcus sp. in Heavy Metal Contaminated Industrial Wastewater: Journal of Science and Technology, p. 29–40.

Otis, R.M., Smith, R.B., and Wold, R.J., 1977, Geophysical surveys of Yellowstone Lake, Wyoming: Journal of Geophysical Research (1896-1977), v. 82, p. 3705–3717, doi:10.1029/JB082i026p03705.

Parsons, M.L., Dortch, Q., Turner, R.E., and Rabalais, N.R., 2006, Reconstructing the development of eutrophication in Louisiana salt marshes: Limnology and Oceanography, v. 51, p. 534–544, doi:10.4319/lo.2006.51.1_part_2.0534.

Pasquier-Cardin, A., Allard, P., Ferreira, T., Hatte, C., Coutinho, R., Fontugne, M., and Jaudon, M., 1999, Magma-derived CO_2 emissions recorded in ^{14}C and ^{13}C content of plants growing in Furnas caldera, Azores: Journal of Volcanology and Geothermal Research, v. 92, p. 195–207, doi:10.1016/S0377-0273(99)00076-1.

Patrick, R.M., and Reimer, C.W., 1975, The Diatoms of the United States: Academy of Natural Sciences of Philadelphia Monograph No. 13, v. 2, 213 p.

Payne, R.J., and Egan, J., 2019, Using palaeoecological techniques to understand the impacts of past volcanic eruptions: Quaternary International, v. 499, p. 278–289, doi:10.1016/j.quaint.2017.12.019.

Pfister, R.D., and Daubenmire, R., 1975, Ecology of Lodgepole Pine, *in* Management of Lodgepole Pine Ecosystems: Symposium Proceedings, p. 27–46.

Pierce, K.L., Cannon, K.P., Meyer, G.A., Trebesch, M.J., and Watts, R.D., 2007, Postglacial Inflation-Deflation Cycles, Tilting, and Faulting in the Yellowstone Caldera Based on Yellowstone Lake Shorelines, *in* Morgan, L.A. ed., Integrated Geoscience Studies in the Greater Yellowstone Area--Volcanic, Tectonic, and Hydrothermal Processes in the Yellowstone Geoecosystem, Reston, VA, U.S. Geological Survey, Professional Paper 1717, p. 127–168.

Pitt, A.M., and Hutchinson, R.A., 1982, Hydrothermal changes related to earthquake activity at Mud Volcano, Yellowstone National Park, Wyoming: Journal of Geophysical Research, v. 87, p. 2762, doi:10.1029/JB087iB04p02762.

Pniewski, F., and Sylwestrzak, Z., 2018, Influence of short periods of increased water temperature on species composition and photosynthetic activity in the Baltic periphyton communities: Biologia, v. 73, p. 1067–1072, doi:10.2478/s11756-018-0122-6.

Podder, M.S., and Majumder, C.B., 2016, The use of artificial neural network for modelling of phycoremediation of toxic elements As(III) and As(V) from wastewater using *Botryococcus braunii*: Spectrochimica Acta Part A: Molecular and Biomolecular Spectroscopy, v. 155, p. 130–145, doi:10.1016/j.saa.2015.11.011.

Ponader, K.C., and Potapova, M.G., 2007, Diatoms from the genus *Achnanthidium* in flowing waters of the Appalachian Mountains (North America): Ecology, distribution and taxonomic notes: Limnologica, v. 37, p. 227–241, doi:10.1016/j.limno.2007.01.004.

Potapova, M., and Snoeijs, P., 1997, The Natural Life Cycle in Wild Populations of *Diatoma moniliformis* (Bacillariophyceae) and Its Disruption in an Aberrant Environment: Journal of Phycology, v. 33, p. 924–937, doi:10.1111/j.0022-3646.1997.00924.x.

Power, M.J., Whitlock, C., and Bartlein, P.J., 2011, Postglacial fire, vegetation, and climate history across an elevational gradient in the Northern Rocky Mountains, USA and

Canada: Quaternary Science Reviews, v. 30, p. 2520–2533, doi:10.1016/j.quascirev.2011.04.012.

PRISM Climate Group, 2004, 30-Year Normals, http://prism.oregonstate.edu.

Prostka, H.J., Smedes, H.W., and Christiansen, R.L., 1975, Geologic map of the Pelican Cone quadrangle, Yellowstone National Park, Wyoming: U.S. Geological Survey Geologic Quadrangle Map GQ-1243 (1:62,500).

Regnéll, J., 1992, Preparing pollen concentrates for AMS dating – a methodological study from a hard-water lake in southern Sweden: Boreas, v. 21, p. 373–377, doi:10.1111/j.1502-3885.1992.tb00042.x.

Reimer, P.J. et al., 2013, IntCal13 and Marine13 Radiocarbon Age Calibration Curves 0–50,000 Years cal BP: Radiocarbon, v. 55, p. 1869–1887, doi:10.2458/azu_js_rc.55.16947.

Reimer, P.J., and Reimer, R.W., 2004, CALIBomb radiocarbon calibration: Queen's University Belfast, Belfast, http://calib.qub.ac.uk/CALIBomb/.

Reynolds, C.S., 1980, Phytoplankton Assemblages and Their Periodicity in Stratifying Lake Systems: Holarctic Ecology, v. 3, p. 141–159.

Richardson, F., and Hall, V.A., 1994, Pollen Concentrate Preparation from Highly Organic Holocene Peat and Lake Deposits for AMS Dating: Radiocarbon, v. 36, p. 407–412, doi:10.1017/S0033822200014582.

Richmond, G.M., 1977, Surficial Geologic Map of the Canyon Village Quadrange, Yellowstone National Park, Wyoming: U.S. Geological Survey Miscellaneous Geologic Investigations I-652 (1:62,500).

Roach, A.W., 1952, Phytosociology of the Nash Crater Lava Flows, Linn County, Oregon: Ecological Monographs, v. 22, p. 169–193, doi:10.2307/1943564.

Roberts, N. et al., 2001, The tempo of Holocene climatic change in the eastern Mediterranean region: new high-resolution crater-lake sediment data from central Turkey: The Holocene, v. 11, p. 721–736, doi:10.1191/09596830195744.

Roberts, M.L., Elder, K.L., Jenkins, W.J., Gagnon, A.R., Xu, L., Hlavenka, J.D., and Longworth, B.E., 2019, ^{14}C Blank Corrections for 25–100 μg Samples at the National Ocean Sciences AMS Laboratory: Radiocarbon, v. 61, p. 1403–1411, doi:10.1017/RDC.2019.74.

Romme, W.H., and Despain, D.G., 1989, Historical Perspective on the Yellowstone Fires of 1988: BioScience, v. 39, p. 695–699, doi:10.2307/1311000.

Salm, C.R., Saros, J.E., Martin, C.S., and Erickson, J.M., 2009, Patterns of seasonal phytoplankton distribution in prairie saline lakes of the northern Great Plains (U.S.A.): Saline Systems, v. 5, p. 1, doi:10.1186/1746-1448-5-1.

Sarna-Wojcicki, A.M., Champion, D.E., and Davis, J.O., 1983, Holocene Volcanism in the Conterminous United States and the Role of Silicic Volcanic Ash Layers in Correlations of Latest Pleistocene and Holocene Deposits, *in* Wright, H.E. ed., Late-Quaternary Environments of the United States, Minneapolis, MN, University of Minnesota Press, v. 2: The Holocene, p. 52–77.

Saros, J.E., and Anderson, N.J., 2015, The ecology of the planktonic diatom Cyclotella and its implications for global environmental change studies: Biological Reviews, v. 90, p. 522–541, doi:10.1111/brv.12120.

Schiller, C.M., Whitlock, C., Alt, M., and Morgan, L.A., 2020, Vegetation responses to Quaternary volcanic and hydrothermal disturbances in the Northern Rocky Mountains and Greater Yellowstone Ecosystem (USA): Palaeogeography, Palaeoclimatology, Palaeoecology, v. 559, p. 109859, doi:10.1016/j.palaeo.2020.109859.

Schnurrenberger, D., Russell, J., and Kelts, K., 2003, Classification of lacustrine sediments based on sedimentary components: Journal of Paleolimnology, v. 29, p. 141–154, doi:10.1023/A:1023270324800.

Schoennagel, T., Turner, M.G., and Romme, W.H., 2003, Influence of Fire Interval and Serotiny on Postfire Lodgepole Pine Density in Yellowstone National Park: Ecology, v. 84, p. 2967–2978.

Schoennagel, T., Waller, D.M., Turner, M.G., and Romme, W.H., 2004, The Effect of Fire Interval on Post-Fire Understorey Communities in Yellowstone National Park: Journal of Vegetation Science, v. 15, p. 797–806.

Schullery, P., 1989, The Fires and Fire Policy: BioScience, v. 39, p. 686–694, doi:10.2307/1310999.

Seymour, V.A., Hinckley, T.M., Morikawa, Y., and Franklin, J.F., 1983, Foliage damage in coniferous trees following volcanic ashfall from Mt. St. Helens: Oecologia, v. 59, p. 339–343, doi:10.1007/BF00378859.

Shanks, W.C., Alt, J., and Morgan, L.A., 2007, Geochemistry of Sublacustrine Hydrothermal Deposits in Yellowstone Lake—Hydrothermal Reactions, Stable-Isotope Systematics, Sinter Deposition, and Spire Formation, *in* Morgan, L.A. ed., Integrated Geoscience Studies in the Greater Yellowstone Area--Volcanic, Tectonic, and Hydrothermal Processes in the Yellowstone Geoecosystem, Reston, VA, U.S. Geological Survey, Professional Paper 1717, p. 201–234.

Shaw Chraïbi, V.L., 2016, A paleolimnological analysis of the hierarchy of environmental controls on the resilience of aquatic communities in Yellowstone National Park, USA [Dissertation]: University of Nebraska, 120 p.

Shuman, B.N., and Marsicek, J., 2016, The structure of Holocene climate change in mid-latitude North America: Quaternary Science Reviews, v. 141, p. 38–51, doi:10.1016/j.quascirev.2016.03.009.

Smedes, H.W., M'Gonigle, J.W., and Prostka, H.J., 1989, Geologic map of the Two Ocean Pass quadrangle, Yellowstone National Park and vicinity, Wyoming: U.S. Geological Survey Geologic Quadrangle Map GQ-1667 (1:62,500).

Smith, B.N., and Epsten, S., 1971, Two Categories of 1CC/12C Ratios for Higher Plantsl: v. 47, p. 5.

Smith, R.B., Jordan, M., Steinberger, B., Puskas, C.M., Farrell, J., Waite, G.P., Husen, S., Chang, W.L., and O'Connell, R., 2009, Geodynamics of the Yellowstone hotspot and mantle plume: Seismic and GPS imaging, kinematics, and mantle flow: Journal of Volcanology and Geothermal Research, v. 188, p. 26–56, doi:10.1016/j.jvolgeores.2009.08.020.

Smith, T.A., and McKibbin, R., 1997, Modelling of Hydrothermal Eruptions: A Review, *in* Proceeedings 19th NZ Geothermal Workshop, p. 123–128.

del Socorro Lozano-García, M., and Xelhuantzi-López, M.S., 1997, Some problems in the late Quaternary pollen records of Central Mexico: Basins of Mexico and Zacapu: Quaternary International, v. 43–44, p. 117–123, doi:10.1016/S1040-6182(97)00027-X.

Sohn, R., Harris, R., Linder, C., Luttrell, K., Lovalvo, D., Morgan, L., Seyfried, W., and Shanks, P., 2017, Exploring the Restless Floor of Yellowstone Lake: Eos, v. 98, doi:https://doi.org/10.1029/2017EO087035.

Spaulding, S.A., and Edlund, M., 2016, Diatoms of North America: Diatoms of North America, https://diatoms.org/.

Stauffer, R.E., and Thompson, J.M., 1984, Arsenic and antimony in geothermal waters of Yellowstone National Park, Wyoming, USA: Geochimica et Cosmochimica Acta, v. 48, p. 2547–2561, doi:10.1016/0016-7037(84)90305-3.

Stegner, W., 1942, Mormon Country: Lincoln, Nebraska, University of Nebraska Press, 362 p.

Stegner, M.A., Turner, M.G., Iglesias, V., and Whitlock, C., 2019, Post-fire vegetation and climate dynamics in low-elevation forests over the last three millennia in Yellowstone National Park: Ecography, v. 42, p. 1226–1236, doi:10.1111/ecog.04445.

Stelten, M.E., Cooper, K.M., Vazquez, J.A., Calvert, A.T., and Glessner, J.J.G., 2015, Mechanisms and Timescales of Generating Eruptible Rhyolitic Magmas at Yellowstone Caldera from Zircon and Sanidine Geochronology and Geochemistry: Journal of Petrology, v. 56, p. 1607–1642, doi:10.1093/petrology/egv047.

Stuiver, M., Reimer, P.J., and Reimer, R.W., 2019, CALIB 7.1:, http://calib.org.

Sturchio, N.C., Pierce, K.L., Murrell, M.T., and Sorey, M.L., 1994, Uranium-Series Ages of Travertines and Timing of the Last Glaciation in the Northern Yellowstone Area, Wyoming-Montana: Quaternary Research, v. 41, p. 265–277, doi:10.1006/qres.1994.1030.

Sugita, S., 1993, A Model of Pollen Source Area for an Entire Lake Surface: Quaternary Research, v. 39, p. 239–244.

Swann, G.E., Leng, M.J., Sloane, H.J., Maslin, M.A., and Onodera, J., 2007, Diatom oxygen isotopes: evidence of a species effect in the sediment record: Geochemistry, Geophysics, Geosystems, v. 8, p. 1–10.

Tennant, R.K., Jones, R.T., Brock, F., Cook, C., Turney, C.S.M., Love, J., and Lee, R., 2013, A new flow cytometry method enabling rapid purification of fossil pollen from terrestrial sediments for AMS radiocarbon dating: Journal of Quaternary Science, v. 28, p. 229–236, doi:10.1002/jqs.2606.

Theriot, E.C., Fritz, S.C., Whitlock, C., and Conley, D.J., 2006, Late Quaternary rapid morphological evolution of an endemic diatom in Yellowstone Lake, Wyoming: Paleobiology, v. 32, p. 38–54, doi:10.1666/02075.1.

Tiller, C.C., 1995, Postglacial sediment stratigraphy of large lakes in Greater Yellowstone: Scenarios of tectonic and climatic forcing [Thesis]: University of Minnesota, 193 p.

Tinker, D.B., Romme, W.H., and Despain, D.G., 2003, Historic range of variability in landscape structure in subalpine forests of the Greater Yellowstone Area, USA: Landscape Ecology, v. 18, p. 427–439.

Tinker, D.B., Romme, W.H., Hargrove, W.W., Gardner, R.H., and Turner, M.G., 1994, Landscape-scale heterogeneity in lodgepole pine serotiny: Canadian Journal of Forest Research, doi:10.1139/x94-118.

Turner, M.G., Hargrove, W.W., Gardner, R.H., and Romme, W.H., 1994, Effects of fire on landscape heterogeneity in Yellowstone National Park, Wyoming: Journal of Vegetation Science, v. 5, p. 731–742, doi:10.2307/3235886.

Tweddle, J.C., and Edwards, K.J., 2010, Pollen preservation zones as an interpretative tool in Holocene palynology: Review of Palaeobotany and Palynology, v. 161, p. 59–76, doi:10.1016/j.revpalbo.2010.03.004.

U.S. Geological Survey, 1972, Geologic Map of Yellowstone National Park: U.S. Geological Survey Miscellaneous Geologic Investigations I-711 (1:125,000).

Vandergoes, M.J., and Prior, C.A., 2003, AMS Dating of Pollen Concentrates—A Methodological Study of Late Quaternary Sediments from South Westland, New Zealand: Radiocarbon, v. 45, p. 479–491, doi:10.1017/S0033822200032823.

Vaughan, R.G., Heasler, H., Jaworowski, C., Lowenstern, J.B., and Keszthelyi, L.P., 2014, Provisional Maps of Thermal Areas in Yellowstone National Park, based on Satellite Thermal Infrared Imaging and Field Observations: U.S. Geological Survey Scientific Investigations Report 2014–5137, 32 p.

Vaughan, R.G., Hungerford, J.D.G., and Keller, W., 2020, A Newly Emerging Thermal Area in Yellowstone: Frontiers in Earth Science, v. 8, doi:10.3389/feart.2020.00204.

Viau, A.E., Ladd, M., and Gajewski, K., 2012, The climate of North America during the past 2000 years reconstructed from pollen data: Global and Planetary Change, v. 84–85, p. 75–83, doi:10.1016/j.gloplacha.2011.09.010.

Vijver, B.V. de, Gremmen, N.J.M., and Beyens, L., 2005, The genus *Stauroneis* (Bacillariophyceae) in the Antarctic region: Journal of Biogeography, v. 32, p. 1791–1798, doi:10.1111/j.1365-2699.2005.01325.x.

Waddington, J.C.B., and Wright, H.E., 1974, Late Quaternary Vegetational Changes on the East Side of Yellowstone Park, Wyoming: Quaternary Research, v. 4, p. 175–184, doi:10.1016/0033-5894(74)90006-4.

Waldrop, H.A., and Pierce, K.L., 1975, Surficial geologic map of the Madison Junction Quadrangle, Yellowstone National Park, Wyoming: U.S. Geological Survey Miscellaneous Geologic Investigations 1-651 (1:62,500).

Werner, C., and Brantley, S., 2003, CO_2 emissions from the Yellowstone volcanic system: Geochemistry, Geophysics, Geosystems, v. 4, doi:10.1029/2002GC000473.

White, D.E., Hutchinson, R.A., and Keith, T.E.C., 1988, The Geology and Remarkable Thermal Activity of Norris Geyser Basin, Yellowstone National Park, Wyoming: U.S. Geological Survey Professional Paper 1456, 83 p.

Whitlock, C., 1993, Postglacial Vegetation and Climate of Grand Teton and Southern Yellowstone National Parks: Ecological Monographs, v. 63, p. 173–198, doi:10.2307/2937179.

Whitlock, C., and Bartlein, P.J., 1993, Spatial Variations of Holocene Climatic Change in the Yellowstone Region: Quaternary Research, v. 39, p. 231–238, doi:10.1006/qres.1993.1026.

Whitlock, C., Bartlein, P.J., and Van Norman, K.J., 1995, Stability of Holocene Climate Regimes in the Yellowstone Region: Quaternary Research, v. 43, p. 433–436, doi:10.1006/qres.1995.1049.

Whitlock, C., Dean, W.E., Fritz, S.C., Stevens, L.R., Stone, J.R., Power, M.J., Rosenbaum, J.R., Pierce, K.L., and Bracht-Flyr, B.B., 2012, Holocene seasonal variability inferred from multiple proxy records from Crevice Lake, Yellowstone National Park, USA: Palaeogeography, Palaeoclimatology, Palaeoecology, v. 331–332, p. 90–103, doi:10.1016/j.palaeo.2012.03.001.

Whitlock, C., Dean, W., Rosenbaum, J., Stevens, L., Fritz, S., Bracht, B., and Power, M., 2008, A 2650-year-long record of environmental change from northern Yellowstone National Park based on a comparison of multiple proxy data: Quaternary International, v. 188, p. 126–138, doi:10.1016/j.quaint.2007.06.005.

Whitlock, C., and Larsen, C., 2001, Charcoal as a Fire Proxy, *in* Smol, J.P., Birks, J.B., and Last, W.M. eds., Tracking Environmental Change Using Lake Sediments Vol. 3, Dordrecht, Kluwer Academic Publishers, v. 3, p. 507.

Whitlock, C., and Millspaugh, S.H., 2001, A paleoecologic perspective on past plant invasions in Yellowstone: Western North American Naturalist, v. 61, p. 316–327.

Whitlock, C., and Millspaugh, S.H., 1996, Testing the assumptions of fire-history studies: an examination of modern charcoal accumulation in Yellowstone National Park, USA: The Holocene, v. 6, p. 7–15, doi:10.1177/095968369600600102.

Whitlock, C., Shafer, S.L., and Marlon, J., 2003, The role of climate and vegetation change in shaping past and future fire regimes in the northwestern US and the implications for ecosystem management: Forest Ecology and Management, v. 178, p. 5–21, doi:10.1016/S0378-1127(03)00051-3.

Whittlesey, L., 1990, Monarch of All These Mighty Wonders: Tourists and Yellowstone's Excelsior Geyser, 1881-1890: Montana: The Magazine of Western History, v. 40, p. 2–15.

Winner, W.E., and Casadevall, T.J., 1983, The Effects of the Mount St. Helens Eruption Cloud on Fir (*Abies* sp.) Needle Cuticles: Analysis with Scanning Electron Microscopy: American Journal of Botany, v. 70, p. 80–87.

Wotzlaw, J.-F., Bindeman, I.N., Stern, R.A., D'Abzac, F.-X., and Schaltegger, U., 2015, Rapid heterogeneous assembly of multiple magma reservoirs prior to Yellowstone supereruptions: Scientific Reports, v. 5, p. 14026, doi:10.1038/srep14026.

Wright, H.E., Mann, D.H., and Glaser, P.H., 1984, Piston Corers for Peat and Lake Sediments: Ecology, v. 65, p. 657–659, doi:10.2307/1941430.

Zdanowicz, C.M., Zielinski, G.A., and Germani, M.S., 1999, Mount Mazama eruption: Calendrical age verified and atmospheric impact assessed: Geology, v. 27, p. 621–624, doi:10.1130/0091-7613(1999)027<0621:MMECAV>2.3.CO;2.

Zhang, J.-F., Xu, B., Turner, F., Zhou, L., Gao, P., Lü, X., and Nesje, A., 2017, Long-term glacier melt fluctuations over the past 2500 yr in monsoonal High Asia revealed by radiocarbon-dated lacustrine pollen concentrates: Geology, v. 45, p. 359–362, doi:10.1130/G38690.1.

Zimmerman, S.R.H., Brown, T.A., Hassel, C., and Heck, J., 2019, Testing Pollen Sorted by Flow Cytometry as the Basis for High-Resolution Lacustrine Chronologies: Radiocarbon, v. 61, p. 359–374, doi:10.1017/RDC.2018.89.

APPENDICES

APPENDIX A

ADDITIONAL AGE-DEPTH MODELS FROM CHAPTER 5

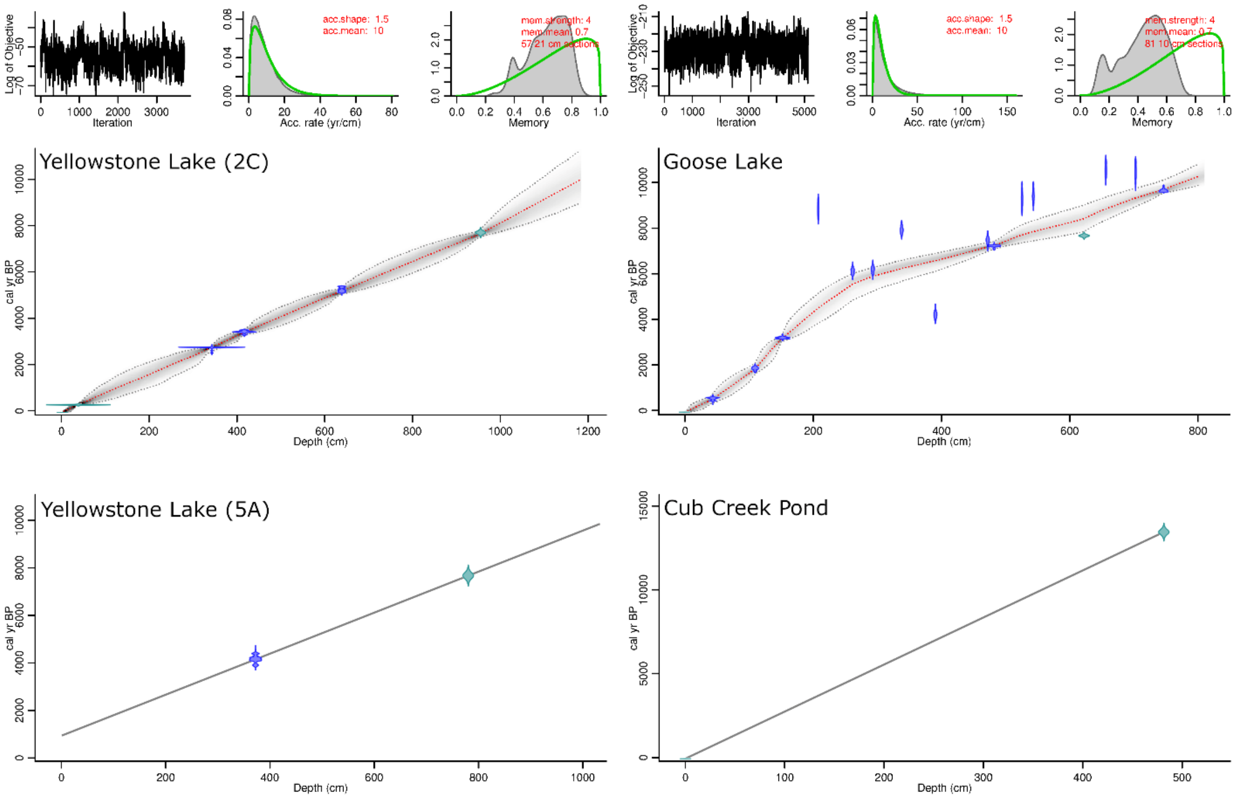

Age-depth models used for new Greater Yellowstone Ecosystem sites, Yellowstone Lake (2C and 5A), Goose Lake, and Cub Creek Pond. Yellowstone Lake (2C) and Goose Lake cores had sufficient age control to produce a Bayesian age-depth model with Bacon, while Yellowstone Lake (5A) and Cub Creek Pond were reconstructed with simple linear interpolation/extrapolation.

APPENDIX B

MAZAMA POLLEN PERCENTAGE DIAGRAMS FROM CHAPTER 5

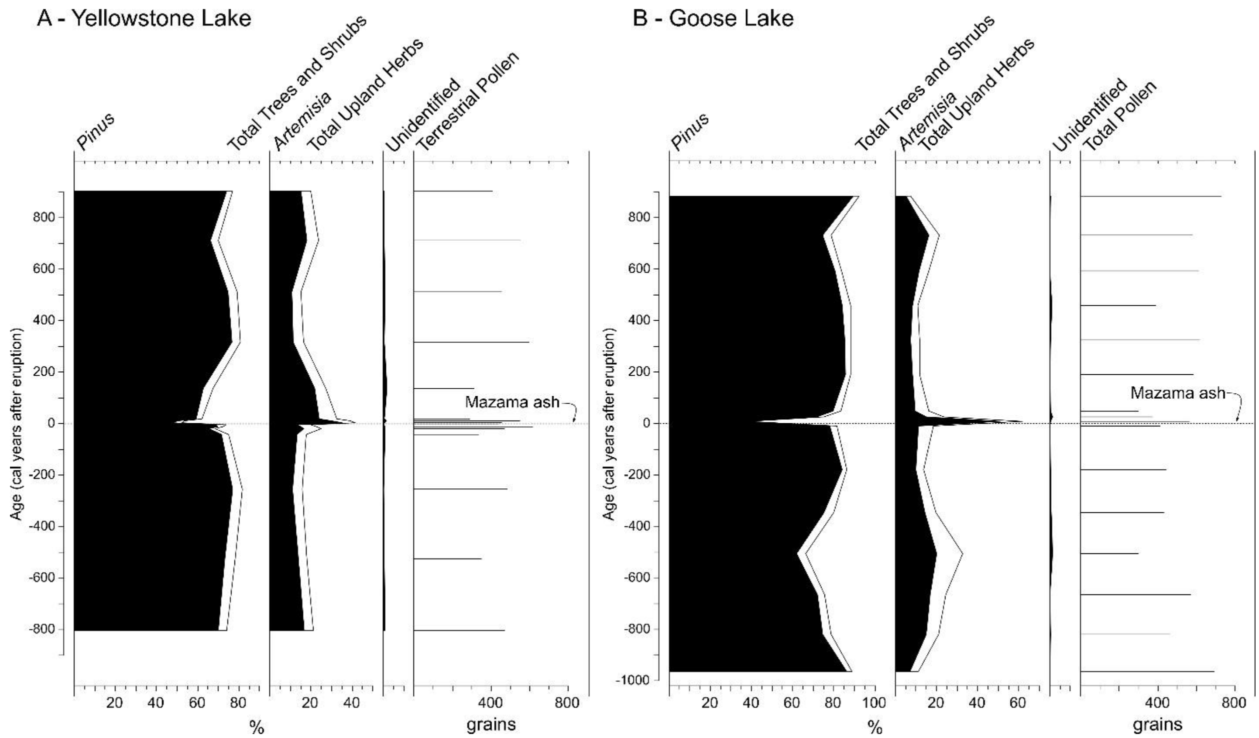

Simplified pollen spectra for Mazama ash sequences with samples covering approximately 1000 cal years before and after ashfall at Yellowstone Lake (2C; A) and Goose Lake (B). Individual taxa percentages are stacked and summed values are overlain.

APPENDIX C

HYDROTHERMAL EXPLOSION DEPOSIT POLLEN PERCENTAGE DIAGRAMS

FROM CHAPTER 5

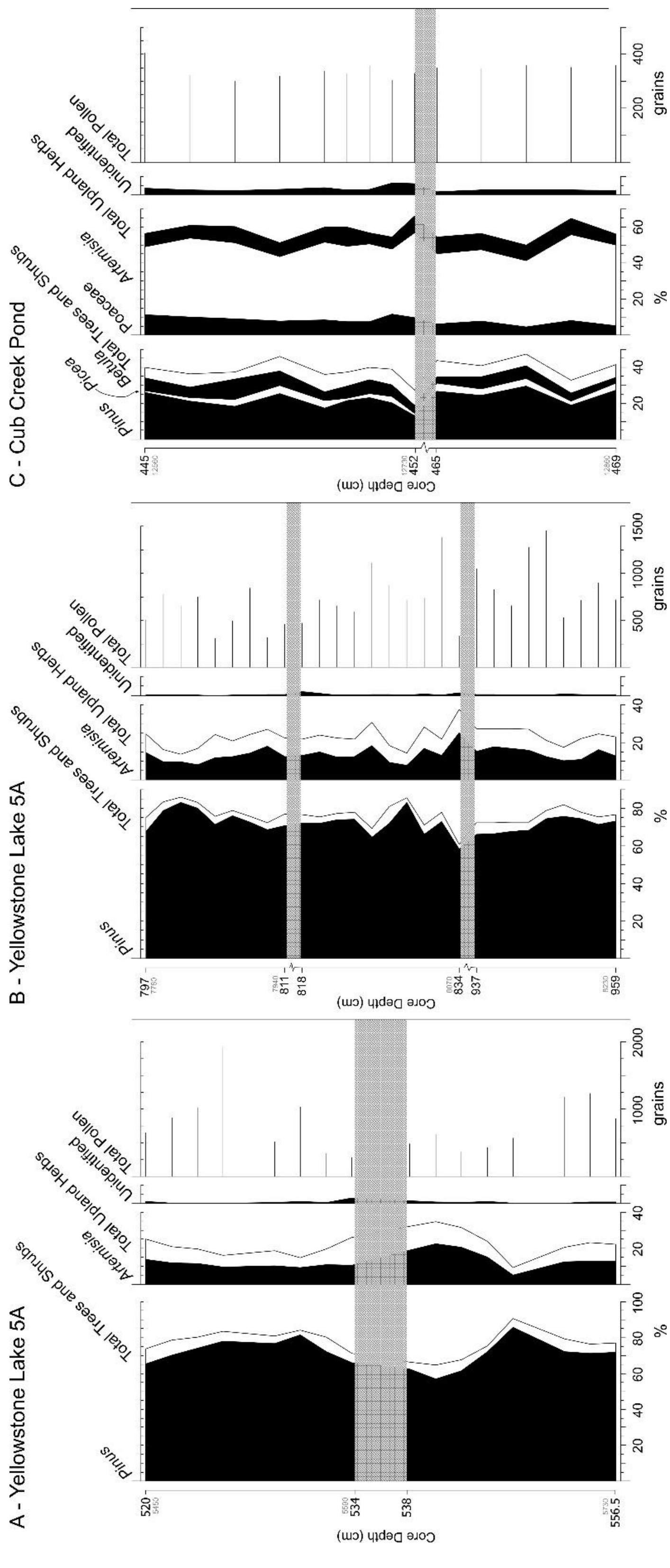

Simplified pollen spectra for hydrothermal explosion sequences with core depths (black) and interpolated ages (gray) for various hydrothermal explosion deposits from Yellowstone Lake (5A; A, B) and Cub Creek Pond (C). Individual taxa percentages are stacked and summed values are overlain.